2024-2025

THÈSE

pour le

DIPLÔME D'ÉTAT DE DOCTEUR EN MÉDECINE

Qualification en MÉDECINE CARDIOVASCULAIRE

From cardiac mechanics to prognosis: left ventricle hemodynamic forces as a novel risk marker in MINOCA

De la mécanique cardiaque au pronostic : les forces hémodynamiques ventriculaires gauches comme nouveau marqueur de risque dans les MINOCA

BALADI Claire

Née le 01 juillet 1995 à Cherbourg (50)

Sous la direction de M. le Professeur BIERE Loïc

Membres du jury

M. le Pr FURBER Alain	Président
M. le Pr BIERE Loïc	Directeur
M. le Pr PRUNIER Fabrice	Membre
M. le Dr GRALL Sylvain	Membre

Soutenue publiquement le :
18 septembre 2025

FACULTÉ DE SANTÉ
UNIVERSITÉ D'ANGERS

ENGAGEMENT DE NON PLAGIAT

Je, soussignée Claire BALADI,
déclare être pleinement consciente que le plagiat de documents ou d'une partie d'un document publiée sur toutes formes de support, y compris l'internet, constitue une violation des droits d'auteur ainsi qu'une fraude caractérisée.
En conséquence, je m'engage à citer toutes les sources que j'ai utilisées pour écrire ce rapport ou mémoire.

signé par l'étudiante le **07**/**09**/**2025**

SERMENT D'HIPPOCRATE

« Au moment d'être admise à exercer la médecine, je promets et je jure d'être fidèle aux lois de l'honneur et de la probité. Mon premier souci sera de rétablir, de préserver ou de promouvoir la santé dans tous ses éléments, physiques et mentaux, individuels et sociaux. Je respecterai toutes les personnes, leur autonomie et leur volonté, sans aucune discrimination selon leur état ou leurs convictions. J'interviendrai pour les protéger si elles sont affaiblies, vulnérables ou menacées dans leur intégrité ou leur dignité. Même sous la contrainte, je ne ferai pas usage de mes connaissances contre les lois de l'humanité. J'informerai les patients des décisions envisagées, de leurs raisons et de leurs conséquences. Je ne tromperai jamais leur confiance et n'exploiterai pas le pouvoir hérité des circonstances pour forcer les consciences. Je donnerai mes soins à l'indigent et à quiconque me les demandera. Je ne me laisserai pas influencer par la soif du gain ou la recherche de la gloire.

Admise dans l'intimité des personnes, je tairai les secrets qui me seront confiés. Reçue à l'intérieur des maisons, je respecterai les secrets des foyers et ma conduite ne servira pas à corrompre les mœurs. Je ferai tout pour soulager les souffrances. Je ne prolongerai pas abusivement les agonies. Je ne provoquerai jamais la mort délibérément.

Je préserverai l'indépendance nécessaire à l'accomplissement de ma mission. Je n'entreprendrai rien qui dépasse mes compétences. Je les entretiendrai et les perfectionnerai pour assurer au mieux les services qui me seront demandés.

J'apporterai mon aide à mes confrères ainsi qu'à leurs familles dans l'adversité. Que les hommes et mes confrères m'accordent leur estime si je suis fidèle à mes promesses ; que je sois déshonorée et méprisée si j'y manque ».

LISTE DES ENSEIGNANTS DE LA FACULTÉ DE SANTÉ D'ANGERS

Doyen de la Faculté : Pr Cédric ANNWEILER
Vice-Doyen de la Faculté et directeur du département de pharmacie : Pr Sébastien FAURE
Directeur du département de médecine : Pr Vincent DUBEE

PROFESSEURS DES UNIVERSITÉS

ABRAHAM Pierre	PHYSIOLOGIE	Médecine
ANGOULVANT Cécile	MEDECINE GENERALE	Médecine
ANNWEILER Cédric	GERIATRIE ET BIOLOGIE DU VIEILLISSEMENT	Médecine
ASFAR Pierre	REANIMATION	Médecine
AUBE Christophe	RADIOLOGIE ET IMAGERIE MEDICALE	Médecine
AUGUSTO Jean-François	NEPHROLOGIE	Médecine
BAUFRETON Christophe	CHIRURGIE THORACIQUE ET CARDIOVASCULAIRE	Médecine
BELLANGER William	MEDECINE GENERALE	Médecine
BELONCLE François	REANIMATION	Médecine
BIERE Loïc	CARDIOLOGIE	Médecine
BIGOT Pierre	UROLOGIE	Médecine
BONNEAU Dominique	GENETIQUE	Médecine
BOUCHARA Jean-Philippe	PARASITOLOGIE ET MYCOLOGIE	Médecine
BOUET Pierre-Emmanuel	GYNECOLOGIE-OBSTETRIQUE	Médecine
BOURSIER Jérôme	GASTROENTEROLOGIE ; HEPATOLOGIE	Médecine
BOUVARD Béatrice	RHUMATOLOGIE	Médecine
BRIET Marie	PHARMACOLOGIE	Médecine
CAMPONE Mario	CANCEROLOGIE ; RADIOTHERAPIE	Médecine
CAROLI-BOSC François-Xavier	GASTROENTEROLOGIE ; HEPATOLOGIE	Médecine
CASSEREAU Julien	NEUROLOGIE	Médecine
CLERE Nicolas	PHARMACOLOGIE / PHYSIOLOGIE	Pharmacie
COLIN Estelle	GENETIQUE	Médecine
CONNAN Laurent	MEDECINE GENERALE	Médecine
COPIN Marie-Christine	ANATOMIE ET CYTOLOGIE PATHOLOGIQUES	Médecine
COUTANT Régis	PEDIATRIE	Médecine
CUSTAUD Marc-Antoine	PHYSIOLOGIE	Médecine
CRAUSTE-MANCIET Sylvie	PHARMACOTECHNIE HOSPITALIERE	Pharmacie
DE CASABIANCA Catherine	MEDECINE GENERALE	Médecine
DERBRE Séverine	PHARMACOGNOSIE	Pharmacie
DESCAMPS Philippe	GYNECOLOGIE-OBSTETRIQUE	Médecine
D'ESCATHA Alexis	MEDECINE ET SANTE AU TRAVAIL	Médecine

DINOMAIS Mickaël	MEDECINE PHYSIQUE ET DE READAPTATION	Médecine
DUBEE Vincent	MALADIES INFECTIEUSES ET TROPICALES	Médecine
DUCANCELLE Alexandra	BACTERIOLOGIE-VIROLOGIE ; HYGIENE HOSPITALIERE	Médecine
DUVERGER Philippe	PEDOPSYCHIATRIE	Médecine
EVEILLARD Matthieu	BACTERIOLOGIE-VIROLOGIE	Pharmacie
FAURE Sébastien	PHARMACOLOGIE PHYSIOLOGIE	Pharmacie
FOURNIER Henri-Dominique	ANATOMIE	Médecine
FOUQUET Olivier	CHIRURGIE THORACIQUE ET CARDIOVASCULAIRE	Médecine
FURBER Alain	CARDIOLOGIE	Médecine
GAGNADOUX Frédéric	PNEUMOLOGIE	Médecine
GOHIER Bénédicte	PSYCHIATRIE D'ADULTES	Médecine
GUARDIOLA Philippe	HEMATOLOGIE ; TRANSFUSION	Médecine
GUILET David	CHIMIE ANALYTIQUE	Pharmacie
HUNAULT-BERGER Mathilde	HEMATOLOGIE ; TRANSFUSION	Médecine
JEANNIN Pascale	IMMUNOLOGIE	Médecine
KAZOUR François	PSYCHIATRIE	Médecine
KEMPF Marie	BACTERIOLOGIE-VIROLOGIE ; HYGIENE HOSPITALIERE	Médecine
KUN-DARBOIS Daniel	CHIRURGIE MAXILLO-FACIALE ET STOMATOLOGIE	Médecine
LACOEUILLE FRANCK	RADIOPHARMACIE	Pharmacie
LACCOURREYE Laurent	OTO-RHINO-LARYNGOLOGIE	Médecine
LAGARCE Frédéric	BIOPHARMACIE	Pharmacie
LANDREAU Anne	BOTANIQUE/ MYCOLOGIE	Pharmacie
LASOCKI Sigismond	ANESTHESIOLOGIE-REANIMATION	Médecine
LEBDAI Souhil	UROLOGIE	Médecine
LEGENDRE Guillaume	GYNECOLOGIE-OBSTETRIQUE	Médecine
LEGRAND Erick	RHUMATOLOGIE	Médecine
LEMEE Jean-Michel	NEUROCHIRURGIE	Médecine
LERMITE Emilie	CHIRURGIE GENERALE	Médecine
LEROLLE Nicolas	REANIMATION	Médecine
LIBOUBAN Hélène	HISTOLOGIE	Médecine
LUQUE PAZ Damien	HEMATOLOGIE BIOLOGIQUE	Médecine
MARCHAIS Véronique	BACTERIOLOGIE-VIROLOGIE	Pharmacie
MARTIN Ludovic	DERMATO-VENEREOLOGIE	Médecine
MAY-PANLOUP Pascale	BIOLOGIE ET MEDECINE DU DEVELOPPEMENT ET DE LA REPRODUCTION	Médecine
MENEI Philippe	NEUROCHIRURGIE	Médecine
MERCAT Alain	REANIMATION	Médecine
ORVAIN Corentin	HEMATOLOGIE ; TRANSFUSION	Médecine
PAISANT Anita	RADIOLOGIE	Médecine
PAPON Nicolas	PARASITOLOGIE ET MYCOLOGIE MEDICALE	Pharmacie

PASSIRANI Catherine	CHIMIE GENERALE	Pharmacie
PELLIER Isabelle	PEDIATRIE	Médecine
PETIT Audrey	MEDECINE ET SANTE AU TRAVAIL	Médecine
PICQUET Jean	CHIRURGIE VASCULAIRE ; MEDECINE VASCULAIRE	Médecine
PODEVIN Guillaume	CHIRURGIE INFANTILE	Médecine
PROCACCIO Vincent	GENETIQUE	Médecine
PRUNIER Delphine	BIOCHIMIE ET BIOLOGIE MOLECULAIRE	Médecine
PRUNIER Fabrice	CARDIOLOGIE	Médecine
PY Thibaut	MEDECINE GENERALE	Médecine
RAMOND-ROQUIN Aline	MEDECINE GENERALE	Médecine
REYNIER Pascal	BIOCHIMIE ET BIOLOGIE MOLECULAIRE	Médecine
RIOU Jérémie	BIOSTATISTIQUE	Pharmacie
RINEAU Emmanuel	ANESTHESIOLOGIE REANIMATION	Médecine
RIQUIN Elise	PEDOPSYCHIATRIE ; ADDICTOLOGIE	Médecine
RODIEN Patrice	ENDOCRINOLOGIE, DIABETE ET MALADIES METABOLIQUES	Médecine
ROQUELAURE Yves	MEDECINE ET SANTE AU TRAVAIL	Médecine
ROUGE-MAILLART Clotilde	MEDECINE LEGALE ET DROIT DE LA SANTE	Médecine
ROUSSEAU Audrey	ANATOMIE ET CYTOLOGIE PATHOLOGIQUES	Médecine
ROUSSEAU Pascal	CHIRURGIE PLASTIQUE, RECONSTRUCTRICE ET ESTHETIQUE	Médecine
ROUSSELET Marie-Christine	ANATOMIE ET CYTOLOGIE PATHOLOGIQUES	Médecine
ROY Pierre-Marie	MEDECINE D'URGENCE	Médecine
SAULNIER Patrick	BIOPHYSIQUE ET BIOSTATISTIQUES	Pharmacie
SERAPHIN Denis	CHIMIE ORGANIQUE	Pharmacie
SCHMIDT Aline	HEMATOLOGIE ; TRANSFUSION	Médecine
TESSIER-CAZENEUVE Christine	MEDECINE GENERALE	Médecine
TRZEPIZUR Wojciech	PNEUMOLOGIE	Médecine
UGO Valérie	HEMATOLOGIE ; TRANSFUSION	Médecine
URBAN Thierry	PNEUMOLOGIE	Médecine
VAN BOGAERT Patrick	PEDIATRIE	Médecine
VENARA Aurélien	CHIRURGIE VISCERALE ET DIGESTIVE	Médecine
VENIER-JULIENNE Marie-Claire	PHARMACOTECHNIE	Pharmacie
VERNY Christophe	NEUROLOGIE	Médecine
WILLOTEAUX Serge	RADIOLOGIE ET IMAGERIE MEDICALE	Médecine

MAÎTRES DE CONFÉRENCES

AMMI Myriam	CHIRURGIE VASCULAIRE ET THORACIQUE	Médecine
BAGLIN Isabelle	CHIMIE THERAPEUTIQUE	Pharmacie

BASTIAT Guillaume	BIOPHYSIQUE ET BIOSTATISTIQUES	Pharmacie
BEAUVILLAIN Céline	IMMUNOLOGIE	Médecine
BEGUE Cyril	MEDECINE GENERALE	Médecine
BELIZNA Cristina	MEDECINE INTERNE	Médecine
BENOIT Jacqueline	PHARMACOLOGIE	Pharmacie
BERNARD Florian	ANATOMIE	Médecine
BESSAGUET Flavien	PHYSIOLOGIE PHARMACOLOGIE	Pharmacie
BLANCHET Odile	HEMATOLOGIE ; TRANSFUSION	Médecine
BOISARD Séverine	CHIMIE ANALYTIQUE	Pharmacie
BOUCHER Sophie	ORL	Médecine
BRIET Claire	ENDOCRINOLOGIE, DIABETE ET MALADIES METABOLIQUES	Médecine
BRILLAND Benoit	NEPHROLOGIE	Médecine
BRIS Céline	BIOCHIMIE ET BIOLOGIE MOLECULAIRE	Pharmacie
BRUGUIERE Antoine	PHARMACOGNOSIE	Pharmacie
CAPITAIN Olivier	CANCEROLOGIE ; RADIOTHERAPIE	Médecine
CHABRUN Floris	BIOCHIMIE ET BIOLOGIE MOLECULAIRE	Pharmacie
CHAO DE LA BARCA Juan-Manuel	BIOCHIMIE ET BIOLOGIE MOLECULAIRE	Médecine
CHOPIN Matthieu	MEDEECINE GENERALE	
CODRON Philippe	NEUROLOGIE	Médecine
DEMAS Josselin	SCIENCES DE LA READAPTATION	Médecine
DESHAYES Caroline	BACTERIOLOGIE VIROLOGIE	Pharmacie
DOUILLET Delphine	MEDECINE D'URGENCE	Médecine
FERRE Marc	BIOLOGIE MOLECULAIRE	Médecine
FORTRAT Jacques-Olivier	PHYSIOLOGIE	Médecine
GHALI Maria	MEDECINE GENERALE	Médecine
GUELFF Jessica	MEDECINE GENERALE	Médecine
HADJ MAHMOUD Dorra	IMMUNOLOGIE	Pharma
HAMEL Jean-François	BIOSTATISTIQUES, INFORMATIQUE MEDICALE	Médicale
HAMON Cédric	MEDECINE GENERALE	Médecine
HELESBEUX Jean-Jacques	CHIMIE ORGANIQUE	Pharmacie
HERIVAUX Anaïs	BIOTECHNOLOGIE	Pharmacie
HINDRE François	BIOPHYSIQUE	Médecine
JOUSSET-THULLIER Nathalie	MEDECINE LEGALE ET DROIT DE LA SANTE	Médecine
JUDALET-ILLAND Ghislaine	MEDECINE GENERALE	Médecine
KHIATI Salim	BIOCHIMIE ET BIOLOGIE MOLECULAIRE	Médecine
LEFEUVRE Caroline	BACTERIOLOGIE ; VIROLOGIE	Médecine
LEGEAY Samuel	PHARMACOCINETIQUE	Pharmacie
LEPELTIER Elise	CHIMIE GENERALE	Pharmacie
LETOURNEL Franck	BIOLOGIE CELLULAIRE	Médecine
MABILLEAU Guillaume	HISTOLOGIE, EMBRYOLOGIE ET CYTOGENETIQUE	Médecine
MALLET Sabine	CHIMIE ANALYTIQUE	Pharmacie
MAROT Agnès	PARASITOLOGIE ET MYCOLOGIE MEDICALE	Pharmacie
MESLIER Nicole	PHYSIOLOGIE	Médecine
MIOT Charline	IMMUNOLOGIE	Médecine
MOUILLIE Jean-Marc	PHILOSOPHIE	Médecine

NAIL BILLAUD Sandrine	IMMUNOLOGIE	Pharmacie
PAILHORIES Hélène	BACTERIOLOGIE-VIROLOGIE	Médecine
PAPON Xavier	ANATOMIE	Médecine
PASCO-PAPON Anne	RADIOLOGIE ET IMAGERIE MEDICALE	Médecine
PENCHAUD Anne-Laurence	SOCIOLOGIE	Médecine
PIHET Marc	PARASITOLOGIE ET MYCOLOGIE	Médecine
PIRAUX Arthur	OFFICINE	Pharmacie
POIROUX Laurent	SCIENCES INFIRMIERES	Médecine
RONY Louis	CHIRURGIE ORTHOPEDIQUE ET TRAUMATOLOGIQUE	Médecine
ROGER Emilie	PHARMACOTECHNIE	Pharmacie
SAVARY Camille	PHARMACOLOGIE-TOXICOLOGIE	Pharmacie
SCHMITT Françoise	CHIRURGIE INFANTILE	Médecine
SCHINKOWITZ Andréas	PHARMACOGNOSIE	Pharmacie
SPIESSER-ROBELET Laurence	PHARMACIE CLINIQUE ET EDUCATION THERAPEUTIQUE	Pharmacie
TEXIER-LEGENDRE Gaëlle	MEDECINE GENERALE	Médecine
VIAULT Guillaume	CHIMIE ORGANIQUE	Pharmacie

AUTRES ENSEIGNANTS

ATER		
BARAKAT Fatima	CHIMIE ANALYTIQUE	Pharmacie
ATCHADE Constantin	GALENIQUE	Pharmacie
PRCE		
AUTRET Erwan	ANGLAIS	Santé
BARBEROUSSE Michel	INFORMATIQUE	Santé
COYNE Ashley	ANGLAIS	Santé
O'SULLIVAN Kayleigh	ANGLAIS	Santé
RIVEAU Hélène	ANGLAIS	
PAST-MAST		
AUBRUCHET Hélène		
BEAUVAIS Vincent	OFFICINE	Pharmacie
BRAUD Cathie	OFFICINE	Pharmacie
CAVAILLON Pascal	PHARMACIE INDUSTRIELLE	Pharmacie
DILÉ Nathalie	OFFICINE	Pharmacie
GUILLET Anne-Françoise	PHARMACIE DEUST PREPARATEUR	Pharmacie
MOAL Frédéric	PHARMACIE CLINIQUE	Pharmacie
CHAMPAGNE Romain	MEECINE PHYSIQUE ET READAPTATION	Médecine
KAASSIS Mehdi	GASTRO-ENTEROLOGIE	Médecine
GUITTON Christophe	MEDECINE INTENSIVE-REANIMATION	Médecine
LAVIGNE Christian	MEDECINE INTERNE	Médecine
PICCOLI Giorgina	NEPHROLOGIE	Médecine

POMMIER Pascal	CANCEROLOGIE-RADIOTHERAPIE	Médecine
SAVARY Dominique	MEDECINE D'URGENCE	Médecine
PLP		
CHIKH Yamina	ECONOMIE-GESTION	Médecine

REMERCIEMENTS

A mon Président de jury,

Monsieur le Professeur Alain FURBER

Vous me faites l'honneur de présider cette thèse.
Je vous remercie pour l'enseignement et la formation dont j'ai pu bénéficier à vos côtés. Veuillez croire à l'expression de ma grande considération et de mon profond respect.

A mon directeur de thèse,

Monsieur le Professeur Loïc BIERE

Merci de m'avoir encouragée dès mes débuts. Tu as marqué mon internat par ta pédagogie, ta disponibilité et ton humour. Ton expertise en cardiologie a été source de motivation tout au long de mon parcours. Merci pour tes remarques pertinentes et pour ton aide dans l'écriture de cette thèse.

Aux membres du jury,

Monsieur le Professeur Fabrice PRUNIER

Vous me faites l'honneur de juger ce travail.
Je vous remercie pour votre accompagnement bienveillant pendant mes années d'internat ainsi que pour la qualité de vos enseignements qui ont enrichi ma formation. Recevez l'expression de ma gratitude et de mon respect sincères.

Monsieur le Docteur Sylvain GRALL

Tu me fais l'honneur de juger ce travail.
Tes enseignements, ta patience et ta bienveillance ont été précieux dès mes premières gardes et tout au long de ma formation. Je t'en suis très reconnaissante, sois assuré de ma profonde estime.

REMERCIEMENTS

A tous ceux ayant participé à ma formation médicale :

A Sophie, merci d'avoir guidé mes premiers pas en cardiologie et de m'avoir appris à travailler avec rigueur.
A Gabriel, pour ton humour et tes précieux conseils.
A Audrey, Antoine, Eloi, pour le plaisir d'avoir travaillé et progressé à vos côtés dans la bonne humeur. Merci pour tout ce que vous m'avez transmis.
A Alban, pour avoir été un chef hors pair aux soins et après. Merci pour ton implication et ta disponibilité, même pour mes questions les plus nulles, ainsi que pour tes innombrables relectures d'ETT.

Au Dr Abi Khalil, merci pour votre soutien, votre gentillesse et votre pédagogie.
Au Dr Rouleau, merci pour le partage de vos précieuses connaissances en échographie interventionnelle et pour votre bienveillance sans égal.
Aux Drs Bénard et Delépine, pour vos enseignements tout au long de ma formation.

A l'ensemble de **l'équipe de cardiologie de Laval**, pour votre dynamisme et votre accueil.

A l'équipe de réa B, pour m'avoir appris la réanimation avec patience et bienveillance.

A Théo et Solenn, merci pour vos conseils avisés tout au long de cette année et pour m'avoir donné les outils nécessaires pour réaliser ce travail. Merci pour votre gentillesse et votre réactivité.

A mes anciens et actuels co-internes : **Hélène**, **Pierre B** (merci pour tes bras), **Anicet** (la 5ème diva le temps d'une journée), **Garance, Grégoire R** (merci pour votre expertise en holterologie), **Tom**, **Grégoire LG** (pour avoir partagé ce premier semestre au rythme de tes chants bretons…), **Audrey** (et notre trinôme de totally spies), **Olivier, Quentin, Nicolas, Antoine S & M, Sarah**. Au plaisir de (re)travailler avec vous.

REMERCIEMENTS

A mes parents, merci pour votre amour inconditionnel et votre soutien indéfectible. C'est grâce à vous que j'ai pu m'épanouir et me réaliser. A **maman**, merci pour tes mots toujours justes et pour ta capacité à trouver la solution à tous mes problèmes. A **papa**, mon meilleur guide à ski, à vélo et dans la vie en général (et je dois l'admettre, souvent devant…). Vous êtes mes exemples de personnes et de médecins, et j'admire la façon dont vous avez su conjuguer vies personnelle et professionnelle. Ces lignes ne seront jamais assez pour vous dire à quel point je vous suis reconnaissante. Je vous aime.

A Blandine, mon premier modèle. J'ai grandi avec tes histoires d'interne des étoiles plein les yeux, et je crois qu'elles m'ont donné envie de suivre la même voie. Merci pour ta présence dans les moments difficiles. Je suis fière d'être ta sœur.
A Matthieu, pour ta gentillesse infinie,
A Armand, petit ninja et dresseur en herbe, je n'ai pas dit mon dernier mot au Stratego,
A Romane, je ne désespère pas d'occuper la même place dans ton cœur que Baptiiiiiste.

Le bonheur pour moi ce sont les moments passés à vos côtés. J'espère que les prochaines années seront plus calmes pour n'en manquer aucun.

A mes grands-parents et plus particulièrement à **papé**, pour m'avoir transmis le sens de la rigueur et le goût du travail bien fait. J'aurais aimé que tu sois là ce jour.

A Richard, Florence, Pascale, Philippe, Camille et **Charles**, merci pour votre gentillesse, votre hospitalité et pour tous les bons moments partagés ensemble, à Vins ou ailleurs.
Avec bien sûr une mention spéciale à **Clément** et aux soirées passées à regarder les étoiles à Vins. Désolée de t'avoir infligé ces spectacles de danse familiaux et merci d'y avoir pris part avec enthousiasme. Et à **Thomas**, le sang, merci d'ensoleiller les réunions de famille par ta bonne humeur et ta spontanéité, et merci pour ton humour que seuls quelques-uns savent vraiment apprécier… C'est toi la relève maintenant, j'espère que tu t'épanouiras pleinement dans cette voie et je te souhaite le meilleur.

A ma belle-famille, pour m'avoir si bien accueillie parmi vous, merci pour votre aide et votre générosité.

A mes amis,

A Anne, des petits chevaux chez nounou aux derniers kilomètres du semi… En passant par quelques soirées au Quinquin... Merci d'avoir toujours été là, avec cette énergie solaire que j'admire tant. Merci pour ton écoute attentive et tes précieux conseils. Je mesure la chance d'avoir une amie extraordinaire comme toi dans ma vie depuis 27 ans. J'espère de tout cœur qu'on va vieillir ensemble.

A Charlotte, on a évolué ensemble dans nos études, des TPE à l'ECN. Ces années lycée font partie des plus belles de ma vie, tu y as tenu et tu y tiens toujours une place essentielle.

A Bastien, **Benji**, et toute la team de Cherbourg. Vous avez ensoleillé mes week-ends et vacances à Cherbourg de cafés au Carré et de verres au Bayou. C'est toujours un vrai plaisir de se retrouver pour se remémorer les vieux souvenirs ou en créer de nouveaux.

REMERCIEMENTS

Aux miskines du désert : Anna, Anne-Emma, Audrey, Charlotte, Clem, Ella. Aux journées interminables à la BU et aux soirées rue Ec. Sans vous, ces études de médecine n'auraient pas eu la même saveur. J'espère que notre amitié perdurera, et qu'on continuera à se retrouver le temps d'un week-end ou d'une semaine au soleil. Et bien sûr à **Théo**, le mâle alpha du groupe.

Aux amis les plus dramas que j'ai, le noyau dur du noyau dur : **Victor**, pas très original mais merci infiniment pour tes innombrables services rendus, **Adèle**, pour tous nos points communs, **Alix**, pour ta gentillesse et ton humour hyperfun, **Dodo**, pour ta bonne humeur à toute épreuve, **Marie-Liesse**, pour ton grand cœur à toute épreuve, **Ivana**, notre maman à tous, **Julian**, pour toujours plus de macaqueries, **Manue,** je suis si heureuse de t'avoir dans ma vie, **Thomas**, pour ta bienveillance sans égal, **Taiana**, pour ton hospitalité et ta joie de vivre solaire, **Gaël**, mon maître à penser en matière d'hémodynamique, **Baptiste R**, pour les séances d'hyrox et surtout les restos post-hyrox, **Marine**, pour ta gentillesse infinie, et **Jérém**, on était partis sur un « bonne continuation » en 2021 mais a priori tu es toujours là…
Merci d'avoir été cette bouffée d'oxygène en 2ème semestre et de continuer à l'être. J'espère que l'avenir sera rempli de nouvelles vacances au ski ou au soleil, de derniers week-ends à Saint-Thibault, de verres au Constant, de kiffance à tue-tête et de tout autre type de moments partagés (ce paragraphe est trop long, il y a trop de monde dans ce groupe).
A **Céline** (nooon je ne t'ai pas oubliée, et je suis trèèès heureuse de t'avoir rencontrée).

A mes sœurs de la cardio, sans qui mon internat n'aurait pas été le même. A **Clem B**, merci infiniment pour ta présence dans les moments difficiles et merci d'avoir égayé mes journées au rythme de sucré-salé et des petits goûters. A **Vithika**, mon rayon de soleil aux explos, merci pour tes précieux conseils et ton écoute attentive, tes réels de petits chiots à n'en plus finir et tes goûts musicaux si proches des miens. A **Clem J**, pour ce semestre à la 70 passé ensemble, pour ta bonne humeur, ta solidarité et ton aide. Pendant un an, je suis allée au travail le sourire aux lèvres devant la perspective d'une journée à vos côtés. Je suis heureuse qu'on se soit trouvées.

A Nassim, pour avoir été mon premier (et meilleur) co-interne. Merci pour ta gentillesse, ta bienveillance et ton humour qui ont ensoleillé mes journées. Surtout, reste le même.
A Pierre H, merci d'avoir partagé avec moi ta base de données, ton amitié (je crois ?) et surtout tes connaissances en matière de pokémons.

A mes co-internes de réa, Marion (meilleure binôme), **Fouritos, Jurgen, Eric, Alex,** et **Max**. Merci pour ce semestre hors du temps riche en bluff et ratatouille, qui m'a presque fait hésiter à changer de bord. Grâce à vous j'ai appris que le corps humain s'étendait au-delà du médiastin.

A Elsa, Alex P, Alex U, Julien, merci pour cette année à Paris. Vous étiez des co-M2 en or et c'était un plaisir de travailler à vos côtés.

Le meilleur pour la fin, à Baptiste, mon meilleur ami, mon pilier, mon partenaire de toute aventure. Merci d'avoir toujours tout rendu si évident. Merci d'avoir accepté mon investissement professionnel sans jamais aucun reproche, d'avoir partagé les rires, les larmes et les craquages de ces années de médecine. Je n'aurais pu rêver mieux et j'espère le faire aussi bien que toi. Je suis tellement fière de toi et de la façon dont on évolue ensemble… « Pourquoi tombons-nous Monsieur ? » … Je t'aime et j'ai hâte de voir ce que les prochaines années nous réservent.

Liste des abréviations

ACS	Acute Coronary Syndrome
AF	Atrial fibrillation
b-SSFP	balanced Steady-State Free-Precession
CCTA	Coronary Computed Tomography Angiography
CMR	Cardiac Magnetic Resonance
CV	Chamber View
ESC	European Society of Cardiology
FLASH	Fast Low-Angle Shot
GLS	Global Longitudinal Strain
HDF	Hemodynamic Force
LGE	Late Gadolinium Enhancement
LV	Left Ventricle
LVEF	Left Ventricular Ejection Fraction
MACE	Major Adverse Cardiovascular Events
MOLLI	Modified Look-Locker Inversion Recovery
MINOCA	Myocardial Infarction with Non-Obstructive Coronary Arteries
PSIR	Phase-Sensitive Inversion Recovery
ROI	Region Of Interest
RVEF	Right Ventricular Ejection Fraction
TSE	Turbo Spin Echo

Plan

FORCES HEMODYNAMIQUES VENTRICULAIRES GAUCHES :

PRINCIPES ET CONTEXTE

La fonction ventriculaire gauche est classiquement appréciée par des paramètres robustes tels que la fraction d'éjection ou la déformation myocardique. Toutefois, ces marqueurs ne reflètent pas l'ensemble de la mécanique cardiaque : le flux sanguin intracavitaire en constitue un déterminant essentiel et son analyse par les forces hémodynamiques (HDFs) permet de détecter plus précocement des altérations mécaniques subtiles. Afin d'éclairer l'article qui suit, une introduction succincte au concept de forces hémodynamiques ventriculaires gauches est proposée ici.

Principes physiques de base

Il est utile de rappeler les **principes physiques** de force et de pression pour appréhender le mécanisme des forces hémodynamiques.

Une force se définit comme une grandeur vectorielle reflétant l'action mécanique exercée par un objet sur un autre. L'application d'une ou plusieurs forces peut entraîner le déplacement, l'accélération ou la déformation de l'objet soumis à cette action. Elle est mesurée en newtons (N), un newton correspondant à la force nécessaire pour donner une accélération de 1 m/s^2 à une masse de 1 kg (1 N = 1 $kg \cdot m/s^2$).

La pression correspond à la force qu'exerce un fluide par unité de surface. Son unité est le pascal (Pa), un pascal correspondant à 1 newton par mètre carré (1 Pa = 1 N/m^2).

Concepts généraux des forces hémodynamiques

Des **gradients de pression** se forment au sein des cavités cardiaques sous l'effet combiné de la contraction du myocarde, du jeu des valves et de l'interaction avec les vaisseaux. Au cours du cycle cardiaque, ces gradients se distribuent de manière hétérogène dans le cœur, générant une multitude de **forces motrices locales** qui dirigent le sang des zones à pression élevée vers celles à pression plus basse. **Les forces hémodynamiques** correspondent à la **résultante globale** de l'ensemble de ces forces locales, exprimée sous forme d'un vecteur unique à chaque instant du cycle cardiaque. Ce vecteur, orienté des zones à haute vers les zones à basse pression, traduit l'action mécanique globale du sang sur les parois, et détermine la direction de l'écoulement intracavitaire. En tant que vecteur, les forces hémodynamiques sont définies par leur **direction**, leur **sens** et leur **intensité**. Dans le ventricule gauche, elles s'exercent selon la **direction longitudinale**, correspondant à l'axe base-apex, et selon le **plan transversal**, correspondant aux directions antéro-inférieure et septo-latérale. La force longitudinale est non seulement la direction la plus efficiente pour le ventricule gauche, mais aussi celle dont la mesure est la plus reproductible et facilement détectable. Nous prendrons donc l'exemple de cette force par la suite pour expliquer leur mécanisme. Lorsque la composante longitudinale du vecteur est dirigée de l'apex vers la base du ventricule gauche (c'est-à-dire lorsque la pression apicale est supérieure à la pression basale), la force est définie comme positive. À l'inverse, lorsqu'il est dirigé de la base vers l'apex (pression basale supérieure à la pression apicale), la force est définie comme négative. Il est ainsi possible d'explorer tout au long du cycle la dynamique des forces via des courbes représentant les variations d'intensité et de sens du vecteur au fil du temps.

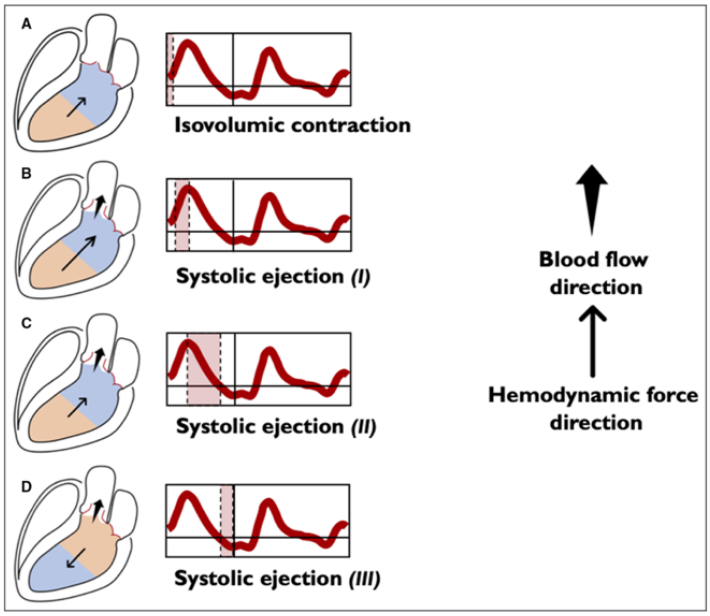

Figure A. Évolution de la composante longitudinale du vecteur de force hémodynamique ventriculaire gauche au cours de la systole (1).

La **Figure A** ci-dessus illustre l'évolution de la composante longitudinale du vecteur de force ventriculaire gauche au cours de la systole. Les gradients de pression sont illustrés entre une zone orange (pression élevée) et une zone bleue (pression basse), orientant à la fois le flux sanguin (flèche large) et la force hémodynamique (flèche fine) de la zone à haute vers la zone à basse pression.

Les quatre phases systoliques suivantes sont successivement représentées :

- Phase A – Contraction isovolumique

Cette phase débute à la fermeture de la valve mitrale et se termine à l'ouverture de la valve aortique. Sous l'effet de la contraction myocardique, un gradient de pression se forme de l'apex vers la base du ventricule gauche, générant une augmentation de la force longitudinale. Ce phénomène traduit une accélération initiale du flux sanguin en direction de la chambre de chasse avant même l'ouverture de la valve aortique. Durant cette période, les valves mitrale et aortique sont toutes deux fermées, empêchant tout flux entre les cavités et vaisseaux. La pression dans l'aorte reste alors supérieure à celle du ventricule gauche.

- Phase B – Début d'éjection systolique

Lorsque la pression intraventriculaire dépasse la pression aortique, la valve aortique s'ouvre

et l'éjection débute. La force longitudinale suit alors une phase ascendante positive jusqu'à atteindre un pic maximal, en lien avec le gradient de pression apex-base croissant.

- Phase C – Milieu d'éjection systolique

Après ce pic, la contraction ventriculaire se poursuit mais le gradient de pression diminue, traduisant une baisse de tension musculaire et une éjection déjà avancée du volume sanguin.

- **Phase D – Fin d'éjection systolique et inversion du gradient de pression**

En fin de systole, le gradient s'inverse avec une pression plus élevée à la base qu'à l'apex. Le flux se poursuit mais ralentit, en raison de la diminution progressive de la pression générée par le ventricule gauche et de l'augmentation concomitante de la pression aortique ; la force hémodynamique longitudinale devient alors négative, s'opposant au flux, jusqu'à la fermeture de la valve aortique et l'entrée en diastole.

La **Figure B** illustre la dynamique diastolique selon le même principe.

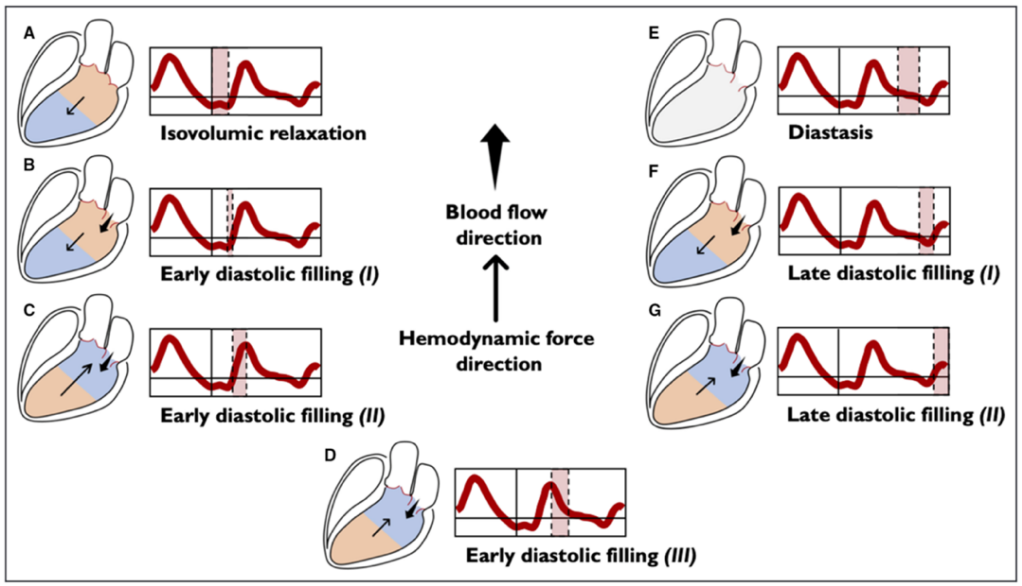

Figure B. Évolution de la composante longitudinale du vecteur de force hémodynamique ventriculaire gauche au cours de la diastole (1).

Les forces hémodynamiques sont normalisées par le volume ventriculaire, la densité du sang et l'accélération de la gravité afin d'obtenir une valeur sans dimension, exprimée en

pourcentage de poids statique du sang. Cette formulation facilite la définition de valeurs de référence et permet une comparaison directe entre patients.

Méthodes de mesure

La méthode de référence pour l'évaluation de l'hémodynamique intracardiaque reste la mesure invasive des pressions par cathétérisme. Parmi les alternatives non invasives, **l'IRM cardiaque de flux 4D** constitue actuellement la technique la plus fiable pour quantifier les forces hémodynamiques du ventricule gauche, car elle permet de mesurer la vitesse du sang dans les trois dimensions de l'espace et à chaque instant du cycle cardiaque. À partir de ces champs de vitesse mesurés, les gradients de pression intraventriculaires peuvent être estimés via l'équation de Navier-Stokes, qui relie les variations spatio-temporelles de la vitesse aux gradients de pression qui les génèrent. Leur intégration sur l'ensemble du volume ventriculaire gauche permet ensuite de calculer la force hémodynamique globale au cours du cycle cardiaque (**Figure C**).

Plus récemment, un modèle mathématique alternatif a permis d'estimer ces forces sans recourir à une mesure directe des vitesses intracavitaires. Cette méthode repose sur l'analyse du mouvement des parois endocardiques et la mesure des diamètres valvulaires mitral et aortique, à partir de **séquences ciné-IRM conventionnelles** acquises dans les plans long axe 2, 3 et 4 cavités. Un modèle 3D du ventricule gauche est alors reconstruit et suivi dynamiquement tout au long du cycle. La vitesse du sang est estimée de manière indirecte :

- **dans la cavité ventriculaire**, en supposant que la masse sanguine suit les déplacements de l'endocarde ;
- **au niveau des valves,** en appliquant le principe de conservation de la masse : le débit transvalvulaire est calculé à partir de la variation de volume ventriculaire entre deux

instants, puis est rapporté à la surface de l'orifice valvulaire pour en déduire la vitesse moyenne du flux.

Ces estimations permettent d'appliquer la forme intégrale de l'équation de Navier–Stokes sur la surface endocavitaire, afin de calculer à chaque instant les forces hémodynamiques globales exercées sur le sang (**Figure 3**). Cette méthode présente un intérêt particulier car elle repose sur des images de routine (ciné-IRM mais applicable également en échocardiographie) facilement accessibles, ouvrant la voie à une application clinique large et non invasive des HDFs.

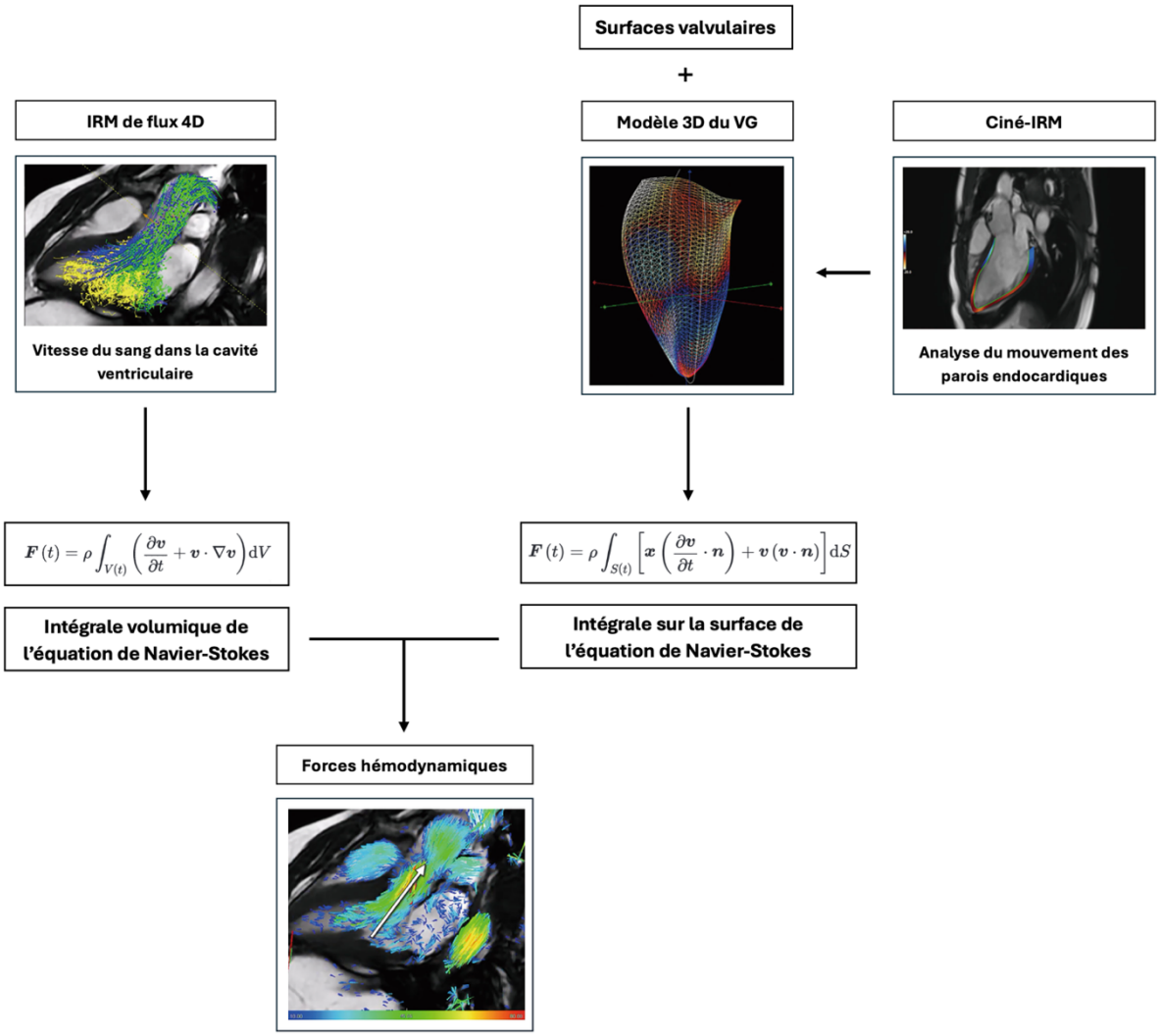

Figure C. Quantification des forces hémodynamiques par IRM 4D Flow ou à partir des séquences ciné-IRM. Avec : F(t) la force hémodynamique nette exercée sur le volume de sang à l'instant t, ρ la densité du sang. Pour l'intégrale volumique de l'équation de Navier-Stokes, v (x, t) représente le champ de vitesse du fluide à chaque point x à l'intérieur du volume ventriculaire gauche V(t) et à tout instant t. Pour l'intégrale sur la surface, v (x, t) représente la vitesse estimée du sang à chaque point x de la surface endocavitaire S(t) et à tout instant t. (2)

Paramètres quantitatifs des forces hémodynamiques

Les forces hémodynamiques sont analysées à partir de **courbes temporelles** décrivant, pour chaque direction, leurs variations de sens et d'intensité au fil du cycle cardiaque. Plusieurs paramètres quantitatifs peuvent en être extraits, moyennés sur l'ensemble du cycle, ou calculés spécifiquement pendant la systole ou la diastole. Une approche fréquente et utilisée dans l'article qui suit consiste à segmenter le cycle cardiaque en **quatre phases fonctionnelles**, s'appuyant sur le sens, positif ou négatif, de la force longitudinale du ventricule gauche (**Figure D**) :

- **Phase d'impulsion systolique** : correspondant à la contraction isovolumique et à l'éjection systolique précoce, jusqu'à négativation de la force longitudinale ;
- **Phase de transition systolo-diastolique** : couvrant toute la période liant la systole à la diastole et durant laquelle la force longitudinale reste négative ;
- **Phase de décélération diastolique** : correspondant à la fin de la diastole, caractérisée par une force longitudinale positive ;
- **Phase de systole atriale** : associée à la contraction de l'oreillette gauche et au remplissage ventriculaire final, avec une force longitudinale ventriculaire gauche se négativant.

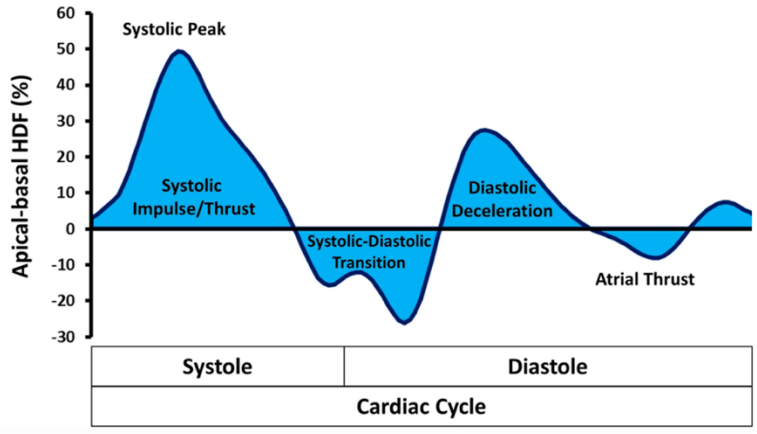

Figure D. Évolution de la force longitudinale ventriculaire gauche au cours du cycle cardiaque (3).

Les forces hémodynamiques peuvent être décrites selon deux dimensions complémentaires : leur **intensité** (amplitude) et leur **direction spatiale** (orientation) au sein du ventricule.

L'amplitude se quantifie de trois façons différentes :

- **Le pic de force** correspond à l'intensité maximale atteinte au cours d'une phase donnée, il reflète la capacité du cœur à générer un gradient de pression élevé (**Figure D**, *systolic peak, reflétant l'intensité maximale pendant la systole*).
- **La valeur quadratique moyenne** (ou *Root Mean Square, RMS*) représente la moyenne des intensités des forces sur une phase cardiaque, calculée en valeur absolue, sans distinction entre forces positives ou négatives.
- **La force moyenne,** correspond à l'aire sous la courbe rapportée à la durée d'une phase spécifique, en ne prenant en compte que les valeurs positives ou, au contraire, uniquement les valeurs négatives.

Les paramètres d'**orientation** sont au nombre de deux :

- **Le ratio de force** compare la composante transversale à la composante longitudinale du vecteur de force intraventriculaire, exprimant dans quelle mesure la force globale s'écarte de l'axe fonctionnel base–apex. Il peut être calculé sur l'ensemble du cycle ou sur des phases spécifiques.
- **L'angle de la force** correspond à l'orientation dominante du vecteur de force au sein du ventricule gauche, variant de 0° (orientation purement transversale) à 90° (orientation strictement longitudinale), et permet d'apprécier visuellement la direction des forces via un histogramme polaire (**Figure F**).

Des altérations de ces paramètres reflètent une hémodynamique cardiaque inefficace. Une amplitude réduite dans l'axe longitudinal témoigne d'une incapacité du ventricule gauche à générer une pression suffisante (**Figure E**), tandis qu'une orientation anormale (angle de force s'éloignant de 90° ou ratio élevé) suggère une déviation du flux sanguin par rapport à l'axe physiologique base-apex (**Figure F**). Ces anomalies sont associées à des phénomènes de remodelage ventriculaire défavorable ou de dysfonction systolique ou diastolique.

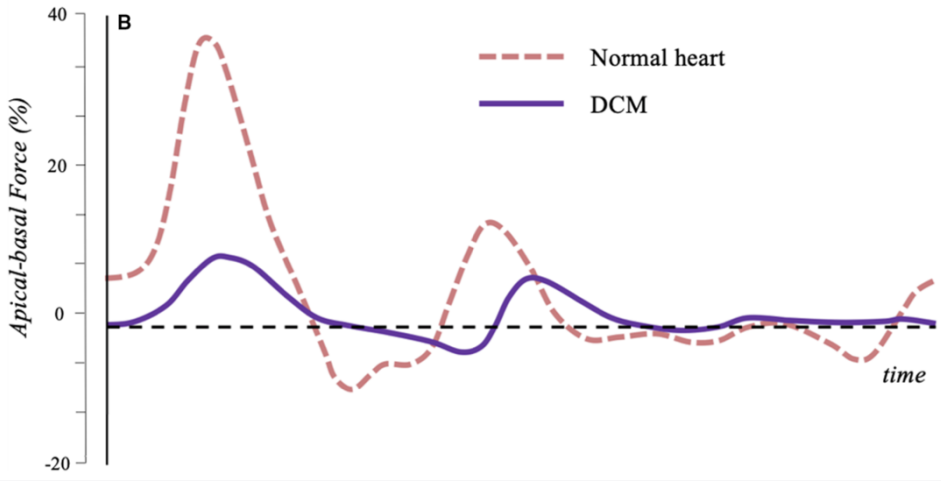

Figure E. Courbes des forces hémodynamiques longitudinales chez un patient sain (courbe rose) et chez un patient présentant une cardiomyopathie dilatée (courbe violette). Les paramètres d'amplitude sont altérés pour ce dernier, reflétant une dysfonction ventriculaire gauche (1).

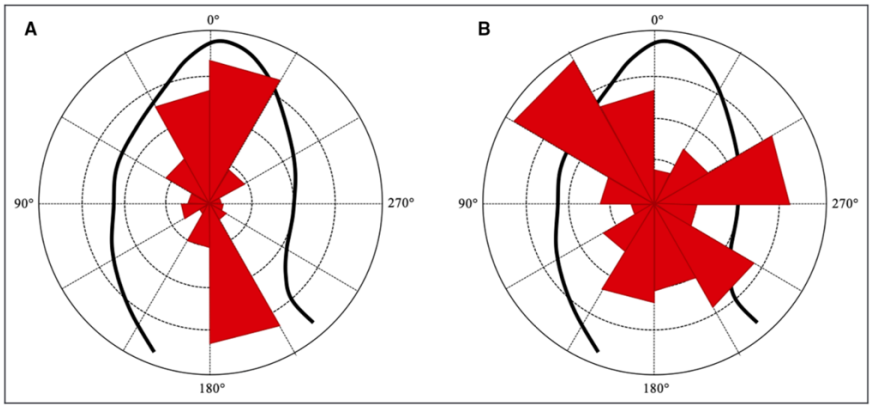

Figure F. Histogramme polaire pondéré par l'intensité des forces (1).
L'orientation et l'intensité des forces hémodynamiques intraventriculaires gauches sur l'ensemble du cycle cardiaque sont représentées par des triangles isocèles rouges.
A. Patient présentant des forces majoritairement orientées selon l'axe longitudinal.
B. Patient présentant des forces majoritairement orientées selon l'axe transversal.

ARTICLE

FROM CARDIAC MECHANICS TO PROGNOSIS: LEFT VENTRICLE HEMODYNAMIC FORCES AS A NOVEL RISK MARKER IN MINOCA

ABSTRACT

INTRODUCTION: Myocardial infarction with non-obstructive coronary arteries (MINOCA) is a heterogeneous entity associated with significant morbidity, where conventional cardiac magnetic resonance (CMR) risk markers may fail to capture risk. Hemodynamic forces (HDFs), derived from cine-CMR and reflecting flow–tissue interactions, detect subtle ventricular dysfunction. Their prognostic value in MINOCA remains unknown.

OBJECTIVE: To assess the prognostic value of specific HDFs parameters in consecutive patients with MINOCA.

METHODS: This retrospective single-centre study included patients admitted for MINOCA who underwent CMR at Angers University Hospital between 2014 and 2023. HDFs parameters were computed using dedicated post-processing software. The primary endpoint was a composite of major adverse cardiovascular events (MACE: all-cause death, stroke, or cardiovascular hospitalization). Cox regression models adjusted for clinical and CMR risk factors were used to evaluate the prognostic impact of HDFs, and incremental value was assessed using nested model comparisons.

RESULTS: During a median follow-up of 2.8 years (IQR 1.1- 5.2), 67 patients (19.1%) experienced MACE. In multivariable models adjusted for left ventricle ejection fraction, strain, late gadolinium enhancement extent, and final diagnosis, higher systolic peak force (HR per 1 SD increase: 0.54, p = 0.004) and longitudinal impulse force (HR per 1 SD increase: 0.58, p = 0.010) independently predicted improved outcomes, whereas an elevated transverse-to-longitudinal force ratio was linked with increased risk (HR per 1 SD increase: 1.31, p = 0.032). In a nested model analysis, each HDF parameter provided incremental prognostic value compared with a model including the previously cited factors; for systolic peak force, the global chi-square increased from 21 to 31 (p = 0.002) with improved reclassification.

CONCLUSION: Hemodynamic forces derived from cine-CMR independently predict adverse outcomes in MINOCA and provide incremental prognostic value beyond established clinical and CMR markers. They represent an easy-to-obtain, highly reproducible parameter that bridges cardiac pathophysiology with patient prognosis, supporting their potential as novel and clinically applicable tools for risk stratification in this population.

GRAPHICAL ABSTRACT

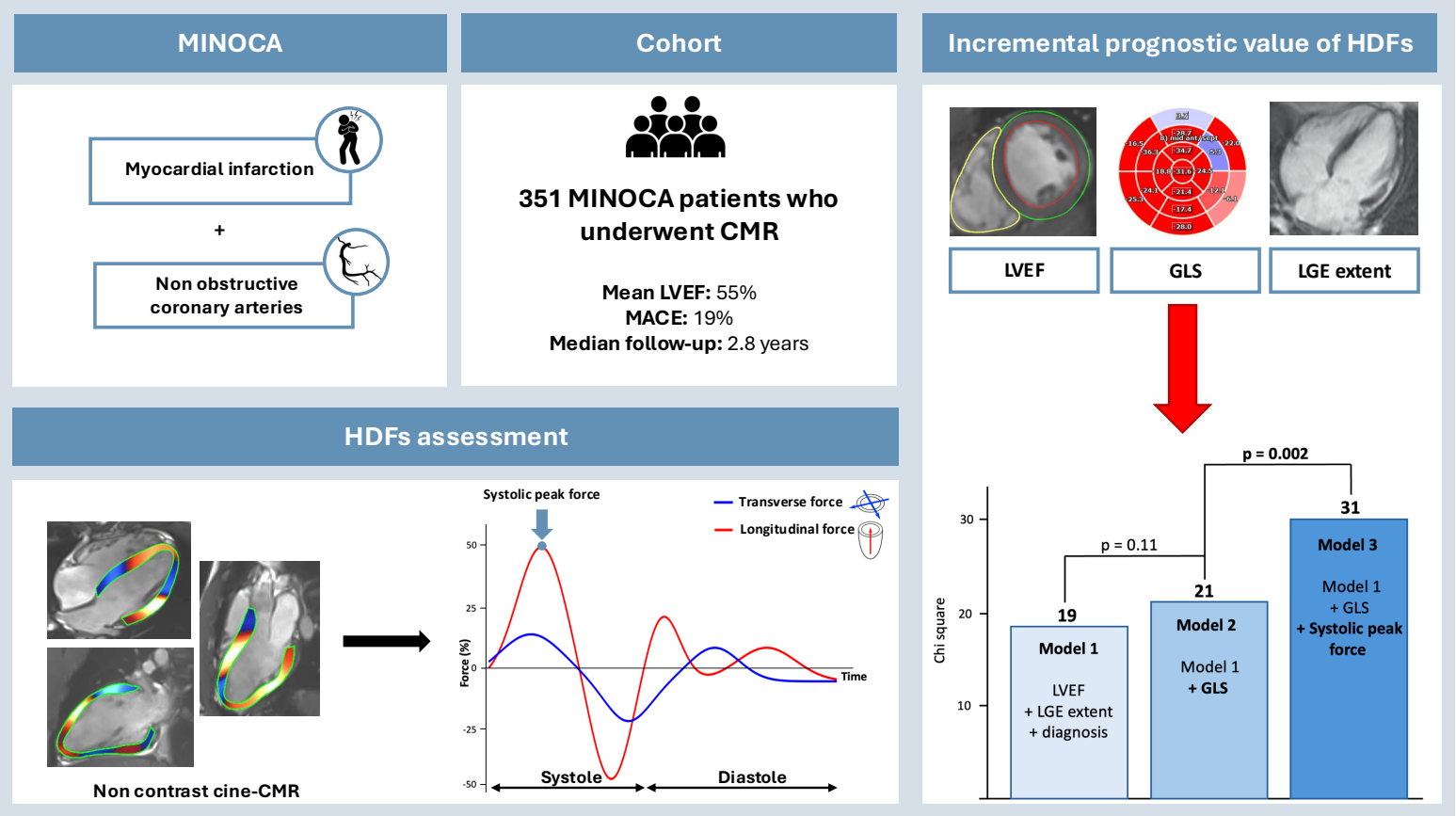

Abbreviations: CMR, cardiac magnetic resonance; GLS, global longitudinal strain; HDFs, hemodynamic forces; LGE, late gadolinium enhancement extent; LVEF, left ventricle ejection fraction; MACE, major adverse cardiovascular events; MINOCA, myocardial infarction with non-obstructive coronary arteries.

Keywords: cardiovascular magnetic resonance imaging; non-contrast CMR; hemodynamic forces; myocardial infarction with non-obstructive coronary arteries; cardiovascular events; outcomes.

INTRODUCTION

Between 1% and 14% of patients with acute coronary syndrome (ACS) have no significant coronary stenosis, an entity known as myocardial infarction with non-obstructive coronary arteries (MINOCA)(4). MINOCA is a heterogeneous working diagnosis that encompasses a broad spectrum of underlying pathophysiological mechanisms and thus aetiologies, including myocarditis, Takotsubo syndrome, and ischemic injury. Accurate identification of the underlying cause is crucial to ensure appropriate management, and cardiac magnetic resonance (CMR) plays a pivotal role in this diagnostic process due to its unique capacity for myocardial tissue characterization (5–8).

Although initially considered relatively benign due to the absence of obstructive coronary disease, MINOCA is now recognized as carrying a significant cardiovascular risk (9–14). Beyond its diagnostic role, CMR has provided several parameters with prognostic relevance across aetiologies, such as left ventricular ejection fraction (LVEF), pattern and extent of late gadolinium enhancement (LGE), and global longitudinal strain (GLS) (15–25). However, risk stratification in this heterogeneous population remains challenging, as these conventional markers can be taken at fault (26,27). Indeed, many patients present with only subtle myocardial involvement, such as mid-range or preserved LVEF and minimal or no LGE, yet remain at risk, highlighting the need for more advanced markers of ventricular function to refine prognostic stratification.

Hemodynamic forces (HDFs) analysis is an emerging contrast-free CMR technique derived from routine cine sequences. After semi-automatic contouring of the ventricular cavities, intraventricular pressure gradients are estimated throughout the cardiac cycle, allowing quantification of the forces that reflect dynamic interaction between the myocardium and intracavitary blood flow (1,28–31). In dilated cardiomyopathy, HDFs have shown incremental prognostic value beyond conventional CMR markers (32,33), while in heart failure with

preserved ejection fraction they have been reported as more sensitive than LVEF or GLS for detecting early systolic dysfunction (34). By capturing subtle disturbances in contraction–flow coupling that conventional indices may overlook, HDFs could provide a powerful tool to refine risk stratification in MINOCA, where their prognostic value has not yet been investigated.

The objective of this study was therefore to determine whether specific HDFs parameters are independently associated with the occurrence of major adverse cardiovascular events (MACE) in a consecutive cohort of patients presenting with MINOCA.

METHODS

Study Population

Between January 2014 and December 2023, we conducted a single-centre, longitudinal cohort study with retrospective enrolment of consecutive patients admitted to Angers University Hospital for MINOCA, who underwent contrast-enhanced CMR for etiological evaluation. Patients were eligible for inclusion if they met the diagnostic criteria proposed by the European Society of Cardiology (ESC) working group on MINOCA, namely: (i) clinical evidence of acute myocardial infarction with troponin elevation, (ii) no obstructive coronary artery disease on angiography, defined as <50% stenosis in any major epicardial vessel, and (iii) absence of an overt alternative explanation for the acute presentation (5,35). In selected cases where coronary angiography was not performed, a CMR obtained during the index hospitalization demonstrating a non-ischemic pattern of myocardial injury was considered sufficient to fulfil the MINOCA definition.

Patients with atrial fibrillation (AF) during CMR acquisition, suboptimal cine image quality,

missing three-chamber cine views, prosthetic mitral or aortic valves, or contraindications to CMR were excluded (**Method S1**). No patient had significant native mitral or aortic valve disease.

Baseline demographic, clinical, biological, and imaging data were collected from hospitalization records. All coronary angiograms were reviewed independently by an interventional cardiologist (AM). Final diagnoses were adjudicated by a Heart Team based on all available information, with a central role of CMR findings. Myocarditis was defined according to the modified Lake Louise criteria, requiring at least one marker of oedema and one marker of non-ischemic myocardial injury (36,37). Ischemic myocardial injury required a clinically compatible presentation with CMR excluding alternative causes and showing ischemic patterns such as wall motion abnormalities, subendocardial or transmural LGE. Takotsubo syndrome was defined by InterTAK criteria, requiring transient LV dysfunction due to stress-induced myocardial stunning (38) and typical CMR features were apical ballooning, oedema and absence of LGE. In selected cases, the presentation was consistent with an underlying cardiomyopathy, while in others CMR was normal and no definitive aetiology could be established at the time of the diagnosis work-up.

This study was conducted according to the Strengthening the Reporting of Observational Studies in Epidemiology (STROBE) reporting guidelines for cohort studies and was approved by the local ethics committee of our institution.

Patients Follow-up and Clinical Outcome

Clinical outcomes were defined according to standardized criteria and collected from hospital records and the French national death registry (INSEE) (39). The primary endpoint was a composite of MACE defined as all-cause death, stroke, and cardiovascular hospitalization (either acute heart failure, sustained ventricular tachycardia, symptomatic atrial fibrillation,

or initial disease recurrence). Follow-up started at the time of the index CMR and continued until the first MACE or the last available clinical contact, with patients censored at that point.

CMR Protocol

CMR was performed in a dedicated laboratory using a 3T scanner (MAGNETOM Skyra, Siemens Healthcare, Erlangen, Germany) with a 32-channel phased-array cardiovascular coil. Cine images were acquired using a segmented, retrospectively gated balanced steady-state free-precession (b-SSFP) sequence, including long-axis (2-, 3-, and 4-chamber) views and contiguous short-axis slices covering the left ventricle (LV) from base to apex. Additional tissue characterization included T2-weighted short tau inversion recovery (TSE) sequences and quantitative T1 and T2 mapping. T1 mapping was performed using a motion-corrected Modified Look-Locker inversion recovery (MOLLI) sequence, and T2 mapping with a motion-corrected fast low-angle shot (FLASH) sequence; both were acquired in three short-axis slices (basal, mid-ventricular, and apical) and one 4-chamber long-axis view.

First-pass perfusion imaging was also performed after the administration of a gadolinium-based contrast agent (Dotarem®, Guerbet, France, 0.1 mmol/kg), injected at a rate of 3–5 mL/s. Ten minutes later, late gadolinium enhancement imaging, combining magnitude and phase-sensitive inversion recovery (PSIR), was performed using a 2D segmented inversion-recovery gradient-echo sequence in the same planes as cine images.

CMR Image Analysis

All CMR examinations were reanalysed in a dedicated core laboratory using Medis software (Medis Suite, Leiden, Netherlands) by three independent cardiovascular imaging specialists (AB, LB, AL). Left and right ventricular end-diastolic and end-systolic volumes, ejection fraction, and LV mass at end-diastole were measured. Corresponding indexed values were calculated. Regional wall motion abnormalities were observed visually. T2-weighted

hyperintensity was visually evaluated. Native T1 and T2 values were obtained after manual delineation of a region of interest (ROI) larger than 1 cm^2, with careful exclusion of the endocavitary blood pool and epicardial fat. For each patient, remote T1 and T2 values were averaged, and maximum values were recorded. The presence of late gadolinium enhancement (LGE) was visually assessed using both magnitude and PSIR sequences and was only considered present if visible in at least two orthogonal planes. Corresponding cine CMR slices were systematically reviewed to avoid misinterpretation of ventricular trabeculations or epicardial fat as LGE. LGE location was then analyzed using the American Heart Association 17-segment model (40), and its distribution was classified as subendocardial, intramyocardial, subepicardial, or transmural.

Left Ventricle Hemodynamic Forces Analysis

LV hemodynamic forces were measured using the QStrain HDF module (Medis Suite, Leiden, Netherlands) by an independent observer (CB), blinded to clinical data and final diagnosis. They were derived from deformation imaging of the 2-, 3-, and 4-chamber views after feature tracking, and measurements of mitral valve width (averaged from the 2- and 4-chamber diameters) and aortic valve width (3-chamber diameter). To account for differences in LV size, HDFs were normalized to LV volume and blood density, and expressed as a percentage of gravitational acceleration. Forces were reported as percentages using the root mean square (RMS), considering absolute values irrespective of their positive or negative sign. A detailed description of the methodology is provided in **Supplementary data (Method S2)**. Three HDFs parameters, each reflecting a distinct physiological aspect, were selected: the systolic peak force, defined as the maximal instantaneous force developed during ventricular systole; the longitudinal impulse force, corresponding to the mean amplitude of the force directed from the apex to the base during early systolic ejection; and the transverse-to-longitudinal force ratio over the cardiac cycle, quantifying the relative

contribution of lateral versus longitudinal forces throughout the entire cycle (**Figure 1**). Greater alignment of forces along the longitudinal axis is considered to reflect more efficient left ventricular function, whereas a higher transverse-to-longitudinal ratio indicates relatively greater transverse forces, suggesting less effective ventricular mechanics.

Statistical methods

Baseline characteristics were summarized for the entire cohort and stratified by diagnosis and MACE. Quantitative variables were expressed as mean ± standard deviation and compared with Student's or Welch's t-tests, or with Wilcoxon rank-sum test for non-normal data. Categorical variables were reported as counts and percentages and compared using chi-square or Fisher's exact tests.

To assess interobserver variability, HDFs were remeasured by an independent blinded evaluator (NB) in a random sample of 35 patients (10% of the study population). Intraobserver variability was assessed in another random set of 35 patients, re-evaluated by the same observer (CB). Reliability was quantified using the intraclass correlation coefficient (ICC) with a two-way mixed-effects model for absolute agreement, and Bland–Altman analysis was used to determine mean bias and 95% limits of agreement.

Cumulative incidence of MACE was estimated with the Kaplan–Meier method and compared with log-rank tests, using stratification by the median value or the optimal cut-off derived from maximally selected rank statistics (MSRS). Univariable and multivariable associations were assessed with Cox proportional hazards models, expressed as hazard ratios (HR) with 95% confidence intervals (CI). The proportional hazards assumption was verified using Schoenfeld residuals, and Martingale residuals were examined to test nonlinearity of continuous variables. Two baseline multivariable Cox models were constructed: (i) a clinical model including age, sex, hypertension, and final diagnosis, and (ii) a CMR model including LVEF, global longitudinal strain, LGE extent, and final diagnosis. Because the diagnosis was

considered a major confounder, it was incorporated in both models. Each of the three previously described HDFs parameters were then separately added to these baseline models to assess its prognostic contribution. Incremental value of HDFs was quantified using likelihood ratio chi-square statistics, changes in Harrell's C-index, and reclassification indices (net reclassification improvement (NRI) and integrated discrimination improvement (IDI)). Annualized event rates were calculated as events per 100 patient-years.

An unsupervised clustering using the k-means method was performed and, by definition, relied exclusively on HDFs similarity patterns, independent of clinical outcomes and patient characteristics. Given the mathematical overlap between several HDFs measures, six non-redundant parameters were retained, each reflecting a distinct pathophysiological dimension: mean and systolic longitudinal forces, mean and systolic transverse forces, systolic peak force, ejection angle. The optimal number of clusters was determined using Silhouette, Davies–Bouldin, and Calinski–Harabasz indices, and survival differences between clusters were assessed with Cox analyses and Kaplan–Meier curves.

Statistical significance was defined as a two-sided p value <0.05. All analyses were performed with R software, version 4.5.1 (R Foundation for Statistical Computing, Vienna, Austria).

RESULTS

Study population

From the initial cohort of 423 consecutive patients hospitalized for MINOCA fulfilling the diagnostic criteria, 363 patients were eligible after exclusion. Of these, 351 patients completed clinical follow-up and constituted the final study cohort. Detailed flowchart of study patients is depicted in **Figure 2**. Baseline subject characteristics stratified by MACE are

presented in **Table 1**, CMR findings in **Table 2**, and baseline and CMR characteristics stratified by final diagnosis in **Supplementary Tables S1 and S2**, respectively.

The mean age of the cohort was 48.5 ± 20.0 years, and 63.5% were male. Cardiovascular risk factors included active smoking in 42.7%, hypertension in 26.8%, dyslipidaemia in 16.0%, and diabetes in 6.3%. LVEF was preserved on average (55.5 ± 10.0%), and mean RVEF was 50.2 ± 9.3%. LGE was present in 71.8% of patients, with a mean extent of 19.2 ± 13.8% of LV mass. Mean global longitudinal strain (GLS) was -19.4 ± 4.5%. Regarding final adjudicated diagnosis, acute myocarditis accounted for 49.0% of cases, ischemic myocardial injury for 21.7%, Takotsubo syndrome for 8.3%, cardiomyopathy for 7.7%, and diagnosis remained inconclusive in 13.4%.

Cardiovascular events

After a median follow-up of 2.8 years (IQR 1.1–5.2), 67 of the 351 patients (19.1%) experienced at least one MACE. Among these, 38 patients died (10.8%), 8 (2.3%) suffered a stroke, 24 (6.8%) required unplanned hospitalization for cardiovascular causes: 10 (2.8%) for recurrence of the initial disease, 7 (2.0%) for sustained ventricular tachycardia, 4 (1.1%) for heart failure, 3 (0.9%) for symptomatic atrial fibrillation.

Hemodynamic forces

In the overall population, mean systolic peak force was 49.1 ± 22.4%, mean longitudinal impulse force was 29.0 ± 13.1%, and the transverse-to-longitudinal force ratio over the entire cardiac cycle was 15.8 ± 5.7. The full distribution of all 15 HDFs parameters is provided in **Supplementary Table S3**. Interobserver reliability was excellent across all HDFs parameters, including systolic peak force (ICC: 0.92 [0.83-0.96]; $p < 0.001$), longitudinal impulse force (ICC: 0.92 [0.82-0.96]; $p < 0.001$), and the transverse-to-longitudinal force ratio (ICC: 0.90 [0.82-0.95]; $p < 0.001$). Comparable results were

observed for intraobserver reliability, with systolic peak force (ICC: 0.90 [0.70-0.96]; p < 0.001), longitudinal impulse force (ICC: 0.90 [0.73-0.95]; p <0.001), and the transverse-to-longitudinal force ratio (ICC: 0.81 [0.65-0.91]; p <0.001). Further details on agreement are shown **in Supplementary Appendix Figure S1 and Table S4.**

Univariable association of HDFs with MACE

In univariable Cox analysis, higher systolic peak (HR per 1 SD increase: 0.44, p <0.001) and longitudinal impulse forces (HR per 1 SD increase 0.47, p <0.001) were protective, whereas an increased transverse-to-longitudinal ratio predicted worse outcomes (HR per 1 SD increase 1.43, p <0.001) (**Table 3**). Kaplan–Meier analyses stratified by MSRS-derived cut-offs confirmed these associations: low systolic peak (≤23.7), low impulse longitudinal force (≤16.4), and high transverse to longitudinal ratio (>17.8) were all significantly linked to higher MACE rates (**Figure 3**). For comparison, the MSRS method was also applied to LVEF, yielding a cut-off of 53.4%. The corresponding Kaplan–Meier curve is shown in **Supplementary Figure S4**. Beyond these three main forces, several other HDFs parameters were also significantly associated with MACE (**Table S5**). Kaplan–Meier curves for all remaining HDFs parameters stratified by MSRS-derived cut-offs and by their median values, are shown in the **Supplementary Appendix** (**Figures S2 and S3**, respectively).

Incremental value of HDFs for prognostication

In the multivariable CMR model adjusted for LVEF, LGE extent, GLS and final diagnosis, all three HDFs parameters remained independent predictors (per 1 SD increase, systolic peak force: HR 0.54, p = 0.004; impulse longitudinal force: HR 0.58, p = 0.010; ratio transverse/longitudinal forces: HR 1.31, p = 0.032) (**Table 4**). In the clinical model adjusted for age, sex, hypertension and diagnosis, systolic peak force (HR 0.63, p = 0.024), impulse longitudinal force (HR 0.65, p = 0.031), and transverse-to-longitudinal ratio (HR 1.48, p <

0.001) were similarly associated per 1 SD increase (**Table 5**). A series of nested multivariable models indicated that the addition of GLS to the baseline model including final diagnosis, LVEF and LGE extent led to a modest but non-significant improvement in model performance (global chi-square 19 vs. 21, p = 0.11), with no significant gain in discrimination as reflected by the C-index, NRI, and IDI (**Figure 4**). In contrast, further extension of the model by incorporating systolic peak HDF improved prediction (global chi-square 31, p = 0.002), with corresponding significant gains in reclassification (NRI, IDI), although the increase in C-index did not reach statistical significance. Comparable nested analyses were also performed for longitudinal impulse force and the transverse-to-longitudinal force ratio, each showing a significant increase in global chi-square when added to the model (**Figures S5–S6**).

Clustering analysis of HDFs parameters

Unsupervised clustering of systolic peak force and 5 other HDFs parameters (described in Methods) identified two optimal groups, as supported by the Silhouette (0.37), Davies–Bouldin (1.05), and Calinski–Harabasz (238) indices, with 123 patients in Cluster 1 and 227 in Cluster 2. Detailed baseline, CMR, and HDFs characteristics by cluster are provided in **Supplementary Tables S6–S7**. In univariable analysis, patients in Cluster 1 had a significantly lower risk of MACE than those in Cluster 2 (HR 0.19, p < 0.001), with Kaplan–Meier curves confirming poorer event-free survival in Cluster 2 (log-rank p-value < 0.001, **Figure 5**). After adjustment, cluster allocation remained independently associated with outcomes: Cluster 1 was at lower risk in both the CMR model (HR 0.27, p = 0.004) and the clinical model (HR 0.40, p = 0.046) (**Tables 4 and 5**). Nested model comparisons further showed a significant chi-square improvement when including cluster allocation (**Figure S7**).

Event rates and hazard ratios across HDFs quartiles

Annualized MACE rates declined across systolic peak quartiles (9.6 to 1.7 per 100 patient-years; **Figure 6**). Cox regression showed a significant risk reduction in Q3 (HR 0.39, p = 0.007) and Q4 (HR 0.18, p < 0.001) compared with Q1, but not in Q2 (HR 0.65, p = 0.13). Comparable results were found for longitudinal impulse force, while the transverse-to-longitudinal force ratio showed a progressive increase across quartiles, as illustrated in **Supplementary Figures S9 and S10.**

Subgroup analyses

Subgroup analyses assessed the consistency of systolic peak HDF prognostic value (**Figure 7**). It was significantly protective in most subgroups, including preserved LVEF (≥50%), limited LGE (<35%), and myocarditis or inconclusive diagnosis. By contrast, no significant association was found in patients with reduced LVEF (<50%), extensive LGE (≥35%), or in those with ischemic injury, Takotsubo syndrome, or cardiomyopathy.

DISCUSSION

Hemodynamic forces derived from cine-CMR offer a simple, reproducible, and physiologically relevant marker that links left ventricle blood flow to prognosis in MINOCA. Their ability to capture risk beyond conventional CMR parameters makes them a valuable tool for improving patient stratification, particularly in a clinical context where these parameters often fail to capture the full spectrum of risk.

Hemodynamic forces as a novel functional marker

By quantifying intraventricular pressure gradients throughout the cardiac cycle, HDFs capture blood flow dynamics, thus providing a dynamic assessment of flow-tissue interactions that

conventional indices cannot. In practical terms, dedicated software analyses standard cine-CMR images by contouring the ventricular cavities, tracking wall motion, and incorporating valve geometry to estimate these pressure differences. The result is a set of force vectors describing how efficiently blood is propelled: in a healthy ventricle, forces are predominantly aligned along the longitudinal axis (apex-base), whereas a predominance of transverse over longitudinal forces reflects less efficient and potentially maladaptive mechanics. This pattern was consistent with our initial analysis of individual force components, and was further reinforced by the clustering approach, which identified a higher-risk phenotype characterized by lower longitudinal forces and an increased transverse-to-longitudinal ratio. This mechanistic dimension extends the existing paradigm of left ventricle function, as described by Vallelonga et Al. (1): following LVEF and strain, HDFs represent a new step in the noninvasive assessment of cardiac function, with the potential to reveal subtle mechanical abnormalities that remain undetected by conventional tools. Other biomechanical parameters have previously demonstrated prognostic significance, notably systolic wall stress (41), which reflects the load borne by the ventricular wall and is closely linked to adverse remodelling, a well-established driver of chamber dilation and poor outcomes (42). Conceptually, HDFs may be viewed as the intracavitary counterpart of wall stress: while wall stress quantifies forces exerted on the myocardium from outside-in, HDFs capture the pressure-driven forces acting within the cavity from inside-out. Both describe different facets of the same process, which, under pathological conditions, may lead to ventricular remodelling and ultimately governs prognosis.

Clinical implications

The strength of HDFs analysis lies not only in its mechanistic insight but also in its practical applicability. HDFs are derived from routine cine-CMR acquisitions, require no contrast agent,

and can be quantified within minutes using semi-automated software. This makes them highly accessible, even in patients with contraindications to gadolinium, and opens perspectives for broader use since similar approaches can also be applied to echocardiography (43). Importantly, HDFs retain prognostic value precisely in settings where conventional markers often fall short, unmasking a subset at risk, who would otherwise escape stratification and could benefit from more tailored management strategies. Whether HDFs are modifiable by therapeutic interventions, and whether such modifications translate into improved patient outcomes, are critical questions that future studies should address. In this context, HDFs could serve not only as an early and reproducible indicator of inefficient ventricular mechanics but also, potentially, as a dynamic target for personalized follow-up and treatment strategies in MINOCA. This hypothesis is supported by recent work from Fabiani et al., who showed that HDFs analysis predicts the response to sacubitril/valsartan in patients with heart failure with reduced ejection fraction, suggesting that hemodynamic forces may help guide therapeutic decision-making and optimize individualized care beyond traditional parameters (44).

Prognostic value across diagnostic subgroups

In our subgroup analyses, the prognostic value of HDFs was most pronounced in patients with subtle myocardial involvement, such as preserved LVEF, minimal LGE, myocarditis, or inconclusive aetiologies, which often correspond to a normal CMR at the time of hospitalization. This strengthens the observation that HDFs can reveal early mechanical dysfunction. In contrast, in patients with more overt myocardial injury, HDFs were not significantly associated with outcomes, although a protective trend was still observed with higher systolic peak forces. This apparent paradox may be partly explained by the limited statistical power in smaller subgroups, but also by a lack of variability in more advanced

disease: when ventricular mechanics are globally impaired, HDFs tend to be uniformly altered, reducing their ability to discriminate between patients. Conversely, in less severe forms of injury where conventional parameters are often uninformative, HDFs retain sufficient interindividual variability to identify high-risk patients.

Limitations and future directions

This study has some limitations. Its retrospective single-centre design and the exclusion of patients with atrial fibrillation or prosthetic valves limit generalizability, while the modest number of adverse events necessitated a broad composite endpoint and constrained multivariable modelling. Clustering analysis added little beyond simple dichotomization, underscoring the practical value of individual HDFs parameters, particularly systolic peak force, which is both physiologically intuitive and reproducible as it reflects the maximum force generated during the cardiac cycle. Finally, despite adjustment for the final diagnosis, the etiologic heterogeneity of MINOCA still complicates interpretation. Subgroup results differed across diagnostic categories but should be interpreted with caution. Validation in large, prospective multicentre cohorts with longer follow-up will be essential, both to confirm the consistency of these associations across different aetiologies and to evaluate the integration of HDFs with other imaging or circulating biomarkers.

CONCLUSION

Hemodynamic forces derived from standard cine-CMR represent a novel tool to characterize left ventricle contraction–flow coupling in MINOCA. They provide independent and incremental prognostic value beyond conventional clinical and CMR markers, supporting their

integration as complementary indices of ventricular function to refine risk stratification in this heterogeneous population.

REFERENCES

1. Vallelonga F, Airale L, Tonti G, Argulian E, Milan A, Narula J, et al. Introduction to Hemodynamic Forces Analysis: Moving Into the New Frontier of Cardiac Deformation Analysis. J Am Heart Assoc. 2021 Dec 21;10(24):e023417.

2. Hou Y, Zhou H, Li Y, Mao T, Luo J, Yang J. Hemodynamic Force Based on Cardiac Magnetic Resonance Imaging: State of the Art and Perspective. J Magn Reson Imaging. 2025 Mar;61(3):1033–47.

3. Lange T, Backhaus SJ, Schulz A, Evertz R, Schneider P, Kowallick JT, et al. Inter-study reproducibility of cardiovascular magnetic resonance-derived hemodynamic force assessments. Sci Rep. 2024 Jan 5;14(1):634.

4. Pasupathy S, Air T, Dreyer RP, Tavella R, Beltrame JF. Systematic Review of Patients Presenting With Suspected Myocardial Infarction and Nonobstructive Coronary Arteries. Circulation. 2015 Mar 10;131(10):861–70.

5. Agewall S, Beltrame JF, Reynolds HR, Niessner A, Rosano G, Caforio ALP, et al. ESC working group position paper on myocardial infarction with non-obstructive coronary arteries. Eur Heart J. 2016 Apr 28;ehw149.

6. Byrne RA, Rossello X, Coughlan JJ, Barbato E, Berry C, Chieffo A, et al. 2023 ESC Guidelines for the management of acute coronary syndromes. Eur Heart J. 2023 Oct 12;44(38):3720–826.

7. Dastidar AG, Rodrigues JCL, Johnson TW, De Garate E, Singhal P, Baritussio A, et al. Myocardial Infarction With Nonobstructed Coronary Arteries. JACC Cardiovasc Imaging. 2017 Oct;10(10):1204–6.

8. Reynolds HR, Maehara A, Kwong RY, Sedlak T, Saw J, Smilowitz NR, et al. Coronary Optical Coherence Tomography and Cardiac Magnetic Resonance Imaging to Determine Underlying Causes of Myocardial Infarction With Nonobstructive Coronary Arteries in Women. Circulation. 2021 Feb 16;143(7):624–40.

9. Pasupathy S, Air T, Dreyer RP, Tavella R, Beltrame JF. Systematic Review of Patients Presenting With Suspected Myocardial Infarction and Nonobstructive Coronary Arteries. Circulation. 2015 Mar 10;131(10):861–70.

10. Dreyer RP, Tavella R, Curtis JP, Wang Y, Pauspathy S, Messenger J, et al. Myocardial infarction with non-obstructive coronary arteries as compared with myocardial infarction and obstructive coronary disease: outcomes in a Medicare population. Eur Heart J. 2020 Feb 14;41(7):870–8.

11. Zeng M, Zhao C, Bao X, Liu M, He L, Xu Y, et al. Clinical Characteristics and Prognosis of MINOCA Caused by Atherosclerotic and Nonatherosclerotic Mechanisms Assessed by OCT. JACC Cardiovasc Imaging. 2023 Apr;16(4):521–32.

12. Gasior P, Desperak A, Gierlotka M, Milewski K, Wita K, Kalarus Z, et al. Clinical Characteristics, Treatments, and Outcomes of Patients with Myocardial Infarction with Non-Obstructive Coronary Arteries (MINOCA): Results from a Multicenter National Registry. J Clin Med. 2020 Aug 27;9(9):2779.

13. Pizzi C, Xhyheri B, Costa GM, Faustino M, Flacco ME, Gualano MR, et al. Nonobstructive Versus Obstructive Coronary Artery Disease in Acute Coronary Syndrome: A Meta-Analysis. J Am Heart Assoc. 2016 Dec;5(12):e004185.

14. Juan-Salvadores P, Jiménez Díaz VA, Rodríguez González De Araujo A, Iglesia Carreño C, Guitián González A, Veiga Garcia C, et al. Clinical Features and Long-Term Outcomes in Very Young Patients with Myocardial Infarction with Non-Obstructive Coronary Arteries. Bil J, editor. J Intervent Cardiol. 2022 July 30;2022:1–7.

15. Konst RE, Parker M, Bhatti L, Kaolawanich Y, Alenezi F, Elias-Smale SE, et al. Prognostic Value of Cardiac Magnetic Resonance Imaging in Patients With a Working Diagnosis of MINOCA—An Outcome Study With up to 10 Years of Follow-Up. Circ Cardiovasc Imaging [Internet]. 2023 Aug [cited 2025 Aug 21];16(8).

16. Bucciarelli V, Bianco F, Francesco AD, Vitulli P, Biasi A, Primavera M, et al. Characteristics and Prognosis of a Contemporary Cohort with Myocardial Infarction with Non-Obstructed Coronary Arteries (MINOCA) Presenting Different Patterns of Late Gadolinium Enhancements in Cardiac Magnetic Resonance Imaging. J Clin Med. 2023 Mar 15;12(6):2266.

17. Bergamaschi L, Foà A, Paolisso P, Renzulli M, Angeli F, Fabrizio M, et al. Prognostic Role of Early Cardiac Magnetic Resonance in Myocardial Infarction With Nonobstructive Coronary Arteries. JACC Cardiovasc Imaging. 2024 Feb;17(2):149–61.

18. Chen L, Qiu B, Abdu FA, Liu L, Zhang W, Wang C, et al. Prognostic Value of Strain by Tissue Tracking Cardiac Magnetic Resonance in Myocardial Infarction With Nonobstructive Coronary Arteries. J Am Heart Assoc. 2025 Apr 15;14(8):e039395.

19. Anzini M, Merlo M, Sabbadini G, Barbati G, Finocchiaro G, Pinamonti B, et al. Long-Term Evolution and Prognostic Stratification of Biopsy-Proven Active Myocarditis. Circulation. 2013 Nov 26;128(22):2384–94.

20. Grün S, Schumm J, Greulich S, Wagner A, Schneider S, Bruder O, et al. Long-Term Follow-Up of Biopsy-Proven Viral Myocarditis. J Am Coll Cardiol. 2012 May;59(18):1604–15.

21. Gräni C, Eichhorn C, Bière L, Murthy VL, Agarwal V, Kaneko K, et al. Prognostic Value of Cardiac Magnetic Resonance Tissue Characterization in Risk Stratifying Patients With Suspected Myocarditis. J Am Coll Cardiol. 2017 Oct;70(16):1964–76.

22. Fischer K, Obrist SJ, Erne SA, Stark AW, Marggraf M, Kaneko K, et al. Feature Tracking Myocardial Strain Incrementally Improves Prognostication in Myocarditis Beyond Traditional CMR Imaging Features. JACC Cardiovasc Imaging. 2020 Sept;13(9):1891–901.

23. Zghyer F, Botheju WSP, Kiss JE, Michos ED, Corretti MC, Mukherjee M, et al. Cardiovascular Imaging in Stress Cardiomyopathy (Takotsubo Syndrome). Front Cardiovasc Med. 2022 Jan 28;8:799031.

24. Naruse Y, Sato A, Kasahara K, Makino K, Sano M, Takeuchi Y, et al. The clinical impact of late gadolinium enhancement in Takotsubo cardiomyopathy: serial analysis of cardiovascular magnetic resonance images. J Cardiovasc Magn Reson. 2011 Jan;13(1):67.

25. Stiermaier T, Busch K, Lange T, Pätz T, Meusel M, Backhaus SJ, et al. Prognostic Value of Different CMR-Based Techniques to Assess Left Ventricular Myocardial Strain in Takotsubo Syndrome. J Clin Med. 2020 Nov 29;9(12):3882.

26. Sanguineti F, Garot P, Mana M, O'h-Ici D, Hovasse T, Unterseeh T, et al. Cardiovascular magnetic resonance predictors of clinical outcome in patients with suspected acute myocarditis. J Cardiovasc Magn Reson. 2015 Jan;17(1):78.

27. Vicente-Ibarra N, Feliu E, Bertomeu-Martínez V, Cano-Vivar P, Carrillo-Sáez P, Morillas P, et al. Role of cardiovascular magnetic resonance in the prognosis of patients with myocardial infarction with non-obstructive coronary arteries. J Cardiovasc Magn Reson. 2021 Mar;23(1):83.

28. Thompson RB, McVeigh ER. Fast measurement of intracardiac pressure differences with 2D breath-hold phase-contrast MRI. Magn Reson Med. 2003 June;49(6):1056–66.

29. Yang G, Kilner PJ, Wood NB, Underwood SR, Firmin DN. Computation of flow pressure fields from magnetic resonance velocity mapping. Magn Reson Med. 1996 Oct;36(4):520–6.

30. Pedrizzetti G, Tanacli R, Lapinskas T, Zovatto L, Pieske B, Tonti G, et al. Integration between volumetric change and strain for describing the global mechanical function of the left ventricle. Med Eng Phys. 2019 Dec;74:65–72.

31. Eriksson J, Bolger AF, Ebbers T, Carlhäll CJ. Assessment of left ventricular hemodynamic forces in healthy subjects and patients with dilated cardiomyopathy using 4D flow MRI. Physiol Rep. 2016 Feb;4(3):e12685.

32. Airale L, Giustiniani A, Ródenas-Alesina E, Lozano-Torres J, Escribano-Escribano P, Vila-Olives R, et al. Unsupervised clustering of intra-ventricular haemodynamic forces for the phenotyping of left ventricular function in non-ischaemic left ventricular cardiomyopathy. Eur Heart J - Cardiovasc Imaging. 2025 Mar 27;26(4):630–9.

33. Vos JL, Raafs AG, Henkens MTHM, Pedrizzetti G, Van Deursen CJ, Rodwell L, et al. CMR-derived left ventricular intraventricular pressure gradients identify different patterns associated with prognosis in dilated cardiomyopathy. Eur Heart J - Cardiovasc Imaging. 2023 Aug 23;24(9):1231–40.

34. Lapinskas T, Pedrizzetti G, Stoiber L, Düngen HD, Edelmann F, Pieske B, et al. The Intraventricular Hemodynamic Forces Estimated Using Routine CMR Cine Images. JACC Cardiovasc Imaging. 2019 Feb;12(2):377–9.

35. Thygesen K, Alpert JS, Jaffe AS, Chaitman BR, Bax JJ, Morrow DA, et al. Fourth universal definition of myocardial infarction (2018). Eur Heart J. 2019 Jan 14;40(3):237–69.

36. Friedrich MG, Sechtem U, Schulz-Menger J, Holmvang G, Alakija P, Cooper LT, et al. Cardiovascular Magnetic Resonance in Myocarditis: A JACC White Paper. J Am Coll Cardiol. 2009 Apr;53(17):1475–87.

37. Ferreira VM, Schulz-Menger J, Holmvang G, Kramer CM, Carbone I, Sechtem U, et al. Cardiovascular Magnetic Resonance in Nonischemic Myocardial Inflammation. J Am Coll Cardiol. 2018 Dec;72(24):3158–76.

38. Ghadri JR, Wittstein IS, Prasad A, Sharkey S, Dote K, Akashi YJ, et al. International Expert Consensus Document on Takotsubo Syndrome (Part I): Clinical Characteristics, Diagnostic Criteria, and Pathophysiology. Eur Heart J. 2018 June 7;39(22):2032–46.

39. Hicks KA, Tcheng JE, Bozkurt B, Chaitman BR, Cutlip DE, Farb A, et al. 2014 ACC/AHA Key Data Elements and Definitions for Cardiovascular Endpoint Events in Clinical Trials. J Am Coll Cardiol. 2015 July;66(4):403–69.

40. American Heart Association Writing Group on Myocardial Segmentation and Registration for Cardiac Imaging:, Cerqueira MD, Weissman NJ, Dilsizian V, Jacobs AK, Kaul S, et al. Standardized Myocardial Segmentation and Nomenclature for Tomographic Imaging of the Heart: A Statement

for Healthcare Professionals From the Cardiac Imaging Committee of the Council on Clinical Cardiology of the American Heart Association. Circulation. 2002 Jan 29;105(4):539–42.

41. Clerfond G, Bière L, Mateus V, Grall S, Willoteaux S, Prunier F, et al. End-systolic wall stress predicts post-discharge heart failure after acute myocardial infarction. Arch Cardiovasc Dis. 2015 May;108(5):310–20.

42. Cohn JN, Ferrari R, Sharpe N. Cardiac remodeling—concepts and clinical implications: a consensus paper from an international forum on cardiac remodeling. J Am Coll Cardiol. 2000 Mar;35(3):569–82.

43. Laenens D, Van Der Bijl P, Stassen J, Rossi AC, Pedrizzetti G, Reiber JHC, et al. Introduction to hemodynamic forces by echocardiography. Int J Cardiol. 2023 Jan;370:442–4.

44. Fabiani I, Pugliese NR, Pedrizzetti G, Tonti G, Castiglione V, Chubuchny V, et al. Haemodynamic forces predicting remodelling and outcome in patients with heart failure treated with sacubitril/valsartan. ESC Heart Fail. 2023 Oct;10(5):2927–38.

LISTE DES FIGURES

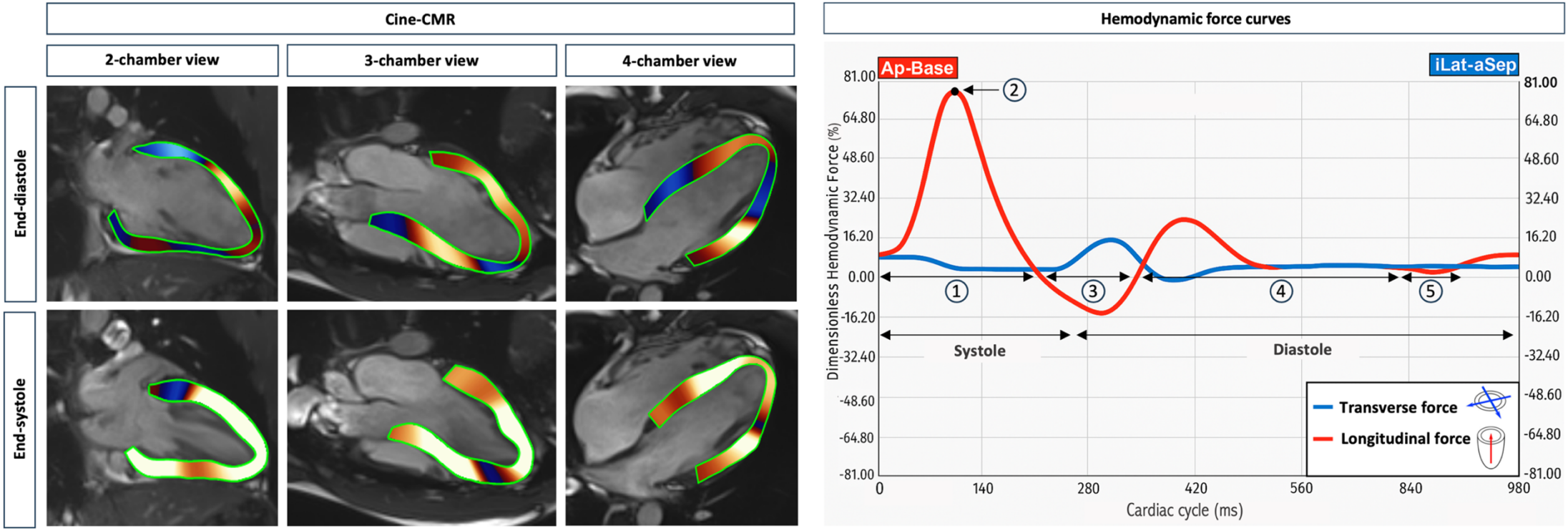

Figure 1. Endocardial and epicardial contouring in 2-, 3- and 4- chamber views at end-diastole and end-systole with the corresponding longitudinal (red) and transverse (blue) hemodynamic force curves.

Phases of the cardiac cycle are numbered as follows: 1: systolic impulse; 2: systolic peak; 3: systolic–diastolic transition; 4: diastolic deceleration; 5: atrial thrust.

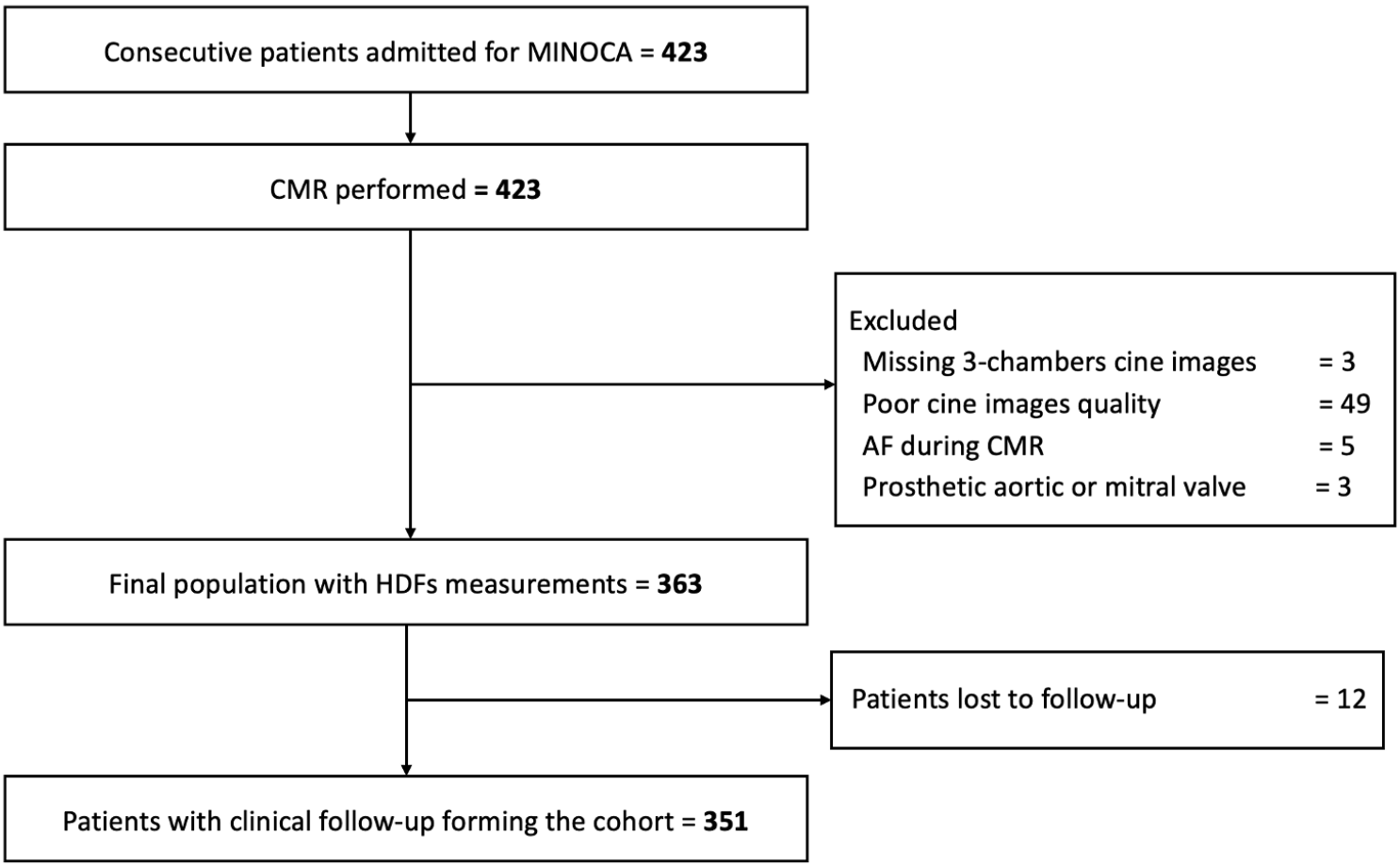

Figure 2. Study flowchart.
AF, atrial fibrillation; CMR, cardiovascular magnetic resonance; HDFs, hemodynamic forces; MINOCA, myocardial infarction with non-obstructive coronary arteries

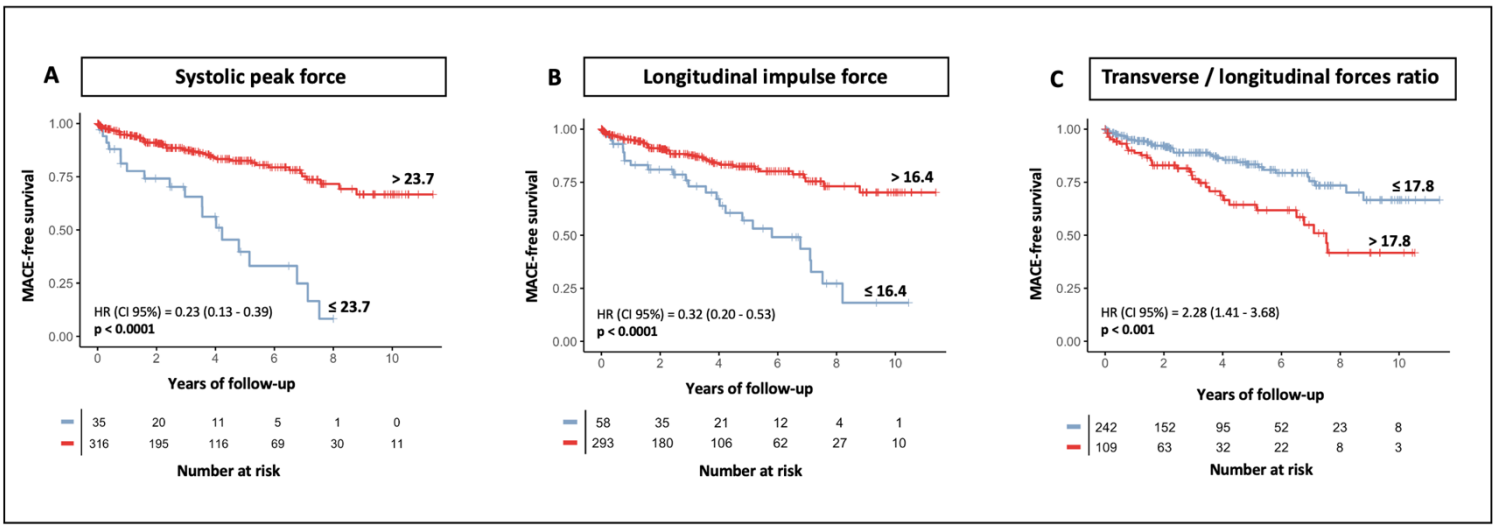

Figure 3. Kaplan–Meier curves of MACE-free survival by hemodynamic forces.
Hazard ratios (HR) and 95% confidence intervals (CI) were derived from Cox regression models, while p-values correspond to log-rank tests.

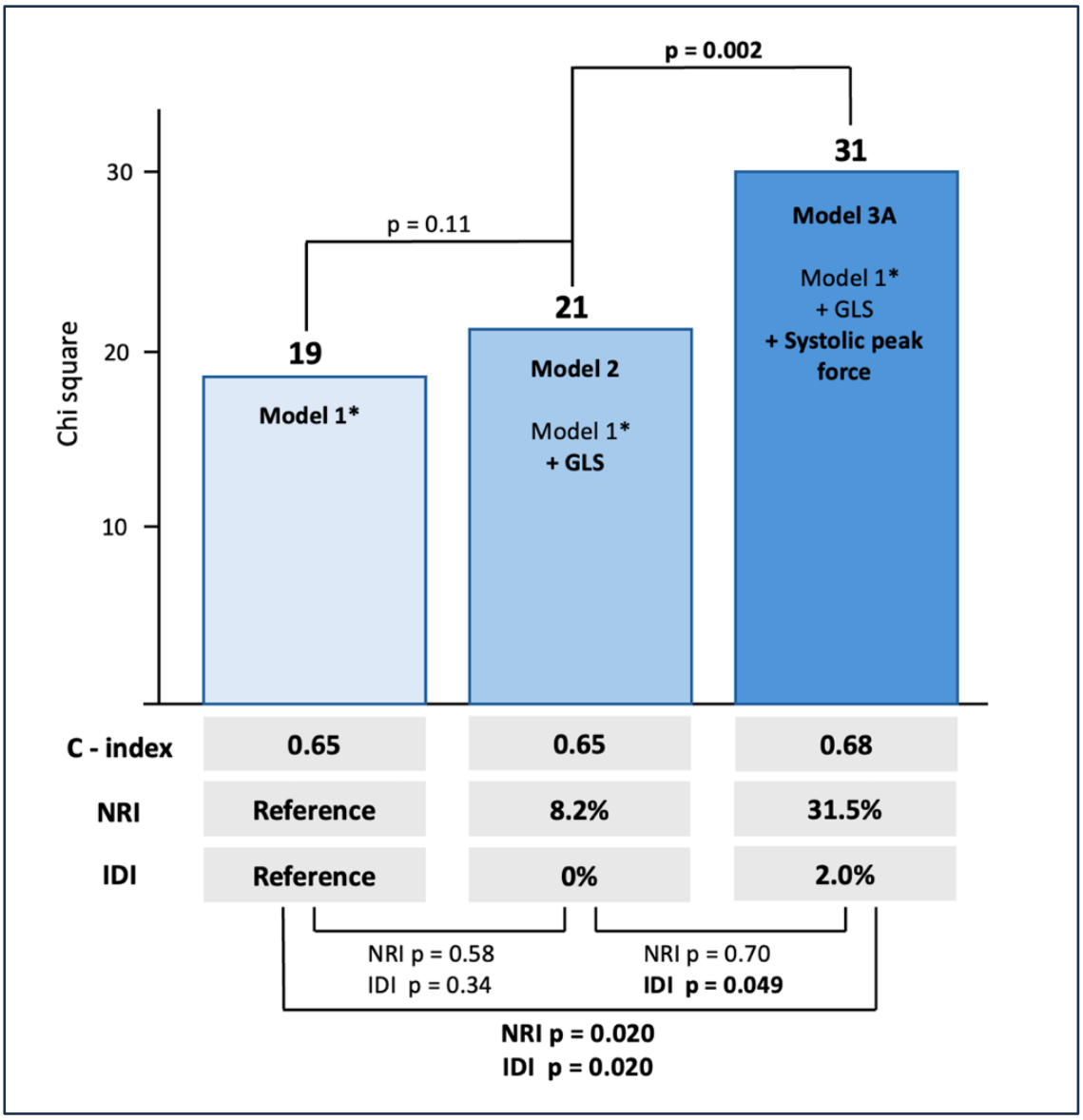

Figure 4. Incremental prognostic value of systolic peak force.
The model 3A is a nested model comprising the model 1 (final diagnosis and traditional CMR prognosticators: LVEF, LGE extent), the model 2 with GLS, and systolic peak force. **Bold** values indicate the 2-tailed p-value reached statistical significance (<0.05).

Abbreviations: CMR, cardiac magnetic resonance; GLS, global longitudinal strain; IDI, integrative discrimination index; LGE, late gadolinium enhancement; LVEF, left ventricle ejection fraction; MINOCA, myocardial infarction with non-obstructive coronary arteries; NRI, net reclassification improvement.

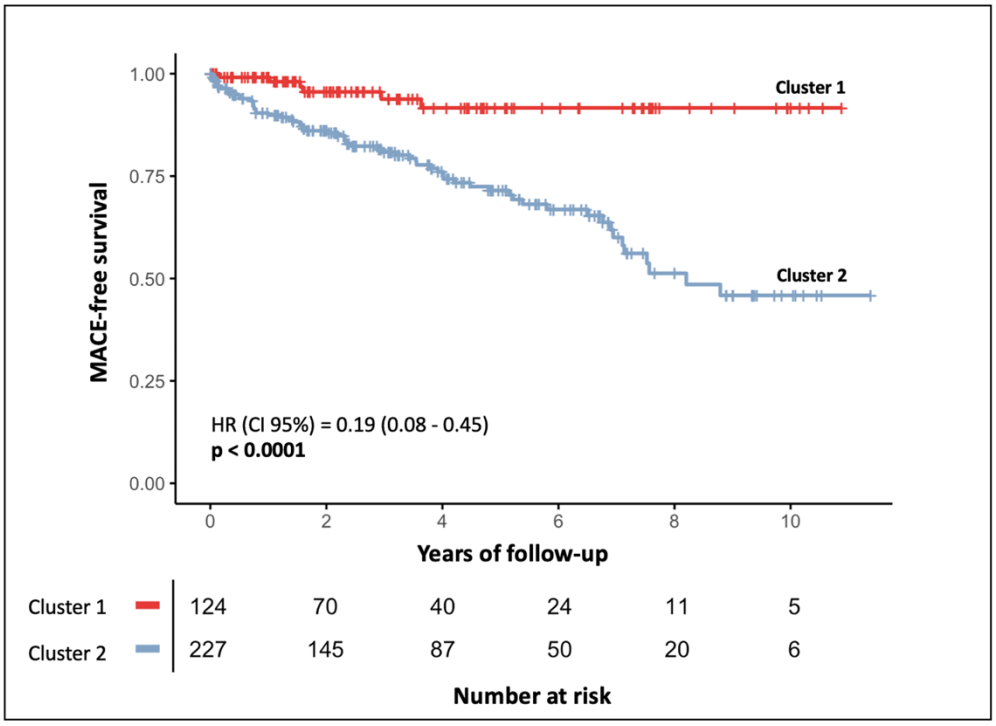

Figure 5. Kaplan–Meier curves of MACE-free survival according to HDF-based clusters.
Hazard ratio (HR) and 95% confidence interval (CI) are derived from Cox regression model, while p-value corresponds to log-rank test.

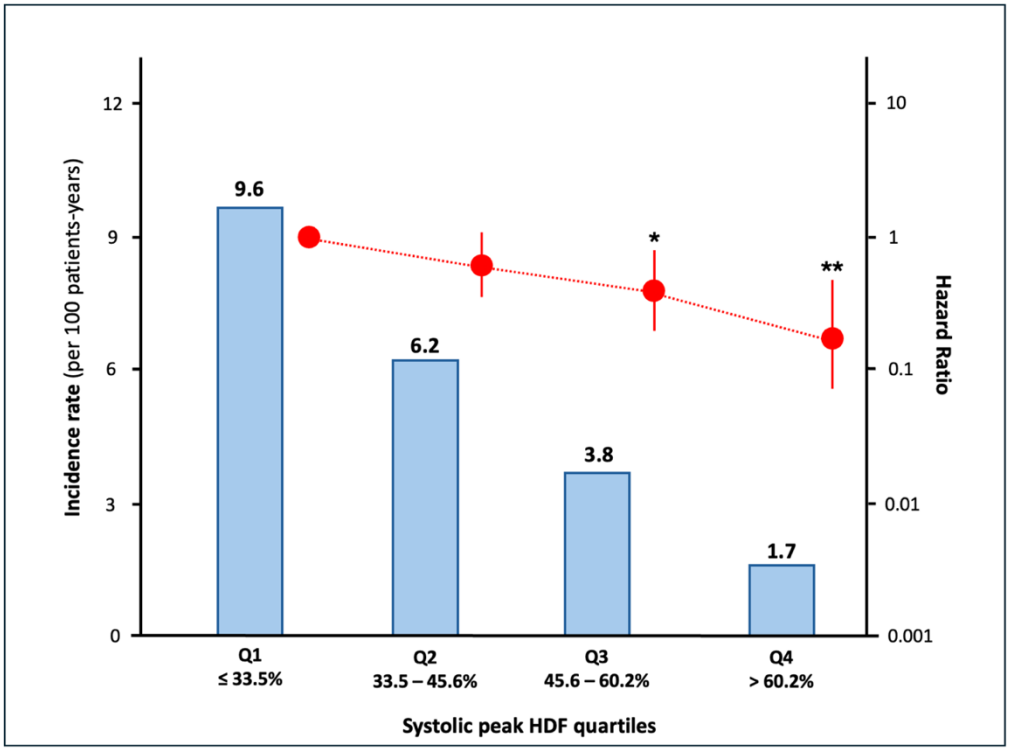

Figure 6. Incidence rate and hazard ratio per systolic peak HDF quartiles.
Hazard ratios (dots) with 95% confidence intervals (whiskers) for MACE according to quartiles of systolic peak force (logarithmic scale, reference: Q1). Annualized incidence rates per 100 patient-years are shown as blue bars. Significant reductions in event rates were observed in Q3 and Q4 compared with Q1 (*p = 0.007, **p < 0.001).

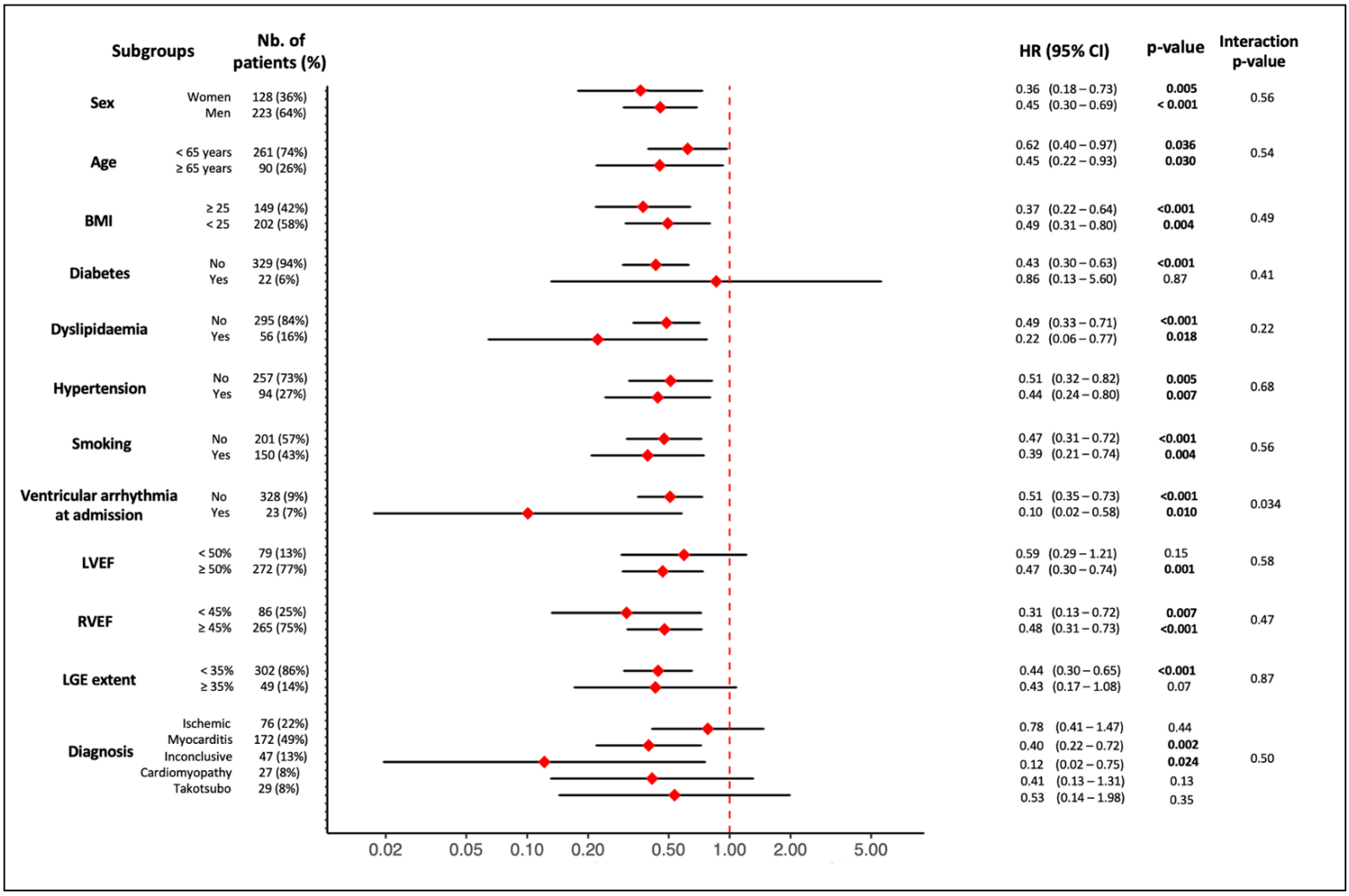

Figure 7. Subgroup analysis of the prognostic value of systolic peak force.

Univariate Cox analysis per 1 standard deviation increase; forest-plot with unadjusted hazard ratio (red squares) and 95% confidence interval (horizontal lines) of MACE.

Abbreviations: BMI, body mass index; CI, confidence interval; HR, hazard ratio; LGE, late gadolinium enhancement; LVEF, left ventricular ejection fraction; and RVEF, right ventricular ejection fraction.

LISTE DES TABLES

Table 1. Baseline characteristics of patients with and without MACE (N=351).

	All patients (N = 351)	**MACE** (N = 67)	**No MACE** (N = 284)	**p-value**
Age, years	48.5 ± 20.0	63.9 ± 18.3	44.9 ± 18.7	**<0.001**
Males, n (%)	223 (63.5%)	42 (62.7%)	181 (63.7%)	0.98
BMI, kg/m^2	25.2 ± 5.2	25.7 ± 5.0	25.1 ± 5.2	0.44
Coronary risk factors, n (%)				
Current or previous smoking	150 (42.7%)	23 (34.3%)	127 (44.7%)	0.16
Hypertension	94 (26.8%)	36 (53.7%)	58 (20.4%)	**<0.001**
Dyslipidemia	56 (16.0%)	16 (23.9%)	40 (14.1%)	0.07
Diabetes	22 (6.3%)	7 (10.4%)	15 (5.3%)	0.16
Admission presentation, n (%)				
Chest pain	291 (82.9%)	42 (62.7%)	249 (87.7%)	**<0.001**
Dyspnea (NYHA III/IV)	22 (6.3%)	9 (13.4%)	13 (4.6%)	**0.020**
Cardiac arrest	9 (2.6%)	2 (3.0%)	7 (2.5%)	0.68
Syncope/ Malaise	9 (2.6%)	3 (4.5%)	6 (2.1%)	0.38
Palpitations	3 (0.9%)	2 (3.0%)	1 (0.4%)	0.09
Cardiogenic shock	2 (0.6%)	1 (1.5%)	1 (0.4%)	0.35
ECG abnormalities	2 (0.6%)	1 (1.5%)	1 (0.4%)	0.35
Other*	13 (3.7%)	7 (10.4%)	6 (2.1%)	**0.005**
Cardiac rhythm at admission, n (%)				
Sinus rhythm	342 (97.4%)	65 (97.0%)	277 (97.5%)	0.68
Atrial fibrillation	9 (2.6%)	2 (3.0%)	7 (2.5%)	0.68
Ventricular arrhythmia	23 (6.6%)	9 (13.4%)	14 (4.9%)	**0.023**
Biological results				
Troponin peak ratio, (x ULN)	234.6 ± 448.4	195.7 ± 299.2	243.7 ± 476.9	0.30
Biological inflammatory syndrome †, n (%)	185 (52.9%)	36 (53.7%)	149 (52.7%)	0.98
TTE findings				
LVEF, (%)	54.2 ± 10.1	50.6 ± 11.3	55.0 ± 9.7	**0.001**
Cinetic abnormalities, n (%)	183 (52.1%)	44 (65.7%)	139 (48.9%)	**0.020**
Pericardial effusion, n (%)	35 (10.0%)	8 (11.9%)	27 (9.5%)	0.71
Invasive coronary angiography, n (%)	245 (69.8%)	59 (88.1%)	186 (65.5%)	**<0.001**

	All patients (N = 351)	MACE (N = 67)	No MACE (N = 284)	p-value
CCTA, n (%)	30 (8.5%)	8 (11.9%)	22 (7.7%)	0.39
Final diagnosis, n (%)				
Myocarditis	172 (49.0%)	22 (32.8%)	150 (52.8%)	**0.005**
Ischemic	76 (21.7%)	19 (28.4%)	57 (20.1%)	0.19
Tako-Tsubo	29 (8.3%)	11 (16.4%)	18 (6.3%)	**0.014**
Cardiomyopathy	27 (7.7%)	7 (10.4%)	20 (7.0%)	0.49
Inconclusive	47 (13.4%)	8 (11.9%)	39 (13.7%)	0.85
Treatments at discharge, n (%)				
Betablockers	270 (76.9%)	56 (83.6%)	214 (75.4%)	0.20
ACEI	172 (49.0%)	46 (68.7%)	126 (44.4%)	**<0.001**
Antiplatelet	125 (35.6%)	30 (44.8%)	95 (33.5%)	0.11
Statin	120 (34.2%)	34 (50.7%)	86 (30.3%)	**0.002**
NSAID	97 (27.6%)	7 (10.4%)	90 (31.7%)	**<0.001**
Colchicine	90 (25.6%)	7 (10.4%)	83 (29.2%)	**0.003**
Hospital length of stay, (days)	5.6 ± 4.3	7.7 ± 6.4	5.1 ± 3.5	**0.002**

Values are n (%) or mean ± standard deviation. **Bold** values indicate the 2-tailed p-value reached statistical significance (<0.05).
* includes: altered general condition, fall, and stroke.
† defined as elevated C-reactive protein (>5 mg/L) and/or leukocytosis (>10×10^9/L)

Abbreviations: ACEI, angiotensin-converting-enzyme inhibitors; BMI, body mass index; CCTA, coronary computed tomography angiography; LVEF, left ventricle ejection fraction; MACE, major adverse cardiovascular events, including death, stroke and cardiovascular hospitalization for: acute heart failure, sustained ventricular tachycardia, symptomatic atrial fibrillation, or initial disease recurrence; NSAID, non-steroidal anti-inflammatory drugs; NYHA, New York heart association; TTE, transthoracic echocardiography; ULN, upper limit of normal.

Table 2. Baseline CMR characteristics, strain and LV hemodynamic forces of patients with and without MACE (N=351).

	Overall N = 351[1]	MACE N = 67[1]	No MACE N = 284[1]	p-value[2]
LV ejection fraction, %	55.5 ± 10.0	51.0 ± 11.2	56.5 ± 9.3	**<0.001**
LV end-diastolic volume index, mL/m^2	89.3 ± 20.7	89.9 ± 24.6	89.2 ± 19.7	0.82
LV end-systolic volume index, mL/m^2	40.4 ± 15.8	45.0 ± 18.9	39.3 ± 14.9	**0.024**
LV mass index, g/m^2	60.3 ± 14.2	66.6 ± 17.3	58.8 ± 13.0	**<0.001**
RV ejection fraction, %	50.2 ± 9.3	49.1 ± 10.5	50.5 ± 8.9	0.25
Presence of T2 TSE hyperintensity, n (%)	164 (51.7%)	31 (56.4%)	133 (50.8%)	0.54
Mapping sequences				
Maximum T2 mapping value, ms	46.7 ± 8.0	46.9 ± 9.0	46.7 ± 7.8	0.89
Remote T2 mapping value, ms	39.5 ± 3.4	39.3 ± 3.1	39.6 ± 3.5	0.60
Maximum T1 mapping value, ms	1,332.8 ± 133.5	1,356.5 ± 141.3	1,327.8 ± 131.6	0.17
Remote T1 mapping value, ms	1,212.4 ± 70.4	1,214.8 ± 72.8	1,211.9 ± 70.1	0.79
Late gadolinium enhancement				
Presence of LGE, n (%)	252 (71.8%)	45 (67.2%)	207 (72.9%)	0.43
Presence of subendocardial LGE, n (%)	79 (22.5%)	20 (29.9%)	59 (20.8%)	0.15
Presence of midwall or subepicardial LGE, n (%)	170 (48.4%)	23 (34.3%)	147 (51.8%)	**0.015**
Presence of transmural LGE, n (%)	54 (15.5%)	19 (28.4%)	35 (12.5%)	**0.002**
LGE extent (%)	19.2 ± 13.8	19.5 ± 14.7	19.2 ± 13.6	0.87
Global longitudinal strain (%)	-19.4 ± 4.5	-17.0 ± 4.7	-20.0 ± 4.3	**<0.001**
LV hemodynamic forces				
Systolic peak force (%)	49.1 ± 22.4	36.6 ± 17.6	52.0 ± 22.4	**<0.001**
Impulse longitudinal force (%)	29.0 ± 13.1	21.9 ± 10.7	30.7 ± 13.1	**<0.001**
Ratio of transverse to longitudinal forces	15.8 ± 5.7	17.4 ± 6.7	15.4 ± 5.4	**0.025**

Values are n (%) or mean ± standard deviation. **Bold** values indicate the 2-tailed p-value reached statistical significance (<0.05).

Abbreviations: CMR, cardiac magnetic resonance; LGE, late gadolinium enhancement; LV, left ventricle; LVEF, left ventricle ejection fraction; MACE, major adverse cardiovascular events, including death, stroke and cardiovascular hospitalization for: acute heart failure, sustained ventricular tachycardia, symptomatic atrial fibrillation, or initial disease recurrence; RV, right ventricle; TSE, turbo spin echo.

Table 3. Univariate analysis of baseline and CMR characteristics for prediction of MACE.

	Hazard Ratio (95% CI)	p-value
Age	1.04 (1.03-1.06)	**<0.001**
Male	1.04 (0.63-1.71)	0.87
BMI	1.01 (0.96-1.05)	0.82
Cardiovascular risk factors		
Hypertension	3.53 (2.18-5.71)	**<0.001**
Dyslipidemia	1.77 (1.01-3.11)	**0.047**
Diabetes	2.00 (0.91-4.40)	0.08
Smoking	0.78 (0.47-1.3)	0.35
Arrhythmias at admission		
Supraventricular arrhythmia	0.96 (0.24-3.94)	0.96
Ventricular arrhythmia	1.89 (0.93-3.82)	0.08
Biological findings		
Troponin peak ratio	1.00 (1.00-1.00)	0.24
Biological inflammatory syndrome	1.09 (0.68-1.76)	0.72
TTE findings		
LVEF	0.97 (0.95-0.99)	**0.001**
Cinetic abnormalities	1.65 (1-2.74)	0.05
Pericardial effusion	1.22 (0.58-2.55)	0.61
CCTA	1.5 (0.72-3.15)	0.28
Invasive coronary angiography	3.11 (1.49-6.51)	**0.003**
Discharge treatment		
Betablockers	1.42 (0.74-2.70)	0.29
Antiplatelet	1.51 (0.93-2.44)	0.10
ACEI	2.10 (1.26-3.53)	**0.005**
Statin	2.13 (1.32-3.44)	**0.002**
NSAID	0.28 (0.13-0.62)	**0.002**
Colchicine	0.32 (0.15-0.70)	**0.004**
Final diagnosis		
Myocarditis (reference)	1.00	-

	Hazard Ratio (95% CI)	p-value
Ischemic	1.94 (1.05-3.58)	**0.035**
Takotsubo syndrome	2.85 (1.38-5.87)	**0.005**
Cardiomyopathy	1.76 (0.75-4.12)	0.20
Inconclusive	1.60 (0.71-3.62)	0.26
CMR findings		
LV ejection fraction	0.96 (0.94-0.98)	**<0.001**
RV ejection fraction	0.99 (0.97-1.02)	0.45
LV end-diastolic volume index	1.00 (0.99-1.02)	0.50
LV end-systolic volume index	1.02 (1.01-1.03)	**0.005**
LV mass index	1.03 (1.02-1.05)	**<0.001**
Presence of T2 TSE hyperintensity	0.84 (0.49-1.45)	0.53
Mapping sequences		
Maximum T2 mapping value	1.00 (0.96-1.04)	0.92
Remote T2 mapping value	1.01 (0.91-1.11)	0.91
Maximum T1 mapping value	1.00 (1.00-1.00)	0.33
Remote T1 mapping value	1.00 (1.00-1.00)	0.84
Pattern of late gadolinium enhancement		
Absence of LGE (reference)	1.00	-
Presence of subendocardial LGE	0.70 (0.30-1.62)	0.40
Presence of midwall or subepicardial LGE	0.44 (0.24-0.82)	**0.010**
Presence of transmural LGE	1.25 (0.68-2.29)	0.47
LGE extent	1.00 (0.98-1.02)	0.90
Global longitudinal strain	1.57 (1.27–1.93)	**<0.001**
LV hemodynamic forces		
Systolic peak force	0.44 (0.31-0.63)	**<0.001**
Impulse longitudinal force	0.47 (0.33-0.66)	**<0.001**
Ratio of transverse to longitudinal forces	1.43 (1.16-1.77)	**<0.001**

Note: Hazard ratios for HDFs parameters and GLS are expressed per 1-standard deviation increase. For other quantitative continuous variables, HR corresponds to a 1-unit increase in their respective measurement scale. *Abbreviations:* Same as Table 1 and 2.

Table 4. Multivariate Cox regression analysis for the prediction of adverse events (CMR model).

	Univariable analysis		Multivariable analysis	
	Hazard Ratio (95% CI)	**p-value**	**Hazard Ratio (95% CI)**	**p-value**
Model 1 (final diagnosis, traditional CMR risk factors)				
LVEF	0.96 (0.94-0.98)	**<0.001**	0.97 (0.94–0.99)	**0.007**
LGE extent	1.11 (0.2-6.07)	0.90	1.01 (0.99–1.03)	0.47
Final diagnosis				
Myocarditis (reference)	1.00	-	1.00	-
Ischemic injury	1.94 (1.05-3.58)	**0.035**	1.92 (1.01-3.64)	**0.047**
Takotsubo syndrome	2.85 (1.38-5.87)	**0.005**	2.04 (0.82-5.05)	0.12
Cardiomyopathy	1.76 (0.75-4.12)	0.20	1.34 (0.55-3.27)	0.51
Inconclusive	1.60 (0.71-3.62)	0.26	2.12 (0.87-5.16)	0.10
Model 2				
Model 1 + **GLS**	1.57 (1.27-1.93)	**<0.001**	1.35 (0.93-1.95)	0.11
Model 3A				
Model 2 + **Systolic peak force**	0.44 (0.31-0.63)	**< 0.001**	0.54 (0.36-0.83)	**0.004**
Model 3B				
Model 2 + **impulse longitudinal force**	0.47 (0.33-0.66)	**< 0.001**	0.58 (0.38-0.88)	**0.010**
Model 3C				
Model 2 + **Ratio of transverse to longitudinal forces**	1.43 (1.16-1.77)	**< 0.001**	1.31 (1.02-1.67)	**0.032**
Model 3D				
Model 2 + **cluster 1 vs. 2**	0.19 (0.08-0.45)	**< 0.001**	0.27 (0.11-0.66)	**0.004**

Note: Hazard ratios hemodynamic force parameters and GLS are expressed per 1-standard deviation increase. For other quantitative continuous variables, HR corresponds to a 1-unit increase in their respective measurement scale.
Abbreviations: Same as Table 2.

Table 5. Multivariate Cox regression analysis for the prediction of adverse events (clinical model).

	Univariable analysis		Multivariable analysis	
	Hazard Ratio (95% CI)	**p-value**	**Hazard Ratio (95% CI)**	**p-value**
Model 4 (traditional risk factors)				
Age (years)	1.04 (1.03-1.06)	**<0.001**	1.04 (1.03-1.06)	**<0.001**
Male	1.04 (0.63-1.71)	0.87	2.08 (1.23–3.53)	**0.006**
Hypertension	3.53 (2.18-5.71)	**<0.001**	1.81 (1.03-3.16)	**0.038**
Model 5 (model 4 + **final diagnosis**)				
+ **Myocarditis** (reference)	1.00	-	1.00	-
Ischemic injury	1.94 (1.05-3.58)	**0.035**	1.08 (0.54–2.14)	0.83
Takotsubo syndrome	2.85 (1.38-5.87)	**0.005**	1.40 (0.53-3.73)	0.50
Cardiomyopathy	1.76 (0.75-4.12)	0.20	1.00 (0.40-2.50)	0.99
Inconclusive	1.60 (0.71-3.62)	0.26	0.85 (0.36-2.03)	0.72
Model 6A				
Model 5 + **Systolic peak force**	0.44 (0.31-0.63)	**< 0.001**	0.63 (0.42-0.94)	**0.024**
Model 6B				
Model 5 + **impulse longitudinal force**	0.47 (0.33-0.66)	**< 0.001**	0.65 (0.44-0.96)	**0.031**
Model 6C				
Model 5 + **Ratio of transverse to longitudinal forces**	1.43 (1.16-1.77)	**< 0.001**	1.48 (1.18-1.86)	**< 0.001**
Model 6D				
Model 5 + **cluster 1 vs. 2**	0.19 (0.08-0.45)	**< 0.001**	0.40 (0.16-0.98)	**0.046**

Note: Hazard ratios for hemodynamic force parameters and GLS are expressed per 1 standard deviation increase. For other continuous variables, HR corresponds to a 1-unit increase in their respective measurement scale.

DONNÉES SUPPLÉMENTAIRES

- **Supplementary Method S1:** Additional exclusion criteria.
- **Supplementary Method S2:** Detailed methodology for the assessment of left ventricular strain and hemodynamic forces.
- **Supplementary Figure S1:** Bland-Altman plots showing inter-observer agreement for HDFs parameters.
- **Supplementary Figure S2:** Kaplan–Meier curves of MACE-free survival by hemodynamic forces, according to the optimal cut-off derived from the maximally selected rank statistics.
- **Supplementary Figure S3:** Kaplan–Meier curves of MACE-free survival by hemodynamic forces, according to the median value.
- **Supplementary Figure S4:** Kaplan–Meier curves of MACE-free survival by LVEF, according to the optimal cut-off derived from the maximally selected rank statistics.
- **Supplementary Figure S5:** Incremental prognostic value of impulse longitudinal HDF
- **Supplementary Figure S6:** Incremental prognostic value of transverse-to-longitudinal forces ratio.
- **Supplementary Figure S7:** Incremental prognostic value of ratio of HDF-derived clusters.
- **Supplementary Figure S8:** Receiver operating characteristic (ROC) curves comparing model discrimination for prediction of MACE
- **Supplementary Figure S9:** Annualized incidence rates of MACE per 100 patient-years across quartiles of longitudinal impulse HDF.

• **Supplementary Figure S10:** Annualized incidence rates of MACE per 100 patient-years across quartiles of transverse to longitudinal forces ratio.

• **Supplementary Table S1:** Baseline characteristics of patients by final diagnosis.

• **Supplementary Table S2:** Baseline CMR characteristics, strain and LV hemodynamic forces by final diagnosis.

• **Supplementary Table S3:** LV hemodynamic forces of patients with and without MACE.

• **Supplementary Table S4:** Intra- and inter-observer reproducibility using intraclass correlation coefficient.

• **Supplementary Table S5:** Univariate analysis of all LV hemodynamic force parameters.

• **Supplementary Table S6:** Baseline characteristics of patients stratified by clusters.

• **Supplementary Table S7:** Baseline CMR characteristics, strain and LV hemodynamic forces of patients stratified by clusters.

SUPPLEMENTARY METHOD S1

Additional exclusion criteria

Additional exclusion criteria included: contraindications to magnetic resonance imaging (e.g., cerebral clips, metallic ocular implants); an estimated glomerular filtration rate (eGFR) <30 mL/min/1.73 m^2; and known allergy to gadolinium-based contrast agents.

SUPPLEMENTARY METHOD S2

Detailed methodology for the assessment of left ventricular strain and hemodynamic forces.

Strain evaluation

LV strain was analysed using post-processing software (Medis Suite, Netherlands). Global longitudinal strain (GLS) of the LV myocardium and endocardium was calculated from the 2-, 3-, and 4-chamber views. After automated contour detection at systole and diastole, with manual corrections when required, the feature tracking module delineated endocardial and epicardial borders throughout the cardiac cycle, from which strain parameters were derived.

LV hemodynamic forces assessment

LV hemodynamic forces (HDFs) were measured using the QStrain HDF module (Medis Suite, Netherlands). They were derived from deformation imaging of the 2-, 3-, and 4-chamber views after feature tracking, and measurements of mitral valve width (averaged from the 2- and 4-chamber diameters) and aortic valve width (3-chamber diameter).
HDFs parameters were measured in the longitudinal and transverse directions over the entire cardiac cycle, as well as separately during systole and diastole, and at specific key time points of the cardiac cycle.

Throughout the cardiac cycle:

- Longitudinal force: the average amplitude of LV longitudinal force across the entire cardiac cycle.
- Transverse force: the average amplitude of LV transverse force across the entire cardiac cycle.
- Ratio: the average ratio between transverse and longitudinal LV forces across the entire cardiac cycle.
- Ejection angle: the dominant angle of the force vector.

During the systole:

- Systolic longitudinal force: the average amplitude of longitudinal force during the systolic phase.
- Systolic transverse force: the average amplitude of transverse force during the systolic phase.
- Systolic ratio: the average ratio between transverse and longitudinal LV forces during the systolic phase.
- Impulse longitudinal force: the average longitudinal force during the initial systolic ejection phase.
- Systolic peak force: the maximum value of longitudinal force reached during the cardiac cycle.

During the diastole:

- Diastolic longitudinal force: the average amplitude of longitudinal force during the diastolic phase.
- Diastolic transverse force: the average amplitude of transverse force during the diastolic phase.
- Diastolic ratio: the average ratio between transverse and longitudinal LV forces during the diastolic phase.
- Systolic-diastolic transition longitudinal force: the average LV longitudinal force during the transition from systole to diastole.
- Diastolic deceleration longitudinal force: the average LV longitudinal force during the early diastolic filling phase.
- Atrial thrust longitudinal force: the average LV longitudinal force during the late diastolic phase.

Figure S1. Bland-Altman plots showing inter-observer agreement for HDFs parameters. Each plot compares measurements from two independent observers, with the mean difference and 95% limits of agreement (±1.96 SD) shown. Most values fall within the agreement limits, and the mean difference is close to zero, reflecting minimal bias and high reproducibility between observers.

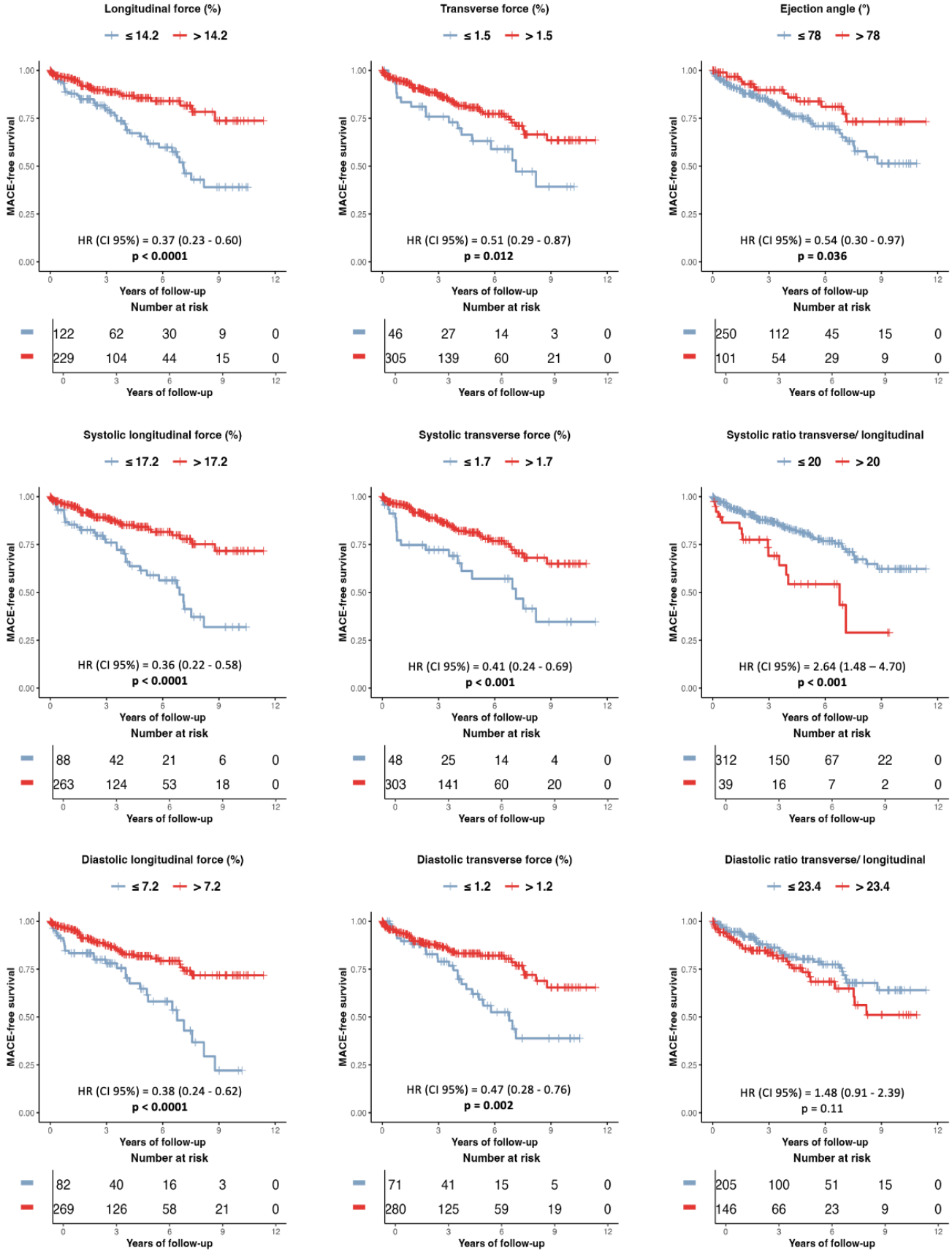
Longitudinal force (%)
≤ 14.2
> 14.2
MACE-free survival
HR (CI 95%) = 0.37 (0.23 - 0.60)
p < 0.0001
Years of follow-up
Number at risk
122 62 30 9 0
229 104 44 15 0
Transverse force (%)
≤ 1.5
> 1.5
HR (CI 95%) = 0.51 (0.29 - 0.87)
p = 0.012
46 27 14 3 0
305 139 60 21 0
Ejection angle (°)
≤ 78
> 78
HR (CI 95%) = 0.54 (0.30 - 0.97)
p = 0.036
250 112 45 15 0
101 54 29 9 0
Systolic longitudinal force (%)
≤ 17.2
> 17.2
HR (CI 95%) = 0.36 (0.22 - 0.58)
p < 0.0001
88 42 21 6 0
263 124 53 18 0
Systolic transverse force (%)
≤ 1.7
> 1.7
HR (CI 95%) = 0.41 (0.24 - 0.69)
p < 0.001
48 25 14 4 0
303 141 60 20 0
Systolic ratio transverse/ longitudinal
≤ 20
> 20
HR (CI 95%) = 2.64 (1.48 – 4.70)
p < 0.001
312 150 67 22 0
39 16 7 2 0
Diastolic longitudinal force (%)
≤ 7.2
> 7.2
HR (CI 95%) = 0.38 (0.24 - 0.62)
p < 0.0001
82 40 16 3 0
269 126 58 21 0
Diastolic transverse force (%)
≤ 1.2
> 1.2
HR (CI 95%) = 0.47 (0.28 - 0.76)
p = 0.002
71 41 15 5 0
280 125 59 19 0
Diastolic ratio transverse/ longitudinal
≤ 23.4
> 23.4
HR (CI 95%) = 1.48 (0.91 - 2.39)
p = 0.11
205 100 51 15 0
146 66 23 9 0

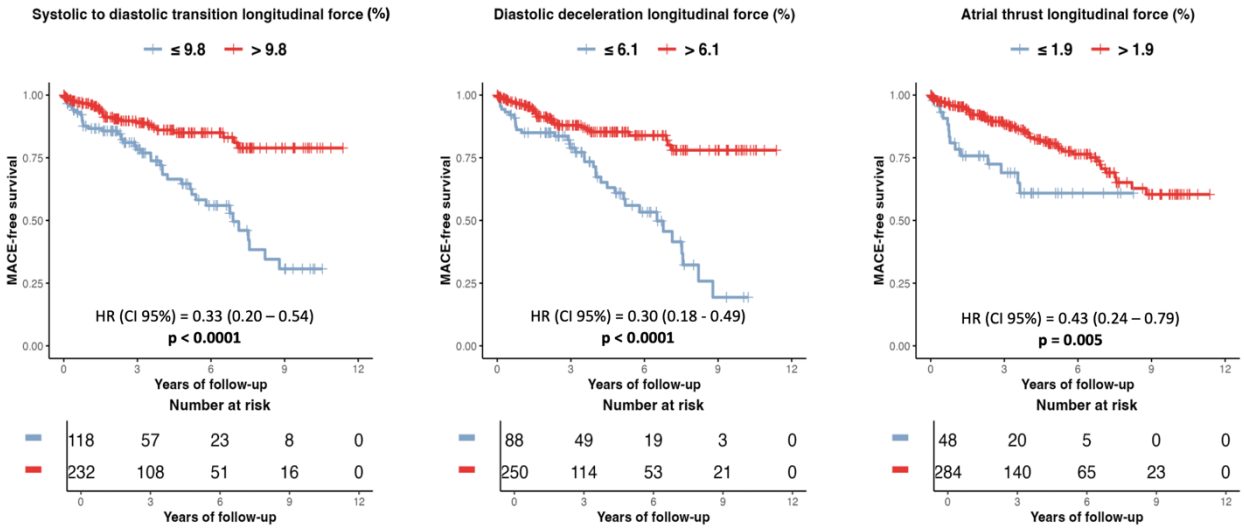

Figure S2. Kaplan–Meier curves of MACE-free survival by hemodynamic forces, according to the optimal cut-off derived from the maximally selected rank statistics. Hazard ratios (HRs) and 95% confidence intervals are derived from Cox regression models, while p values correspond to log-rank tests.

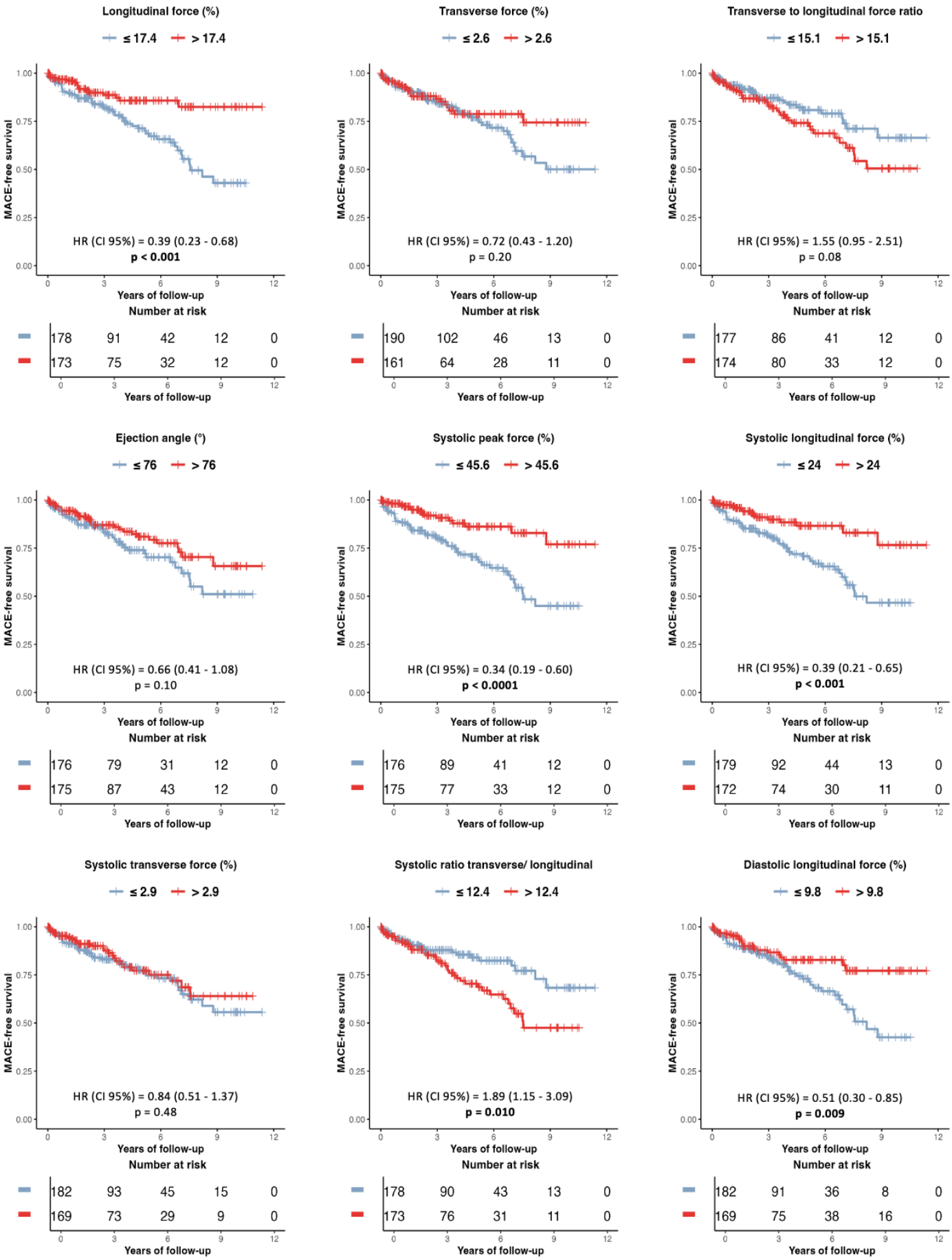
Longitudinal force (%)
≤ 17.4
> 17.4
MACE-free survival
HR (CI 95%) = 0.39 (0.23 - 0.68)
p < 0.001
Years of follow-up
Number at risk
178 91 42 12 0
173 75 32 12 0
Years of follow-up
Transverse force (%)
≤ 2.6
> 2.6
MACE-free survival
HR (CI 95%) = 0.72 (0.43 - 1.20)
p = 0.20
Years of follow-up
Number at risk
190 102 46 13 0
161 64 28 11 0
Years of follow-up
Transverse to longitudinal force ratio
≤ 15.1
> 15.1
MACE-free survival
HR (CI 95%) = 1.55 (0.95 - 2.51)
p = 0.08
Years of follow-up
Number at risk
177 86 41 12 0
174 80 33 12 0
Years of follow-up
Ejection angle (°)
≤ 76
> 76
MACE-free survival
HR (CI 95%) = 0.66 (0.41 - 1.08)
p = 0.10
Years of follow-up
Number at risk
176 79 31 12 0
175 87 43 12 0
Years of follow-up
Systolic peak force (%)
≤ 45.6
> 45.6
MACE-free survival
HR (CI 95%) = 0.34 (0.19 - 0.60)
p < 0.0001
Years of follow-up
Number at risk
176 89 41 12 0
175 77 33 12 0
Years of follow-up
Systolic longitudinal force (%)
≤ 24
> 24
MACE-free survival
HR (CI 95%) = 0.39 (0.21 - 0.65)
p < 0.001
Years of follow-up
Number at risk
179 92 44 13 0
172 74 30 11 0
Years of follow-up
Systolic transverse force (%)
≤ 2.9
> 2.9
MACE-free survival
HR (CI 95%) = 0.84 (0.51 - 1.37)
p = 0.48
Years of follow-up
Number at risk
182 93 45 15 0
169 73 29 9 0
Years of follow-up
Systolic ratio transverse/ longitudinal
≤ 12.4
> 12.4
MACE-free survival
HR (CI 95%) = 1.89 (1.15 - 3.09)
p = 0.010
Years of follow-up
Number at risk
178 90 43 13 0
173 76 31 11 0
Years of follow-up
Diastolic longitudinal force (%)
≤ 9.8
> 9.8
MACE-free survival
HR (CI 95%) = 0.51 (0.30 - 0.85)
p = 0.009
Years of follow-up
Number at risk
182 91 36 8 0
169 75 38 16 0
Years of follow-up

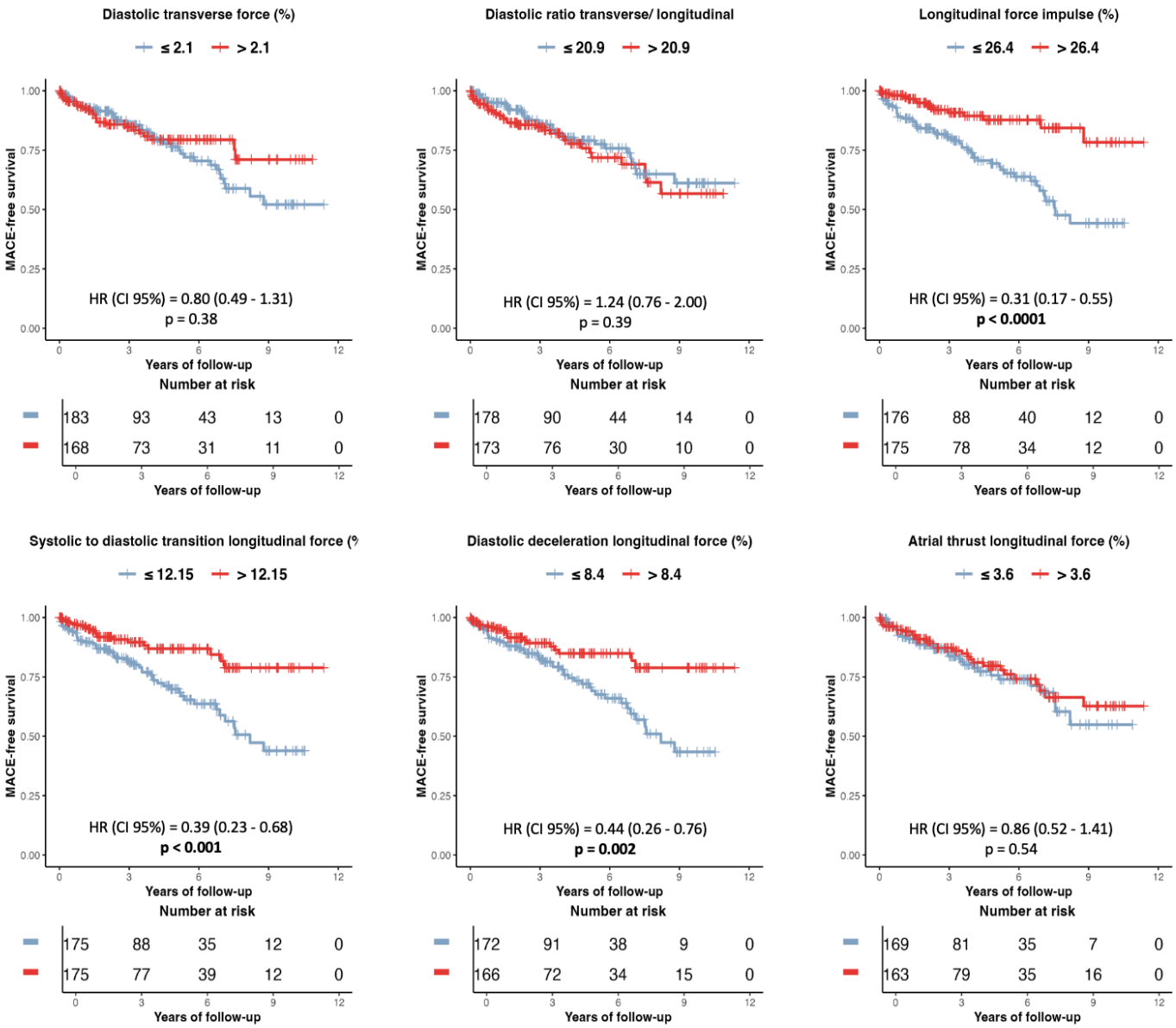

Figure S3. Kaplan–Meier curves of MACE-free survival by hemodynamic forces, according to the median value. Hazard ratios (HRs) and 95% confidence intervals are derived from Cox regression models, while p values correspond to log-rank tests.

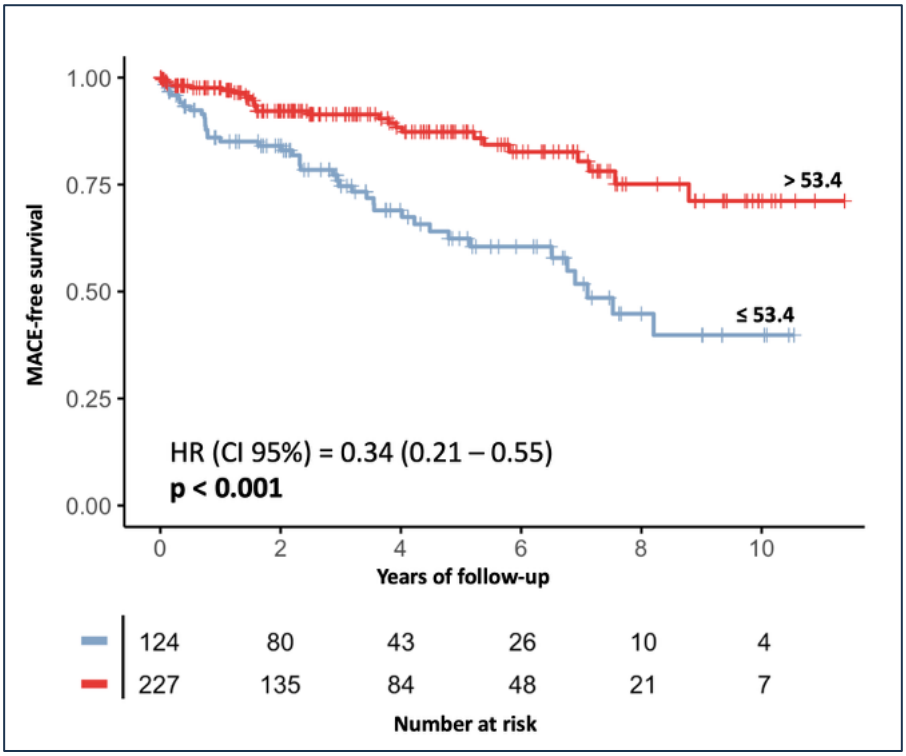

Figure S4. Kaplan–Meier curves of MACE-free survival by LVEF, according to the optimal cut-off derived from the maximally selected rank statistics. Hazard ratios (HR) and 95% confidence intervals (CI) are derived from Cox regression models, while p-values correspond to log-rank tests.

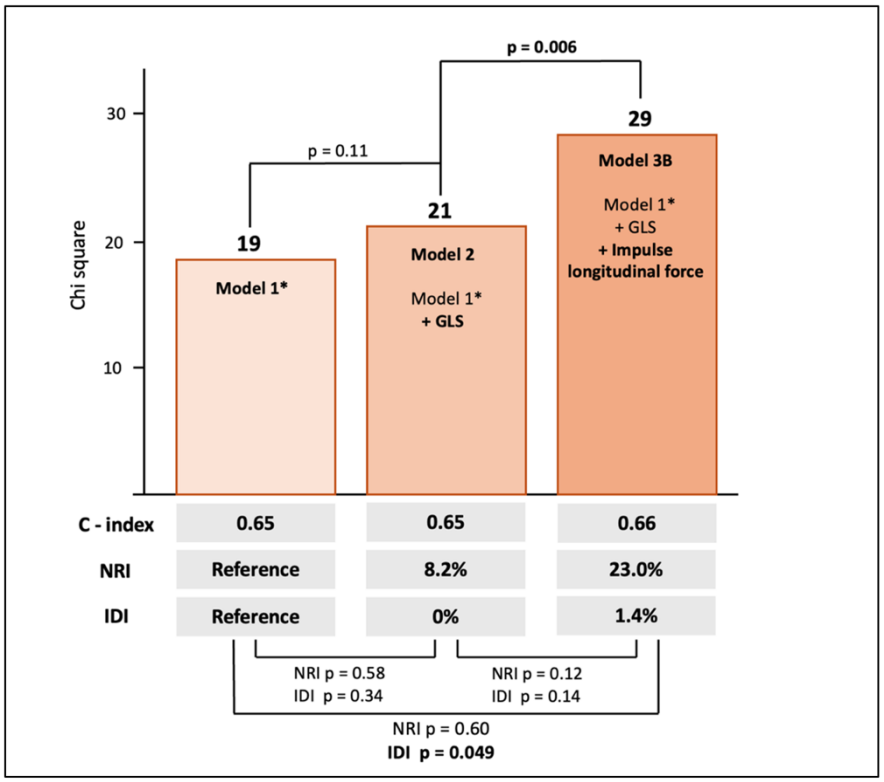

Figure S5. Incremental prognostic value of impulse longitudinal force. The model 3B is a nested model comprising the model 1 (final diagnosis, LVEF, LGE extent), the model 2 with GLS, and impulse force. **Bold** values indicate the 2-tailed p-value reached statistical significance (<0.05). *Abbreviations: Same as Figure 4.*

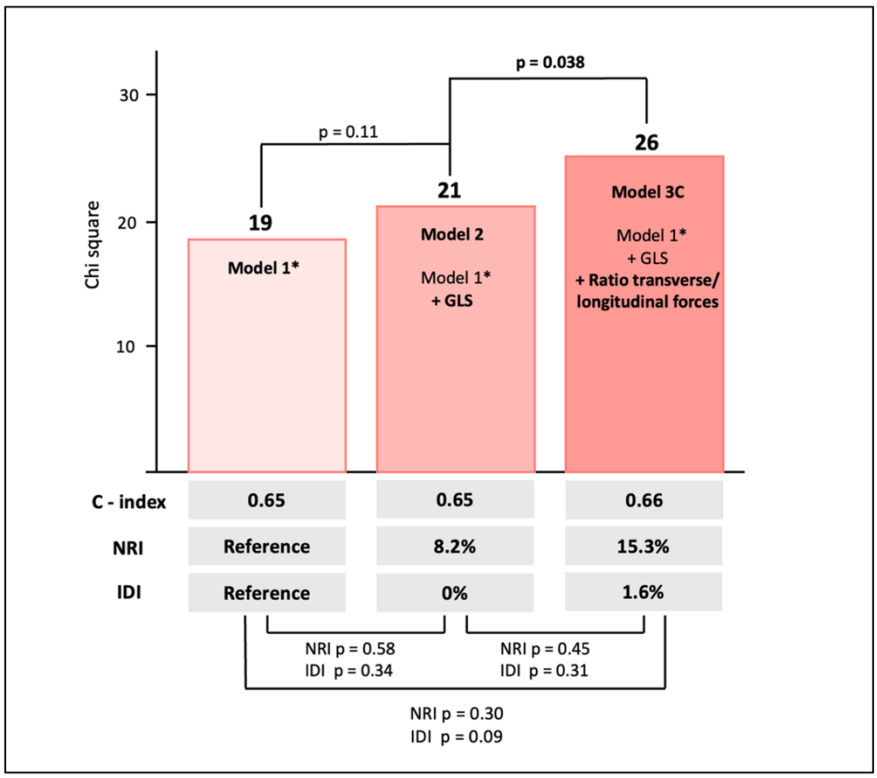

Figure S6. Incremental prognostic value of transverse-to-longitudinal forces ratio. The model 3C is a nested model comprising the model 1 (final diagnosis, LVEF, LGE extent), the model 2 with GLS, and the ratio. **Bold** values indicate the 2-tailed p-value reached statistical significance (<0.05). *Abbreviations: Same as Figure 4.*

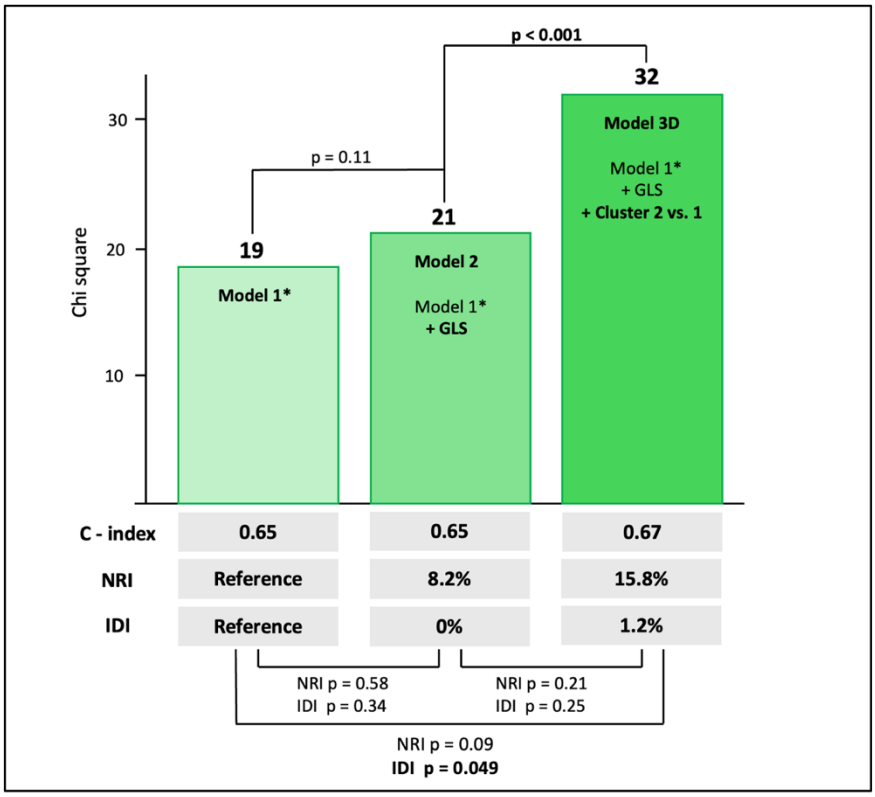

Figure S7. Incremental prognostic value of HDF-derived clusters. The model 3D is a nested model comprising the model 1 (final diagnosis, LVEF, LGE extent), the model 2 with GLS and the cluster 2 vs. 1. **Bold** values indicate the 2-tailed p-value reached statistical significance (<0.05). *Abbreviations: Same as Figure 4.*

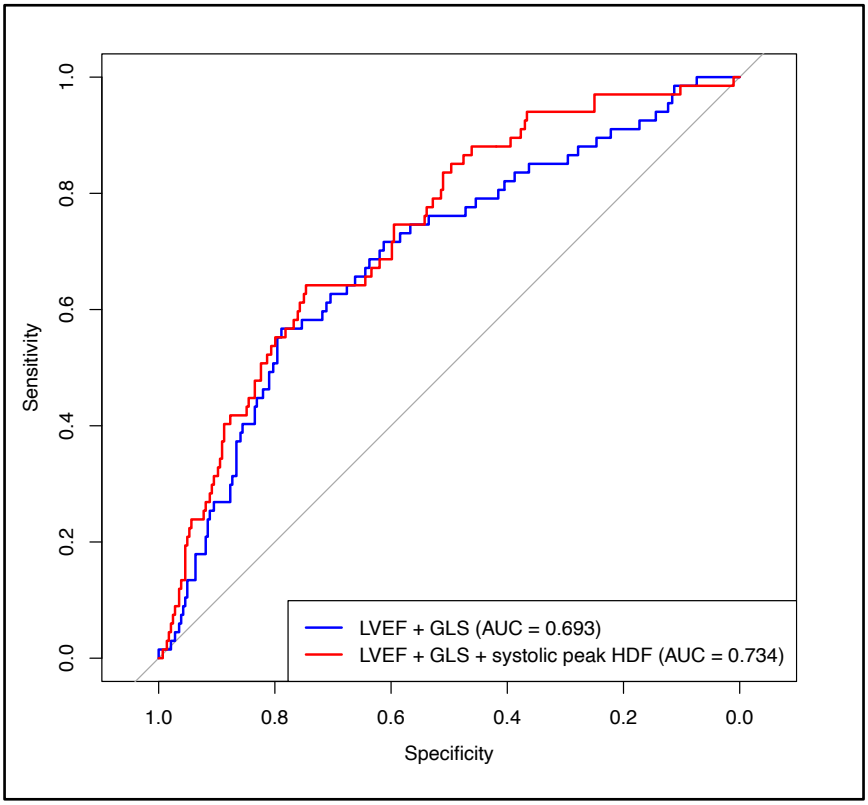

Figure S8. Receiver operating characteristic (ROC) curves comparing model discrimination for prediction of MACE. The baseline model including left ventricle ejection fraction (LVEF) and global longitudinal strain (GLS) is shown in blue, and the extended model additionally incorporating systolic peak hemodynamic force (HDF) is shown in red. The addition of systolic peak force improved the area under the curve (AUC) from 0.69 to 0.73 (DeLong p-value = 0.08).

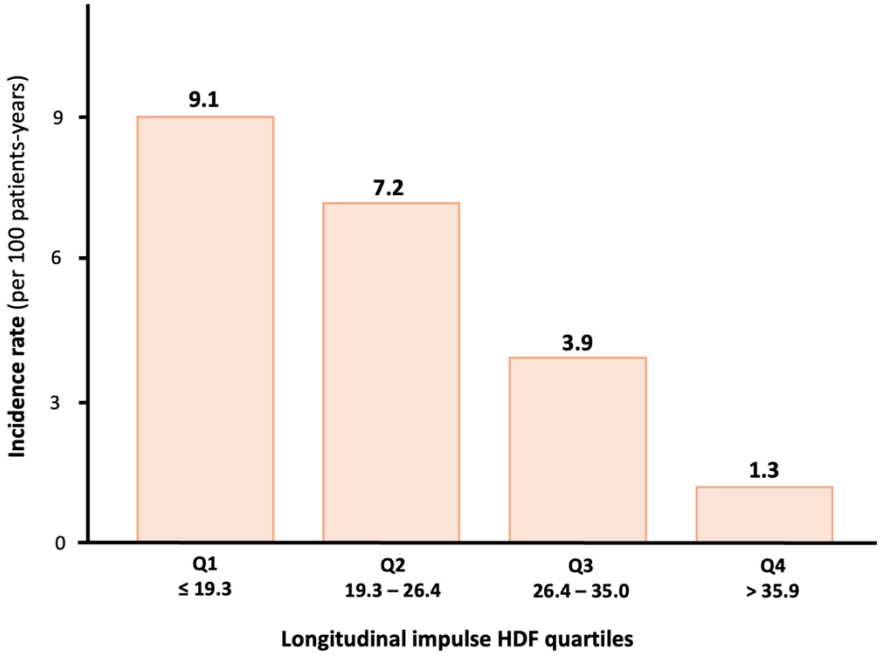

Figure S9. Annualized incidence rates of MACE per 100 patient-years across quartiles of longitudinal impulse HDF. Incidence decreased progressively from Q1 (9.1/100 patients-years (py)) to Q4 (1.3/100 py). In Cox regression (Q1 as reference), risk reduction was non-significant in Q2 (HR 0.79, p = 0.41), but significant in Q3 (HR 0.43, p = 0.018) and Q4 (HR 0.14, p < 0.001).

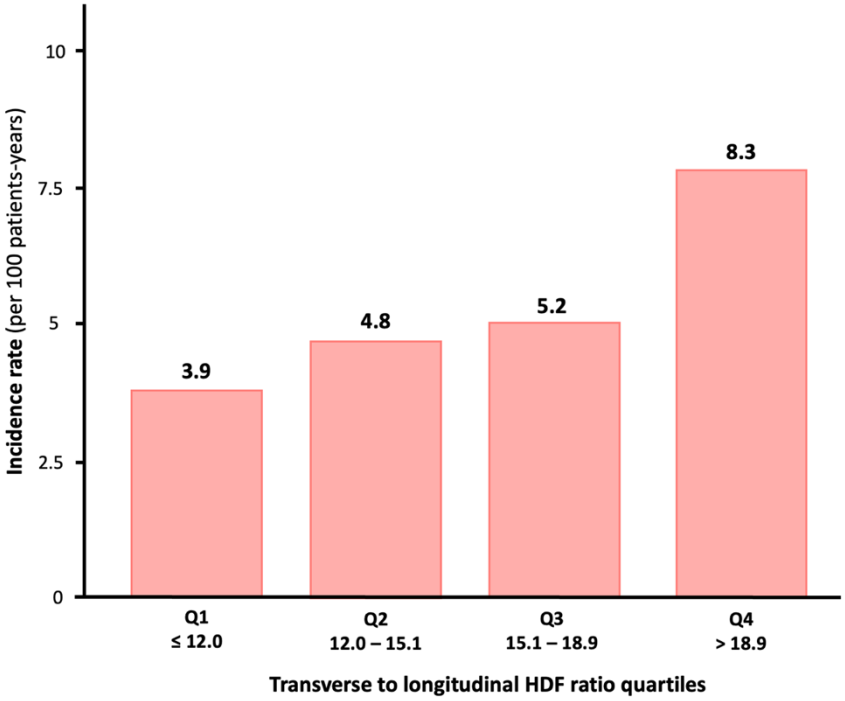

Figure S10. Annualized incidence rates of MACE per 100 patient-years across quartiles of transverse to longitudinal HDF ratio.
Incidence increased progressively from Q1 (3.9/100 patients-years (py)) to Q4 (8.3/100 py). In Cox regression (Q1 as reference), risk increase was non-significant in Q2 (HR 1.24, p = 0.58), and Q3 (HR 1.31, p = 0.48) but reached significance in Q4 (HR 2.09, p = 0.033).

Table S1. Baseline characteristics of patients by final diagnosis (N=351).

	All patients (N = 351)	**Myocarditis** (N = 172)	**Ischemic** (N = 76)	**Non conclusive** (N = 47)	**Tako-Tsubo** (N = 29)	**Other diagnosis** (N = 27)	**p-value**
Age, years	48.5 ± 20.0	38.1 ± 16.8	57.5 ± 16.7	53.7 ± 19.4	70.2 ± 12.6	57.0 ± 17.8	**<0.001**
Males, n (%)	223.0 (63.5%)	141.0 (82.0%)	40.0 (52.6%)	26.0 (55.3%)	0.0 (0.0%)	16.0 (59.3%)	**<0.001**
BMI, kg/m^2	25.2 ± 5.2	24.8 ± 5.0	26.2 ± 5.4	24.4 ± 4.0	25.0 ± 6.4	27.0 ± 5.8	**0.045**
Coronary risk factors, n (%)							
Current or previous smoking	150.0 (42.7%)	72.0 (41.9%)	36.0 (47.4%)	26.0 (55.3%)	7.0 (24.1%)	9.0 (33.3%)	0.07
Hypertension	94.0 (26.8%)	21.0 (12.2%)	29.0 (38.2%)	18.0 (38.3%)	16.0 (55.2%)	10.0 (37.0%)	**<0.001**
Dyslipidemia	56.0 (16.0%)	10.0 (5.8%)	21.0 (27.6%)	13.0 (27.7%)	8.0 (27.6%)	4.0 (14.8%)	**<0.001**
Diabetes	22.0 (6.3%)	5.0 (2.9%)	5.0 (6.6%)	4.0 (8.5%)	3.0 (10.3%)	5.0 (18.5%)	**0.022**
Admission presentation, n (%)							
Chest pain	291 (82.9%)	157 (91.3%)	57 (75.0%)	42 (89.4%)	20 (69.0%)	15 (55.6%)	**< 0.001**
Dyspnea (NYHA III/IV)	22 (6.3%)	4 (2.3%)	5 (6.6%)	2 (4.3%)	4 (13.8%)	7 (25.9%)	**< 0.001**
Cardiac arrest	9 (2.6%)	3 (1.7%)	5 (6.6%)	0 (0%)	0 (0%)	1 (3.7%)	0.13
Syncope/ Malaise	9 (2.6%)	3 (1.7%)	2 (2.6%)	2 (4.3%)	2 (6.9%)	0 (0%)	0.34
Palpitations	3 (0.9%)	1 (0.6%)	0 (0%)	0 (0%)	0 (0%)	2 (7.4%)	0.05
Cardiogenic shock	2 (0.6%)	1 (0.6%)	0 (0%)	0 (0%)	0 (0%)	1 (3.7%)	0.34
ECG abnormalities	2 (0.6%)	0 (0%)	0 (0%)	0 (0%)	1 (3.4%)	1 (3.7%)	**0.025**
Other*	13 (5.2%)	3 (1.7%)	7 (9.2%)	1 (2.1%)	2 (6.9%)	0 (0%)	**0.035**
Cardiac rhythm, n (%)							

	All patients (N = 351)	**Myocarditis** (N = 172)	**Ischemic** (N = 76)	**Non conclusive** (N = 47)	**Tako-Tsubo** (N = 29)	**Other diagnosis** (N = 27)	**p-value**
Sinus rhythm	342 (97.4%)	167 (97.1%)	75 (98.7%)	47 (100%)	26 (89.7%)	27 (100%)	0.05
Atrial fibrillation	9 (2.6%)	5 (2.9%)	1 (1.3%)	0 (0%)	3 (10.3%)	0 (0%)	0.05
Ventricular arrhythmia	23 (6.6%)	12 (7.0%)	9 (11.8%)	0 (0%)	0 (0%)	2 (7.4%)	0.07
Biological results							
Troponin peak ratio, (x ULN)	234.6 ± 448.4	273.8 ± 520.4	355.7 ± 495.2	35.8 ± 88.0	146.3 ± 145.9	84.2 ± 158.8	**<0.001**
Biological inflammatory syndrome[†], n (%)	185 (52.9%)	111 (64.5%)	28 (36.8%)	20 (42.6%)	15 (51.7%)	11 (42.3%)	**<0.001**
TTE findings							
LVEF, (%)	54.2 ± 10.1	56.6 ± 7.4	54.2 ± 10.1	57.8 ± 6.5	38.9 ± 10.4	48.9 ± 13.5	**<0.001**
Cinetic abnormalities, n (%)	183 (52.1%)	78 (45.3%)	47 (61.8%)	13 (27.7%)	29 (100.0%)	16 (59.3%)	**<0.001**
Pericardial effusion, n (%)	35 (10.0%)	22 (12.8%)	5 (6.6%)	3 (6.4%)	2 (6.9%)	3 (11.1%)	0.48
Invasive coronary angiography, n (%)	245 (69.8%)	85 (49.4%)	75 (98.7%)	38 (80.9%)	25 (86.2%)	22 (81.5%)	**<0.001**
CCTA, n (%)	30 (8.5%)	18 (10.5%)	4 (5.3%)	4 (8.5%)	2 (6.9%)	2 (7.4%)	0.74
Treatments at discharge, n (%)							
Betablockers	270 (76.9%)	135 (78.5%)	64 (84.2%)	26 (55.3%)	26 (89.7%)	19 (70.4%)	**0.001**
ACEI	172 (49.0%)	69 (40.1%)	48 (63.2%)	13 (27.7%)	27 (93.1%)	15 (55.6%)	**<0.001**
Antiplatelet	125 (35.6%)	28 (16.3%)	58 (76.3%)	21 (44.7%)	9 (31.0%)	9 (33.3%)	**<0.001**
Statin	120 (34.2%)	25 (14.5%)	55 (72.4%)	22 (46.8%)	12 (41.4%)	6 (22.2%)	**<0.001**
NSAID	97 (27.6%)	82 (47.7%)	3 (3.9%)	10 (21.3%)	0 (0.0%)	2 (7.4%)	**<0.001**

	All patients (N = 351)	**Myocarditis** (N = 172)	**Ischemic** (N = 76)	**Non conclusive** (N = 47)	**Tako-Tsubo** (N = 29)	**Other diagnosis** (N = 27)	**p-value**
Colchicine	90 (25.6%)	75 (43.6%)	3 (3.9%)	11 (23.4%)	0 (0.0%)	1 (3.7%)	**<0.001**
Outcomes, n (%)							
MACE	67 (19.1%)	22 (12.8%)	19 (25.0%)	8 (17.0%)	11 (37.9%)	7 (25.9%)	**0.008**
Death	38 (10.8%)	7 (4.1%)	13 (17.1%)	4 (8.5%)	8 (27.6%)	6 (22.2%)	**<0.001**
Disease recurrence	18 (%)	9 (%)	6 (%)	3 (%)	0 (0%)	0 (0%)	0.07
Hospitalization for heart failure	4 (1.1%)	2 (1.2%)	1 (1.3%)	0 (0%)	0 (0%)	1 (3.7%)	0.65
Sustained TV	7 (2.0%)	5 (2.9%)	2 (2.6%)	0 (0%)	0 (0%)	0 (0%)	0.56
Hospitalization for symptomatic AF	3 (0.9%)	0 (0%)	0 (0%)	1 (2.1%)	2 (6.9%)	0 (0%)	**0.003**
Stroke	8 (2.3%)	0 (0%)	3 (3.9%)	1 (2.1%)	3 (10.3%)	1 (3.7%)	**0.009**
Hospital length of stay, (days)	5.6 ± 4.3	5.0 ± 3.7	6.3 ± 3.5	4.7 ± 4.9	8.1 ± 5.6	6.5 ± 5.6	**<0.001**

Values are n (%) or mean ± standard deviation. **Bold** values indicate the 2-tailed p-value reached statistical significance (<0.05).
* includes: altered general condition, fall, and stroke.
† defined as elevated C-reactive protein (>5 mg/L) and/or leukocytosis (>10×10^9/L)

Abbreviations: Same as Table 1.

Table S2. Baseline CMR characteristics, strain and LV hemodynamic forces by final diagnosis (N=351).

	Overall N = 351	**Myocarditis** N = 172	**Ischemic** N = 76	**Normal** N = 47	**Tako-Tsubo** N = 29	**Other diagnosis** N = 27	**p-value**
LV ejection fraction, %	55.5 ± 10.0	56.7 ± 8.6	55.0 ± 9.8	60.6 ± 6.7	43.9 ± 10.2	52.5 ± 13.0	**<0.001**
LV end-diastolic volume index, mL/m^2	89.3 ± 20.7	91.4 ± 20.3	87.1 ± 20.5	85.8 ± 18.4	88.7 ± 19.0	89.1 ± 28.1	0.40
LV end-systolic volume index, mL/m^2	40.4 ± 15.8	40.0 ± 13.9	40.1 ± 16.8	33.9 ± 9.6	50.0 ± 15.8	44.5 ± 25.8	**<0.001**
LV mass index, g/m^2	60.3 ± 14.2	59.9 ± 12.1	60.1 ± 15.4	60.0 ± 16.7	59.9 ± 12.1	64.2 ± 20.2	**0.63**
RV ejection fraction, %	50.2 ± 9.3	49.3 ± 8.4	51.3 ± 10.3	52.5 ± 8.5	50.3 ± 10.0	49.7 ± 11.3	0.19
Presence of T2 TSE hyperintensity, n (%)	164 (51.7%)	100 (63.7%)	44 (63.8%)	1 (2.3%)	14 (53.8%)	5 (22.7%)	**<0.001**
Mapping sequences							
Maximum T2 mapping value, ms	46.7 ± 8.0	47.2 ± 6.3	49.9 ± 10.5	39.7 ± 2.7	53.4 ± 7.0	40.0 ± 3.6	**<0.001**
Remote T2 mapping value, ms	39.5 ± 3.4	39.4 ± 3.5	39.2 ± 2.7	39.6 ± 2.6	40.3 ± 5.7	39.4 ± 2.1	0.97
Maximum T1 mapping value, ms	1,332.8 ± 133.5	1,320.2 ± 122.2	1,401.2 ± 130.8	1,209.9 ± 60.6	1,480.5 ± 102.5	1,316.6 ± 100.5	**<0.001**
Remote T1 mapping value, ms	1,212.4 ± 70.4	1,203.1 ± 65.5	1,200.8 ± 70.8	1,209.9 ± 60.6	1,268.1 ± 85.3	1,254.0 ± 67.6	**<0.001**
Late gadolinium enhancement							
Presence of LGE, n (%)	252 (71.8%)	166 (96.5%)	74 (97.4%)	3 (6.4%)	3 (10.3%)	6 (22.2%)	**<0.001**
Presence of subendocardial LGE, n (%)	79 (22.5%)	4 (2.3%)	73 (96.1%)	0 (0.0%)	1 (3.4%)	1 (3.7%)	**<0.001**
Presence of midwall or subepicardial LGE, n (%)	170 (48.4%)	163 (94.8%)	4 (5.3%)	1 (2.1%)	1 (3.4%)	1 (3.7%)	**<0.001**
Presence of transmural LGE, n (%)	54 (15.5%)	9 (5.2%)	43 (56.6%)	1 (2.2%)	1 (3.4%)	0 (0.0%)	**<0.001**
LGE extent (%)	19.2 ± 13.8	25.8 ± 14.1	17.9 ± 7.3	6.2 ± 1.2	7.9 ± 5.9	15.9 ± 17.2	**<0.001**

	Overall N = 351	**Myocarditis** N = 172	**Ischemic** N = 76	**Normal** N = 47	**Tako-Tsubo** N = 29	**Other diagnosis** N = 27	**p-value**
Global longitudinal strain							
Myocardial GLS (%)	-19.4 ± 4.5	-20.5 ± 3.9	-19.0 ± 4.6	-21.0 ± 2.8	-13.7 ± 4.9	-17.2 ± 4.7	**<0.001**
LV hemodynamic forces							
Longitudinal force (%)	18.1 ± 7.3	19.8 ± 7.5	17.0 ± 7.0	18.2 ± 5.9	11.5 ± 4.4	17.2 ± 7.1	**<0.001**
Transverse force (%)	2.7 ± 1.1	2.9 ± 1.0	2.5 ± 1.2	2.8 ± 1.0	1.8 ± 0.7	2.8 ± 1.0	**<0.001**
Ratio of transverse to longitudinal forces	15.8 ± 5.7	15.5 ± 5.6	15.2 ± 4.7	15.9 ± 5.9	16.6 ± 5.1	18.4 ± 8.1	0.22
Ejection angle (°)	76.4 ± 3.7	76.5 ± 3.5	76.8 ± 3.5	76.4 ± 3.8	75.6 ± 3.8	75.2 ± 5.2	0.35
Systolic peak force (%)	49.1 ± 22.4	55.1 ± 23.3	44.9 ± 20.5	48.2 ± 18.2	29.1 ± 12.2	44.9 ± 21.4	**<0.001**
Systolic longitudinal force (%)	25.5 ± 11.4	28.7 ± 11.9	22.8 ± 10.1	25.8 ± 9.6	15.4 ± 6.8	23.2 ± 9.9	**<0.001**
Systolic transverse force (%)	3.1 ± 1.4	3.4 ± 1.3	2.9 ± 1.7	3.2 ± 1.3	2.0 ± 0.9	3.2 ± 1.3	**<0.001**
Systolic ratio of transverse to longitudinal forces	13.3 ± 5.5	13.0 ± 5.9	13.0 ± 4.9	13.2 ± 4.5	13.3 ± 4.2	15.9 ± 7.2	0.25
Diastolic longitudinal force (%)	10.4 ± 4.4	10.8 ± 4.1	10.4 ± 4.3	10.5 ± 4.6	7.4 ± 3.4	10.7 ± 5.5	**<0.001**
Diastolic transverse force (%)	2.2 ± 1.1	2.4 ± 1.2	2.0 ± 0.9	2.3 ± 1.1	1.7 ± 0.8	2.3 ± 1.1	**0.016**
Diastolic ratio of transverse to longitudinal forces	23.2 ± 11.2	23.1 ± 10.4	21.5 ± 10.3	23.4 ± 11.6	25.4 ± 12.8	25.5 ± 15.3	0.66
Impulse longitudinal force (%)	29.0 ± 13.1	32.4 ± 13.6	26.7 ± 12.3	28.8 ± 10.8	17.5 ± 7.6	27.0 ± 12.3	**<0.001**
Systolic-diastolic transition longitudinal force (%)	12.8 ± 5.8	14.3 ± 5.7	11.8 ± 5.1	12.9 ± 5.7	8.2 ± 4.4	11.2 ± 6.3	**<0.001**
Diastolic deceleration longitudinal force (%)	9.2 ± 4.7	9.9 ± 4.4	8.6 ± 3.8	9.9 ± 5.7	5.9 ± 4.1	8.6 ± 5.3	**<0.001**
Atrial thrust longitudinal force (%)	4.3 ± 2.7	3.9 ± 2.4	4.8 ± 3.0	4.8 ± 2.9	4.1 ± 2.7	4.7 ± 2.9	0.10

Values are n (%) or mean ± standard deviation. **Bold** values indicate the 2-tailed p-value reached significance (<0.05). *Abbreviations: Same as Table 2.*

Table S3. LV hemodynamic forces of patients with and without MACE (N=351).

	Overall N = 351[1]	**MACE** N = 67[1]	**No MACE** N = 284[1]	**p-value**[2]
LV hemodynamic forces				
Longitudinal force (%)	18.1 ± 7.3	14.3 ± 6.3	19.0 ± 7.2	**<0.001**
Transverse force (%)	2.7 ± 1.1	2.4 ± 1.2	2.8 ± 1.0	**0.023**
Ratio of transverse to longitudinal forces	15.8 ± 5.7	17.4 ± 6.7	15.4 ± 5.4	**0.025**
Ejection angle (°)	76.4 ± 3.7	75.6 ± 4.0	76.6 ± 3.6	0.06
Systolic peak force (%)	49.1 ± 22.4	36.6 ± 17.6	52.0 ± 22.4	**<0.001**
Systolic longitudinal force (%)	25.5 ± 11.4	19.5 ± 9.3	27.0 ± 11.4	**<0.001**
Systolic transverse force (%)	3.1 ± 1.4	2.7 ± 1.8	3.2 ± 1.3	**<0.001**
Systolic ratio of transverse to longitudinal forces	13.3 ± 5.5	14.8 ± 6.8	12.9 ± 5.1	**0.030**
Diastolic longitudinal force (%)	10.4 ± 4.4	8.9 ± 4.4	10.7 ± 4.3	**0.002**
Diastolic transverse force (%)	2.2 ± 1.1	1.9 ± 1.0	2.3 ± 1.1	**0.004**
Diastolic ratio of transverse to longitudinal forces	23.2 ± 11.2	23.4 ± 12.3	23.1 ± 10.9	0.82
Impulse longitudinal force (%)	29.0 ± 13.1	21.9 ± 10.7	30.7 ± 13.1	**<0.001**
Systolic-diastolic transition longitudinal force (%)	12.8 ± 5.8	10.2 ± 5.8	13.4 ± 5.6	**<0.001**
Diastolic deceleration longitudinal force (%)	9.2 ± 4.7	7.4 ± 5.3	9.7 ± 4.4	**0.002**
Atrial thrust longitudinal force (%)	4.3 ± 2.7	4.1 ± 2.6	4.3 ± 2.7	0.46

Values are mean ± standard deviation. **Bold** values indicate the 2-tailed p-value reached statistical significance (<0.05).

Table S4. Intra- and inter-observer reproducibility using intraclass correlation coefficient.

HDFs parameters	Inter-observer correlation coefficient	Intra-observer correlation coefficient
Longitudinal force (%)	0.94	0.88
Transverse force (%)	0.92	0.85
Transverse-longitudinal forces ratio	0.90	0.81
Ejection angle (°)	0.89	0.79
Systolic peak force (%)	0.92	0.90
Systolic longitudinal force (%)	0.90	0.89
Systolic transverse force (%)	0.93	0.84
Systolic transverse-longitudinal forces ratio	0.96	0.79
Diastolic longitudinal force (%)	0.90	0.96
Diastolic transverse force (%)	0.83	0.79
Diastolic transverse-longitudinal forces ratio	0.67	0.75
Impulse longitudinal force (%)	0.92	0.90
Systolic-diastolic transition longitudinal force (%)	0.89	0.97
Diastolic deceleration longitudinal force (%)	0.93	0.91
Atrial thrust longitudinal force (%)	0.81	0.93

Results show ICC values > 0.75 for every HDF parameter (except for diastolic ratio), showing good intra and inter observer reproducibility. Corresponding p-values were all below 0.001.

Table S5. Univariate analysis of all LV hemodynamic force parameters.

	Hazard Ratio (95% CI)	p-value
Longitudinal force	0.49 (0.35–0.69)	**<0.001**
Transverse force	0.81 (0.62–1.06)	0.13
Ratio of transverse to longitudinal forces	1.43 (1.16–1.77)	**<0.001**
Ejection angle	0.75 (0.59–0.95)	**0.016**
Systolic peak force	0.44 (0.31–0.63)	**<0.001**
Systolic longitudinal force	0.49 (0.35–0.68)	**<0.001**
Systolic transverse force	0.80 (0.60–1.05)	0.11
Systolic ratio of transverse to longitudinal forces	1.38 (1.11–1.71)	**0.003**
Diastolic longitudinal force	0.67 (0.49–0.91)	**0.010**
Diastolic transverse force	0.76 (0.57–1.00)	**0.049**
Diastolic ratio of transverse to longitudinal forces	1.08 (0.86–1.37)	0.50
Impulse longitudinal force	0.47 (0.33–0.66)	**<0.001**
Systolic-diastolic transition longitudinal force	0.57 (0.42–0.78)	**<0.001**
Diastolic deceleration longitudinal force	0.64 (0.46–0.87)	**0.005**
Atrial thrust longitudinal force	0.87 (0.66–1.14)	0.30

Abbreviations: Same as Table 1 and 2.

Note: Hazard ratios for hemodynamic force parameters are expressed per 1 standard deviation increase.

Table S6. Baseline characteristics of patients stratified by clusters (N=351).

	All patients (N = 351)	**Cluster 1** N = 124	**Cluster 2** N = 227	**p-value**
Age, years	48.5 ± 20.0	37.3 ± 16.1	54.6 ± 19.3	**<0.001**
Males, n (%)	223 (63.5%)	89 (71.8%)	134 (59.0%)	**0.004**
BMI, kg/m^2	25.2 ± 5.2	25.2 ± 5.8	25.2 ± 4.8	0.95
Coronary risk factors, n (%)				
Current or previous smoking	150 (42.7%)	56 (45.2%)	94 (41.4%)	0.88
Hypertension	94 (26.8%)	19 (15.3%)	75 (33.0%)	**<0.001**
Dyslipidemia	56 (16.0%)	10 (8.1%)	46 (20.3%)	**0.001**
Diabetes	22 (6.3%)	2 (1.6%)	20 (8.8%)	**0.013**
Admission presentation, n (%)				
Chest pain	291 (82.9%)	113 (91.1%)	178 (78.4%)	**0.018**
Dyspnea (NYHA III/IV)	22 (6.3%)	4 (3.2%)	18 (7.9%)	**0.044**
Cardiac arrest	9 (2.6%)	3 (2.4%)	6 (2.6%)	0.73
Syncope/ Malaise	9 (2.6%)	1 (0.8%)	8 (3.5%)	0.50
Palpitations	3 (0.9%)	1 (0.8%)	2 (0.9%)	0.29
Cardiogenic shock	2 (0.6%)	0 (0.0%)	2 (0.9%)	0.54
ECG abnormalities	2 (0.6%)	1 (0.8%)	1 (0.4%)	1.00
Other*	13 (3.7%)	1 (0.8%)	12 (5.3%)	**0.037**
Cardiac rhythm at admission, n (%)				
Sinus rhythm	342 (97.4%)	123 (99.2%)	219 (96.5%)	0.17
Atrial fibrillation	9 (2.6%)	1 (0.8%)	8 (3.5%)	0.17
Ventricular arrhythmia	23 (6.6%)	6 (4.8%)	17 (7.5%)	0.73
Biological results				
Troponin peak ratio, (x ULN)	234.6 ± 448.4	270.5 ± 552.8	214.9 ± 379.5	0.69
Biological inflammatory syndrome †, n (%)	185 (52.9%)	69 (55.6%)	116 (51.3%)	0.67
TTE findings				
LVEF, (%)	54.2 ± 10.1	57.1 ± 6.9	52.6 ± 11.2	**<0.001**
Cinetic abnormalities, n (%)	183 (52.1%)	46 (37.1%)	137 (60.4%)	**<0.001**
Pericardial effusion, n (%)	35 (10.0%)	8 (6.5%)	27 (11.9%)	0.13
Invasive coronary angiography, n (%)	245 (69.8%)	65 (52.4%)	180 (79.3%)	**<0.001**

	All patients (N = 351)	Cluster 1 N = 124	Cluster 2 N = 227	p-value
CCTA, n (%)	30 (8.5%)	10 (8.1%)	20 (8.8%)	0.93
Final diagnosis, n (%)				
Myocarditis	172 (49.0%)	78 (62.9%)	94 (41.4%)	**<0.001**
Ischemic	76 (21.7%)	19 (15.3%)	57 (25.1%)	**0.036**
Tako-Tsubo	29 (8.3%)	2 (1.6%)	27 (11.9%)	**<0.001**
Cardiomyopathy	27 (7.7%)	9 (7.3%)	18 (7.9%)	1.00
Inconclusive	47 (13.4%)	16 (12.9%)	31 (13.7%)	0.90
Treatments at discharge, n (%)				
Betablockers	270 (76.9%)	92 (74.2%)	178 (78.4%)	0.24
ACEI	172 (49.0%)	42 (33.9%)	130 (57.3%)	**<0.001**
Antiplatelet	125 (35.6%)	27 (21.8%)	98 (43.2%)	**<0.001**
Statin	120 (34.2%)	25 (20.2%)	95 (41.9%)	**<0.001**
NSAID	97 (27.6%)	50 (40.3%)	47 (20.7%)	**<0.001**
Colchicine	90 (25.6%)	44 (35.5%)	46 (20.3%)	**0.002**
Outcomes, n (%)				
MACE	67 (19.1%)	6 (4.8%)	61 (26.9%)	**<0.001**
Death	38 (10.8%)	2 (1.6%)	36 (15.9%)	**0.001**
Disease recurrence	18 (5.1%)	5 (4.0%)	13 (5.7%)	0.48
Hospitalization for heart failure	4 (1.1%)	0.0 (0.0%)	4.0 (1.8%)	0.30
Sustained TV	7 (2.0%)	0.0 (0.0%)	7.0 (3.1%)	0.05
Hospitalization for symptomatic AF	3 (0.9%)	0.0 (0.0%)	3.0 (1.3%)	0.56
Stroke	8 (2.3%)	0.0 (0.0%)	8.0 (3.5%)	0.05
Hospital length of stay, (days)	5.6 ± 4.3	4.9 ± 3.6	6.0 ± 4.6	**0.006**

Values are n (%) or mean ± standard deviation. **Bold** values indicate the 2-tailed p-value reached statistical significance (<0.05).
* includes: altered general condition, fall, and stroke.
† defined as elevated C-reactive protein (>5 mg/L) and/or leukocytosis (>10×10^9/L)

Abbreviations: Same as Table 1

Table S7. Baseline CMR characteristics, strain and LV hemodynamic forces of patients stratified by clusters (N=351).

	Overall N = 351	**Cluster 1** N = 124	**Cluster 2** N = 227	**p-value**
LV ejection fraction, %	55.5 ± 10.0	60.6 ± 6.4	52.6 ± 10.4	**<0.001**
LV end-diastolic volume index, mL/m^2	89.3 ± 20.7	87.9 ± 18.8	90.0 ± 21.7	0.73
LV end-systolic volume index, mL/m^2	40.4 ± 15.8	34.9 ± 10.5	43.4 ± 17.4	**<0.001**
LV mass index, g/m^2	60.3 ± 14.2	58.8 ± 12.8	61.1 ± 14.9	0.52
RV ejection fraction, %	50.2 ± 9.3	52.9 ± 7.8	48.8 ± 9.7	**<0.001**
Presence of T2 TSE hyperintensity, n (%)	164 (51.7%)	57 (50.0%)	107 (52.7%)	0.48
Mapping sequences				
Maximum T2 mapping value, ms	46.7 ± 8.0	45.4 ± 7.0	47.6 ± 8.4	0.45
Remote T2 mapping value, ms	39.5 ± 3.4	39.4 ± 2.9	39.6 ± 3.7	0.74
Maximum T1 mapping value, ms	1,332.8 ± 133.5	1,318.0 ± 128.7	1,341.2 ± 135.9	0.07
Remote T1 mapping value, ms	1,212.4 ± 70.4	1,206.9 ± 67.5	1,215.6 ± 72.0	**0.027**
Late gadolinium enhancement				
Presence of LGE, n (%)	252 (71.8%)	98 (79.0%)	154 (67.8%)	**0.013**
Presence of subendocardial LGE, n (%)	79 (22.5%)	19.0 (15.3%)	60.0 (26.4%)	**0.036**
Presence of midwall or subepicardial LGE, n (%)	170 (48.4%)	78.0 (62.9%)	92.0 (40.5%)	**<0.001**
Presence of transmural LGE, n (%)	54 (15.5%)	11.0 (8.9%)	43.0 (19.1%)	**0.015**
LGE extent (%)	19.2 ± 13.8	20.7 ± 13.7	18.4 ± 13.8	0.10
Global longitudinal strain				
Myocardial GLS (%)	-19.4 ± 4.5	-22.1 ± 2.9	-18.0 ± 4.6	**<0.001**
Endocardial GLS (%)	-22.3 ± 5.2	-25.2 ± 3.2	-20.7 ± 5.4	**<0.001**
LV hemodynamic forces				
Longitudinal force (%)	18.1 ± 7.3	25.4 ± 6.3	14.1 ± 4.0	**<0.001**
Transverse force (%)	2.7 ± 1.1	3.5 ± 1.0	2.2 ± 0.7	**<0.001**
Ratio of transverse to longitudinal forces	15.8 ± 5.7	14.4 ± 4.4	16.6 ± 6.2	**<0.001**
Ejection angle (°)	76.4 ± 3.7	77.0 ± 3.2	76.0 ± 3.9	**<0.001**
Systolic peak force (%)	49.1 ± 22.4	71.6 ± 19.3	36.7 ± 11.9	**<0.001**
Systolic longitudinal force (%)	25.5 ± 11.4	37.1 ± 9.5	19.2 ± 6.1	**<0.001**

	Overall N = 351	**Cluster 1** N = 124	**Cluster 2** N = 227	**p-value**
Systolic transverse force (%)	3.1 ± 1.4	4.3 ± 1.4	2.5 ± 0.9	**<0.001**
Systolic ratio of transverse to longitudinal forces	13.3 ± 5.5	12.1 ± 4.2	13.9 ± 6.1	**<0.001**
Diastolic longitudinal force (%)	10.4 ± 4.4	13.2 ± 4.4	8.9 ± 3.5	**<0.001**
Diastolic transverse force (%)	2.2 ± 1.1	2.8 ± 1.2	1.9 ± 1.0	**<0.001**
Diastolic ratio of transverse to longitudinal forces	23.2 ± 11.2	22.4 ± 10.2	23.6 ± 11.7	**<0.001**
Impulse longitudinal force (%)	29.0 ± 13.1	42.4 ± 11.0	21.7 ± 6.9	**<0.001**
Systolic-diastolic transition longitudinal force (%)	12.8 ± 5.8	17.1 ± 5.5	10.5 ± 4.4	**<0.001**
Diastolic deceleration longitudinal force (%)	9.2 ± 4.7	11.9 ± 4.4	7.7 ± 4.1	**<0.001**
Atrial thrust longitudinal force (%)	4.3 ± 2.7	4.7 ± 2.9	4.1 ± 2.5	0.06

Values are n (%) or mean ± standard deviation. **Bold** values indicate the 2-tailed p-value reached statistical significance (<0.05)

Abbreviations: Same as Table 2.

TABLE DES MATIERES

BALADI Claire

De la mécanique cardiaque au pronostic : les forces hémodynamiques ventriculaires gauches comme nouveau marqueur de risque dans les MINOCA

RÉSUMÉ

INTRODUCTION : L'infarctus du myocarde à coronaires non obstructives (MINOCA) est une entité hétérogène associée à une morbidité significative, pour laquelle les marqueurs classiques de l'IRM cardiaque peuvent manquer de sensibilité pour évaluer le risque. Les forces hémodynamiques (HDFs), dérivées des séquences ciné-IRM et reflétant les interactions entre flux sanguin et paroi myocardique, permettent de détecter des dysfonctions ventriculaires subtiles. Leur rôle pronostique dans les MINOCA reste inconnu.
OBJECTIF : Évaluer la valeur pronostique de paramètres HDFs spécifiques chez des patients présentant un MINOCA.
MÉTHODES : Cette étude rétrospective monocentrique a inclus des patients hospitalisés pour MINOCA au CHU d'Angers entre 2014 et 2023 et ayant bénéficié d'une IRM cardiaque. Le critère de jugement principal était un critère composite d'événements cardiovasculaires majeurs (MACE : décès toute cause, accident vasculaire cérébral ou hospitalisation pour motif cardiovasculaire). Des modèles de Cox ajustés sur des variables cliniques et d'IRM ont été utilisés pour évaluer l'impact pronostique des HDFs. La valeur incrémentale a été testée par comparaisons de modèles emboîtés.
RÉSULTATS : Après un suivi médian de 2,8 ans (IQR 1,1–5,2), 67 patients (19,1 %) ont présenté un événement cardiovasculaire majeur. Dans les modèles multivariés ajustés sur la fraction d'éjection ventriculaire gauche, le strain, l'étendue du rehaussement tardif et le diagnostic final, des forces longitudinales de pic systolique (HR +1 DS = 0,54 ; p = 0,004) et d'impulsion (HR +1 DS = 0,58 ; p = 0,010) plus élevées étaient indépendamment associées à un meilleur pronostic, tandis qu'un ratio forces transversale/longitudinale élevé était associé à un risque accru de MACE (HR + 1 DS = 1,31 ; p = 0,032). Dans une analyse par modèles emboîtés, chaque paramètre HDF apportait une valeur pronostique incrémentale par rapport au modèle précédent. Pour la force de pic systolique, le chi-deux passait de 21 à 31 (p = 0,002) avec amélioration de la reclassification.
CONCLUSION : Les forces hémodynamiques dérivées des images ciné-IRM prédisent indépendamment les événements indésirables chez les patients présentant un MINOCA et apportent une valeur pronostique supplémentaire aux marqueurs cliniques et IRM établis.

Mots-clés : imagerie par résonance magnétique cardiaque ; IRM sans contraste ; forces hémodynamiques ; infarctus du myocarde à coronaires non-obstructives ; évènements cardiovasculaires.

From cardiac mechanics to prognosis: left ventricle hemodynamic forces as a novel risk marker in MINOCA

ABSTRACT

INTRODUCTION: Myocardial infarction with non-obstructive coronary arteries (MINOCA) is a heterogeneous entity associated with significant morbidity, where conventional cardiac magnetic resonance (CMR) markers may fail to capture risk. Hemodynamic forces (HDFs), derived from cine-CMR and reflecting flow–tissue interactions, detect subtle ventricular dysfunction. Their prognostic value in MINOCA remains unknown.
OBJECTIVE: To assess the prognostic value of specific HDFs parameters in consecutive patients with MINOCA.
METHODS: This retrospective single-centre study included patients admitted for MINOCA who underwent CMR at Angers University Hospital between 2014 and 2023. The primary endpoint was a composite of major adverse cardiovascular events (MACE: all-cause death, stroke, or cardiovascular hospitalization). Cox regression models adjusted for clinical and CMR risk factors were used to evaluate the prognostic impact of HDFs, and incremental value was assessed using nested model comparisons.
RESULTS: During a median follow-up of 2.8 years (IQR 1.1 - 5.2), 67 patients (19.1%) experienced MACE. In multivariable models adjusted for left ventricular ejection fraction, strain, late gadolinium enhancement extent, and final diagnosis, higher systolic peak force (HR +1 SD = 0.54, p = 0.004) and longitudinal impulse force (HR +1 SD = 0.58, p = 0.010) independently predicted improved outcomes, whereas an elevated transverse-to-longitudinal forces ratio was associated with increased risk (HR + 1 SD = 1.31, p = 0.032). In a nested model analysis, each HDF parameter provided incremental prognostic value compared with a model including the previously cited factors; for systolic peak force, the global chi-square increased from 21 to 31 (p = 0.002) with improved reclassification.
CONCLUSION: Hemodynamic forces derived from cine-CMR independently predict adverse outcomes in MINOCA and provide incremental prognostic value beyond established clinical and CMR markers.

Keywords: cardiovascular magnetic resonance imaging ; non-contrast CMR; hemodynamic forces ; myocardial infarction with non-obstructive coronary arteries ; cardiovascular events.

FACULTÉ DE SANTÉ
UNIVERSITÉ D'ANGERS